Aeolian Research 3 (2011) 87–144

Contents lists available at ScienceDirect

Aeolian Research

journal homepage: www.elsevier.com/locate/aeolia

Review

# The magnetic properties of Quaternary aeolian dusts and sediments, and their palaeoclimatic significance

B.A. Maher *

*Centre for Environmental Magnetism & Palaeomagnetism, Lancaster Environment Centre, University of Lancaster, LA1 4YQ, UK*

ARTICLE INFO

*Article history:*
Received 1 October 2010
Revised 28 January 2011
Accepted 28 January 2011
Available online 26 March 2011

*Keywords:*
Mineral dust
Palaeoclimate
Magnetic susceptibility
Sediment provenance
Loess
Deep-sea, lake and desert sediments

ABSTRACT

Changes in the sources, properties and fluxes of mineral aerosol ('dust') have significance as both indicators and agents of climate change, through radiative, cloud condensation and ocean biogeochemical effects. Quaternary aeolian sediments, worldwide in distribution, can comprise high-resolution archives of past climatic and environmental change, by incorporating chronological, physico-chemical and magnetic information.

The magnetic record for a sediment sequence may reflect changes in sediment source, and diagenetic (post-depositional) loss and/or transformation and/or gain of magnetic minerals. Each potential pathway requires careful evaluation, to achieve robust understanding of the palaeo-environmental and/or palaeoclimatic information carried by sediment magnetic properties.

The most important minerals for studies of aeolian dusts are those carrying a magnetic remanence at room temperature. For the arid zone, the weakly but very magnetically stable minerals, haematite and goethite, form key magnetic tracers for aeolian transport through space and time. Elsewhere, the strongly magnetic ferrimagnets, magnetite and maghemite, arising from lithogenic and/or *in situ* sources, can dominate sediment magnetic properties. Magnetic measurements, sensitive even to trace concentrations of these iron minerals, can readily discriminate between different magnetic mineral assemblages, and are also relatively rapid, non sample-destructive, and cost-effective. Combined with robust chronological control, magnetic measurements are a powerful means of identifying palaeoclimatic and palaeoenvironmental change from palaeo-dust records. In the case of the classic loess/palaeosol sequences of East Asia, it has been possible to obtain quantitative magnetic climofunctions, enabling spatially- and temporally-dense reconstructions of palaeoprecipitation.



**Contents**



* Tel.: +44 1524 510268; fax: +44 1524 510269.
*E-mail address:* b.maher@lancaster.ac.uk

1875-9637/$ - see front matter © 2011 Elsevier B.V. All rights reserved.
doi:10.1016/j.aeolia.2011.01.005

## 1. Introduction

Aeolian sediments can comprise key natural archives of past climatic and environmental changes. Aeolian sediments of Quaternary age occur in every ocean and on every continent (on land and/or in ice), and incorporate chronological, physico-chemical, and magnetic records of changes in dust flux, source and properties.

Palaeo-dust records show that the emission, transport, deposition and post-depositional weathering of aeolian dust are all strongly linked with climate state (e.g. Harrison et al., 2001; Kohfeld, 2002; Kohfeld et al., 2005). During glacial climate stages, for example, increases in dust flux were globally 'synchronous' and were on average two to five times greater than in interglacial stages (Fig. 1, and e.g. Kohfeld and Harrison, 2001). However, dust fluxes also demonstrate major *within*-stage variability, both in temporal (sub-millennial) and spatial terms, such variability particularly exemplified by most of the world's sequences of loess (deposits of windblown dust). The transport and deposition of mineral dust not only reflects and responds to climate but may play an active role in climate modification, whether directly via radiative effects (e.g. Sokolik and Toon, 1999; Alfaro et al., 2004; IPCC, 2007) or indirectly via modification of clouds (Sassen et al., 2003; Spracklen et al., 2008) or of ocean uptake of atmospheric carbon dioxide (Martin, 1990; Bopp et al., 2003; Moore and Braucher, 2008). Given the significance of aeolian dust as not just a proxy recorder of climate conditions but also as an active agent of climate change, sampling, analysis and understanding of palaeo-dust records represent timely and important scientific tasks.

The large changes in dust fluxes recorded by the palaeo-dust record may reflect a variety of processes, encompassing multi-factorial changes in (a) the location and areal extent of dust source areas, (b) transport path and efficacy, and (c) the trapping efficiency of the depositional zone. For the last glacial maximum (LGM), for example, comparisons between palaeo-data and modelled dust fluxes indicate that the areal extent of dust sources must have been greatly extended (e.g. Mahowald et al., 1999; Werner et al., 2002; Tegen et al., 2002). Expansion of dust source areas appears to have been quasi-synchronous across the northern and southern hemispheres (Winckler et al., 2008; Maher et al., 2010), resulting, depending on location, from changes in vegetative cover (e.g. Aleinikoff et al., 2008; Tegen and Fung, 1995); sub-aerial erosion of emergent continental shelves (Bigler et al., 2006); and deflation from glacigenic and periglacial deposits (Mahowald et al., 2006; Sugden et al., 2009).

In terms of transport, variations in pressure gradients and resultant wind speeds and/or gustiness (Rea and Hovan, 1995; Engelstaedter and Washington, 2007; McGee et al., 2010) have been inferred from changes in palaeo-dust particle size, whilst others have additionally suggested the role of changes in transport path, length of path and particle rain-out (e.g. Arnold et al., 1998; Ruth et al., 2003; Fischer et al., 2007a, 2007b; Lambert et al., 2008). Dust deposition rates are likely to have varied not only in response to enhanced dust emissions and transport, but also due to surface roughness changes, especially related to vegetation change (e.g. Marticorena et al., 1997). Present-day (PD) and LGM sources and properties of aeolian dust, and their possible impacts on climate via radiative and ocean biogeochemical forcings, are the subject

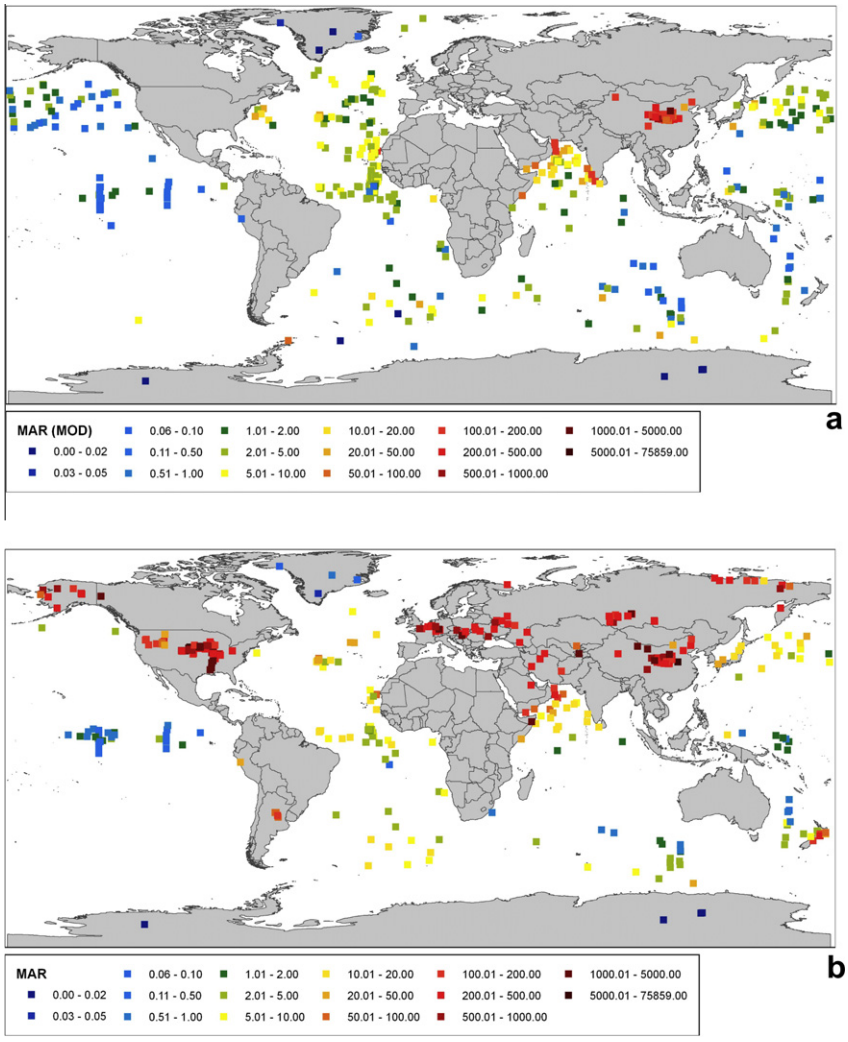


**Fig. 1.** Measured aeolian mass accumulation rates (MARs, g $m^{-2}$ $yr^{-1}$) for (a) the present day (MOD = modern) and (b) for the LGM. All data drawn from the 'DIRTMAP3' database (Maher and Kohfeld, 2009, http://www.lec.lancs.ac.uk/research/LU_themes/inqua_working_group.php). From Maher et al. (2010).

of a recent review (Maher et al., 2010), which also includes the latest global synthesis of PD and LGM dust fluxes ('DIRTMAP3', see Fig. 1).

Here, the palaeoclimatic significance of the *magnetic properties* of aeolian dusts and sediments is reviewed. Magnetic behaviour and the magnetic properties of a range of iron oxides and oxyhydroxides are first briefly introduced, and the sources of such minerals for dusts and aeolian sediments considered. Magnetic data for modern dusts (relatively scarce compared with the available palaeo-data) are then presented, followed by a review of a global range of magnetic studies of palaeo-dust fluxes, sources and properties. The examples discussed are drawn both from the marine and continental (including ice-core) realms. Attention is paid particularly to the worldwide occurrences of loess sequences and their interbedded palaeosols, and the potential role of these sediments as quantitative archives of palaeoclimate, and especially of palaeoprecipitation.

The ubiquity of 'magnetic minerals' (i.e. defined in this context as minerals capable of carrying a magnetic remanence, see Section 2 below) provides the potential for rich magnetic records of past and present changes in climate and environment. The *palaeomagnetic* properties of aeolian sediments can provide records of sediment age, via reversal magnetostratigraphy, secular variation or palaeointensity changes. Their *environmental* or mineral magnetic properties can provide not only a basis for high-resolution magnetic cyclostratigraphy but also unique information on sediment source, and on climate, recorded through post-depositional weathering and soil development. The *magnetic fabric* of sediments can sometimes provide information on pathways of sediment transport and deposition, especially in least weathered aeolian sediments; increased magnetic lineation associated with deposition from a preferential direction of flow, whether wind or water. (This aspect of sedimentary magnetism will not be considered here; see e.g. Kodama, 1995 for a review of magnetic fabrics).

Magnetic measurements of sediments and soils are sensitive even to trace concentrations of the most ubiquitous iron oxides, goethite and haematite. For example, the remanent magnetisation due to less than 1 part per $10^7$–$10^8$ of haematite can be readily measured. For ferrimagnets like magnetite, the sensitivity increases to <1 ppb. Magnetic measurements can be made relatively rapidly and non-destructively. Combined with robust chronological control, magnetic measurements demonstrably provide a powerful means of identifying and quantifying palaeoclimatic and palaeoenvironmental change.

Changes in sediment magnetic properties can reflect changes in the supply of allocthonous magnetic minerals, and/or authigenic

formation of magnetic minerals, and/or their post-depositional dissolution. Hence, sediment magnetic properties require careful, site-specific evaluation, ideally based on thorough investigation of a range of magnetic parameters (e.g. Table 1), in order to achieve robust understanding both of the magnetic minerals carrying the measured signal and the nature of the recording process, and hence its palaeoclimatic significance.

## 2. Magnetic properties of minerals in dusts and sediments

All materials display magnetic behaviour – when placed in a magnetic field, they respond by producing magnetic fields of their own. Indeed, some minerals (like magnetite) spontaneously generate magnetisation, without application of any external field. Here is provided a brief introduction to material magnetic properties (drawn from Maher, 2007 and Maher et al., 1999); more detailed discussion is available from e.g. Jiles (1998).

Magnetic fields arise at the atomic level, from the electric currents generated by the spin of electrons about their own axes and their orbital motion around their central nucleus. The movements of these charged particles (which can be thought of as describing tiny current loops) produce magnetic moments, $\boldsymbol{m}$. When a material is subjected to an applied magnetic field, $\boldsymbol{H}$, the magnetic moments will respond and produce an induced magnetisation, $\boldsymbol{M_i}$, the magnetic moment per unit volume (ampere/metre, A m), or per unit mass (A m$^2$ kg$^{-1}$).

The relationship between the induced magnetisation, $\boldsymbol{M_i}$ and the applied field, $\boldsymbol{H}$ is

$$\boldsymbol{M_i} = \mathrm{K}\boldsymbol{H} \text{ or } \chi\boldsymbol{H}$$

where K or $\chi$ is the *magnetic susceptibility*. The volumetric magnetic susceptibility, K, is dimensionless. The mass susceptibility, $\chi = \mathrm{K}/\rho$ (where $\rho$ = the sample density), in units of m$^3$ kg$^{-1}$, is commonly used in environmental studies of magnetic materials.

It is important to note that $\chi$ can vary in complex ways as a function of the sample characteristics, including magnetic mineralogy, concentration, grain size, shape and stress, and method of measurement, for example, at different temperatures and frequency of applied field.

Three basic types of magnetic response can be observed when $\boldsymbol{M_i}$ is measured upon application of an external magnetic field, $\boldsymbol{H}$ (Fig. 2). Diamagnetic materials acquire a small induced magnetisation, which is aligned opposite to the applied field direction (Fig. 2a). Examples of diamagnetic substances include water ($\chi \sim -0.9 \times 10^{-8}$ m$^3$ kg$^{-1}$), quartz ($\chi \sim -0.6 \times 10^{-8}$ m$^3$ kg$^{-1}$), and calcium carbonate ($\chi \sim -0.5 \times 10^{-8}$ m$^3$ kg$^{-1}$). Paramagnetic materials display weak but positive magnetic susceptibility (Fig. 2b). They contain unpaired electrons which generate net (non-cancelled) electron spin moments, which align themselves with the applied field direction. Thus, their magnetic susceptibility at room temperature is low (but higher than the diamagnets) and positive; examples include such iron-bearing minerals as biotite ($\chi \sim 50 \times 10^{-8}$ m$^3$ kg$^{-1}$), and the iron oxyhydroxide, lepidocrocite ($\chi \sim 70 \times 10^{-8}$ m$^3$ kg$^{-1}$).

In contrast to these weakly magnetic responses, the third type of magnetic behaviour, ferromagnetism, displays much stronger and spontaneous magnetisations, and magnetic remanence-carrying capability (Fig. 2c). Ferromagnetic materials are strong magnets because of the close packing of atoms within their crystal structures. This close packing enables positive interactions between uncancelled electron spins, leading to large and stable induced magnetisations (i.e. orders of magnitude higher than those of diamagnets and paramagnets). As seen in Fig. 2c, ferromagnets display steep increases in magnetisation with applied field, until they reach saturation magnetisation ($\mathbf{M_s}$). Ferromagnets also display irreversible magnetisation; upon removal of the saturating field, their magnetisation falls not to zero but to the saturation remanent magnetisation (SIRM). The exchange interactions which produce this strong magnetic behaviour can take on different con-

**Table 1**
Summary of routine, room-temperature magnetic parameters, units, instrumentation and magnetic significance. Adapted from Maher et al. (2009a,b).

| | |
|---|---|
| Magnetic susceptibility, $\chi$ (normalised to sample mass)<br>***Magnetic concentration*** | The ratio of magnetisation induced in a sample to the intensity of the magnetising field. Measured *within* a small ac field (~0.1 mT, ~2.5× the Earth's magnetic field) and is reversible (i.e. no magnetic remanence is induced). Often roughly proportional to the concentration of strongly magnetic (e.g. magnetite-like) minerals. Weakly magnetic minerals, like haematite, have much lower susceptibility values; water, organic matter have negative susceptibility<br>*Instrumentation:* single sample susceptibility meter<br>*Units:* m$^3$ kg$^{-1}$ |
| Frequency dependent susceptibility, $\chi_{fd}$<br>***Ultrafine magnetic grain size (on the superparamagnetic/ single domain size boundary at room temperature)*** | The variation of susceptibility with frequency of ac measurement field. Frequency dependence of susceptibility reflects the presence of SP grains, unstable (high susceptibility) at low frequency/ longer 'observation time', and stable (lower susceptibility) at higher frequency/shorter 'observation time'<br>*Instrumentation:* e.g. the Bartington Instruments MS2B susceptibility sensor enables measurement at 2 frequencies (0.46 kHz and 4.6 kHz)<br>*Units:* m$^3$ kg$^{-1}$ or normalised to the low-frequency $\chi$, $(X_{LF} - X_{HF})/X_{LF}$ |
| Anhysteretic remanent magnetisation, ARM or anhysteretic susceptibility, $\chi_{ARM}$<br>***Ultrafine magnetite*** | If a sample is subjected to a decreasing ac field with a small dc field superimposed, it acquires an anhysteretic remanence. ARM is sensitive both to the concentration and grain size of ferrimagnetic (magnetite-like) grains, highest for grains close to the SP/SD boundary and lowest for coarse multidomain (MD) magnetic grains (e.g. >~5 μm in magnetite). If ARM normalised for the dc field strength (desirable as different labs. use different dc fields), it is termed an anhysteretic susceptibility<br>*Instrumentation:* anhysteretic magnetiser (max. ac field 100 mT, dc field often ~0.08 mT); fluxgate magnetometer<br>*Units*: ARM, A(mperes) m$^2$, $\chi_{ARM}$ m$^3$ kg$^{-1}$ |
| Saturation remanence, SIRM<br>***Concentration of remanence-bearing minerals*** | The highest level of magnetic remanence that can be induced by application of a 'saturating' magnetic field (in many labs. the highest dc field is 1 T, sufficient to saturate magnetite but not haematite or goethite). SIRM is an indicator of the concentration of magnetic minerals in a sample but also responds (albeit less sensitively than ARM) to magnetic grain size<br>*Instrumentation:* Pulse magnetiser and/or electromagnet; fluxgate magnetometer |
| Remanence ratios, $IRM_{n\ mT}$/SIRM%<br>***Degree of magnetic 'softness' or 'hardness' (MD vs SD magnetite; magnetite vs haematite)*** | A 'soft' mineral (e.g. coarse MD magnetite) will acquire remanence easily, at low fields (e.g. $IRM_{20\ mT}$/SIRM of 90%). A 'hard' mineral (e.g. haematite) will magnetise only at high fields (e.g. $IRM_{20\ mT}$/SIRM of <5%, IRM 300 mT/SIRM of ~30%) |

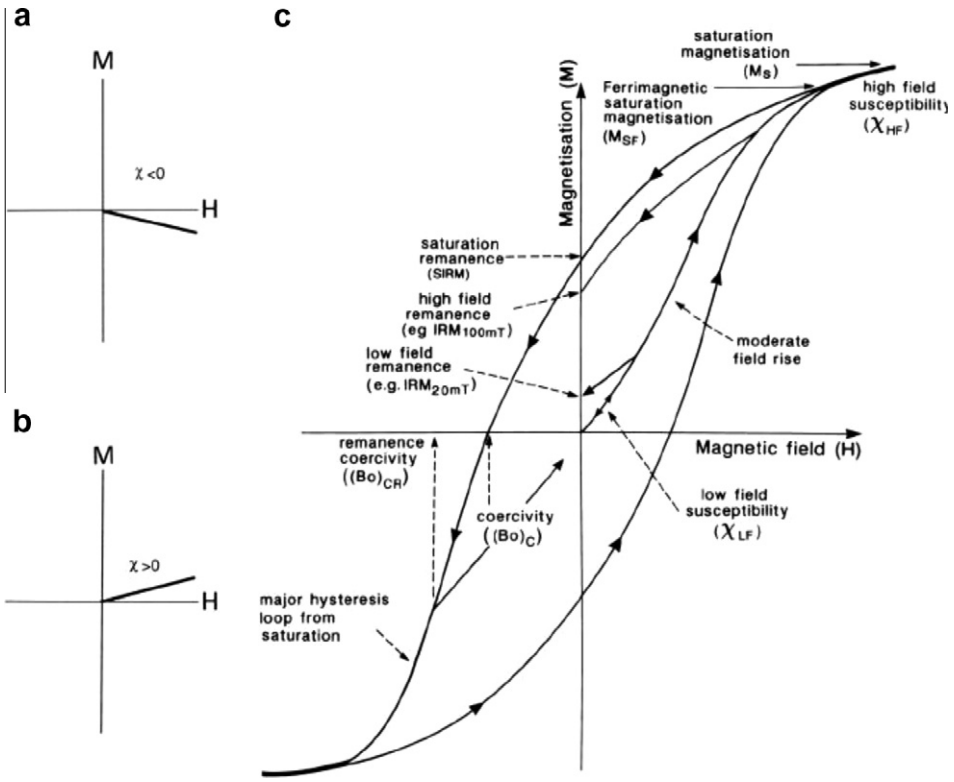


**Fig. 2.** Magnetic response (M) to applied magnetic fields (H); (a) the weak and negative behaviour of a diamagnetic material; (b) the weak and positive response of a paramagnetic material; (c) a magnetic hysteresis (M–H) loop for a typical natural material containing a mixture of ferromagnetic and paramagnetic minerals, and the magnetic parameters often used in environmental magnetic investigations. Redrawn from Maher et al. (1999).

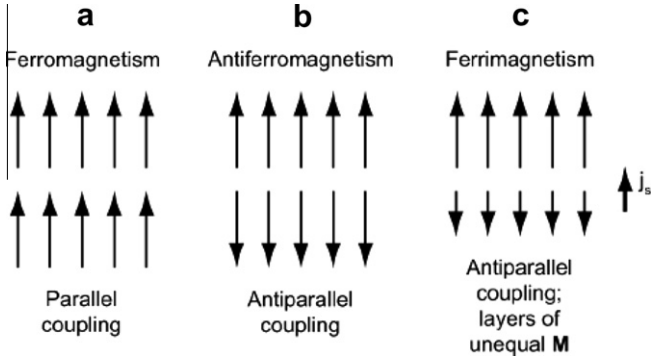


**Fig. 3.** Ferromagnetic (a), perfectly antiferromagnetic (b) and ferromagnetic (c) exchange coupling.

figurations, reflecting different mineral structures. In ferromagnets, the alignment of the exchange coupling is entirely parallel (Fig. 3a); in (imperfect) antiferromagnets, the coupling is (almost) anti-parallel (Fig. 3b); in ferrimagnets, the coupling is opposite but unequal (Fig. 3c). Examples of ferromagnets include the true ferromagnet, iron ($\chi$ ~200,000 × $10^{-8}$ $m^3$ $kg^{-1}$, SIRM ~80 A $m^2$ $kg^{-1}$); the imperfect antiferromagnet, haematite ($\chi$ ~60 × $10^{-8}$ $m^3$ $kg^{-1}$, SIRM ~0.25 A $m^2$ $kg^{-1}$); and the mixed $Fe^{2+}/Fe^{3+}$ ferrimagnet, magnetite ($\chi$ ~50,000 × $10^{-8}$ $m^3$ $kg^{-1}$, SIRM ~15 A $m^2$ $kg^{-1}$).

A further valuable characteristic of ferromagnetic minerals is that their susceptibility and remanence properties display apparent grain size-dependence (Fig. 4). Grain size exerts no intrinsic control on magnetisation, but it physically controls the number of magnetic domains into which any magnetic mineral crystal can sub-divide. Magnetic domains – regions within a crystal with uniform directions of magnetisation – are typically a few hundreds of nanometers in diameter, and separated from other domains by domain walls, of ~5–200 nm thickness. Domains form in order to lower the total energy state of the crystal; for example, a large, multidomain (MD) magnetite grain (i.e. >~2 μm) can exist in a nearly demagnetised state, by sub-dividing into many domains each magnetised in different directions. Small grains (e.g. <~0.03 μm in magnetite) are too small to form any domains. Magnetite grains of between ~0.03 and 0.07 μm can form one single, stable domain (SSD). It is energetically easier to magnetise and demagnetise MD grains than SSD grains, and MD grains will also have weaker magnetisations than SSD grains. The least stable magnetic grains are those which are *superparamagnetic* (SP) at room temperature (i.e. for magnetite, <~30 nm in diameter). The magnetic moments of such grains are constantly disordered by thermal agitation; they can carry no magnetic remanence but do contribute a disproportionately high magnetic susceptibility (depending on the frequency of measurement, see Table 1).

This high susceptibility reflects temporary alignment of their ~$10^5$ magnetic moments within a low magnetic field, giving rise to 'super'-paramagnetic behaviour.

The magnetic properties of natural samples can be analysed using many different measurement protocols and experiments. However, because environmental materials often contain different and distinctive magnetic minerals, with different compositions, concentrations and grain sizes, it is often possible to use a quite small number of magnetic parameters to identify their major magnetic components and/or to characterise, or magnetically 'fingerprint', individual samples (e.g. Tables 1 and 2, and Fig. 5). It might be noted that measurements of magnetic susceptibility normally constitute just the first, and most basic, step in any sediment magnetic analysis, followed by more detailed magnetic characterisation, preferably supplemented by independent mineralogical analysis (e.g. electron microscopy, Mossbauer analysis) of a representative subset of samples (e.g. Hounslow and Maher, 1996). A

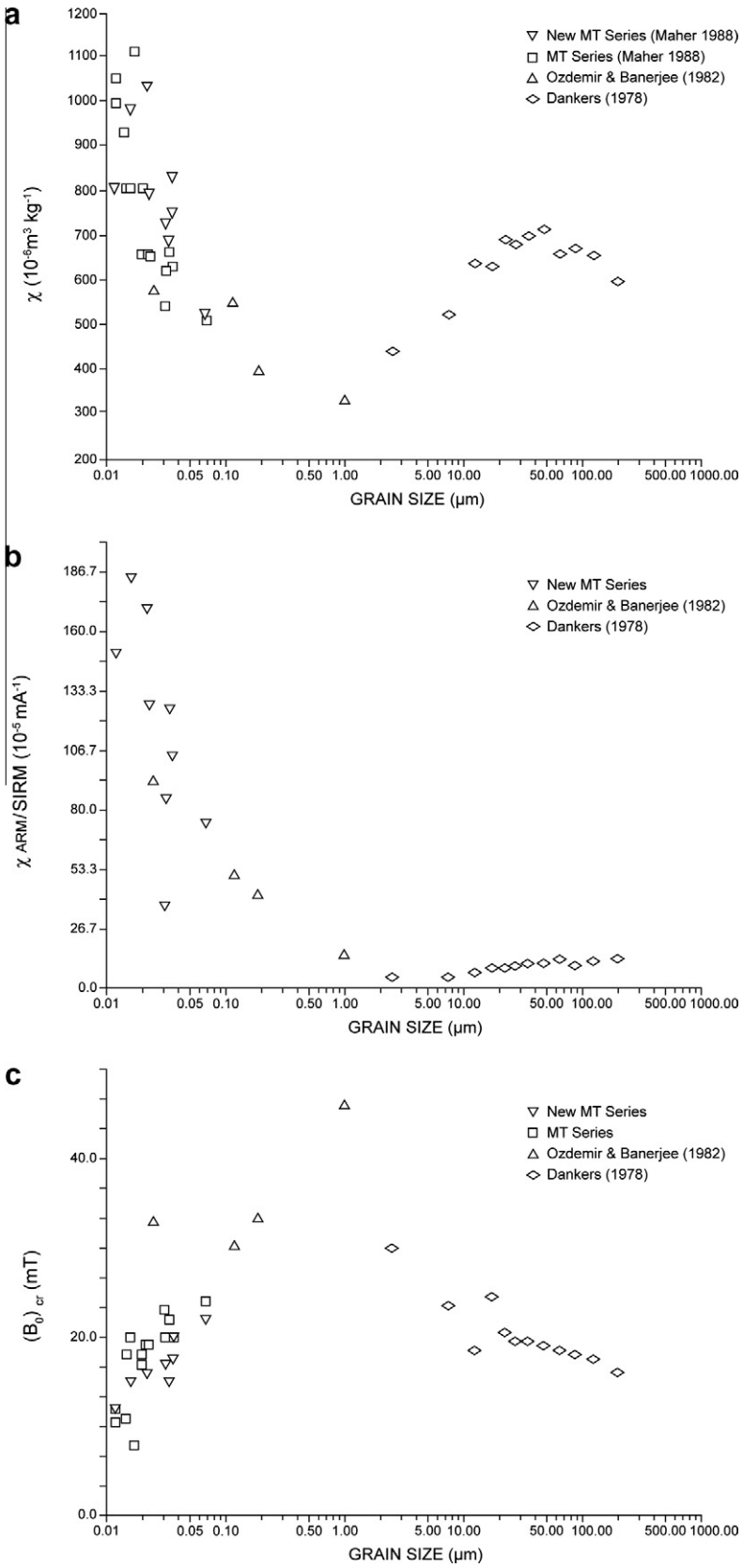


**Fig. 4.** The variation of magnetic properties with grain size in magnetites of known grain size distributions, (a) $\chi$; (b) $\chi_{ARM/SIRM}$ ratio; (c) coercivity of remanence $(B_0)_{CR}$.

'user-friendly' practical guide to magnetic analysis of environmental materials is provided by Walden et al. (1999).

Most natural samples contain a mixture of different magnetic components (i.e. different minerals, in different concentrations

**Table 2**
Magnetic mineral identification along a sequence of magnetic analyses. From Maher et al. (1999).

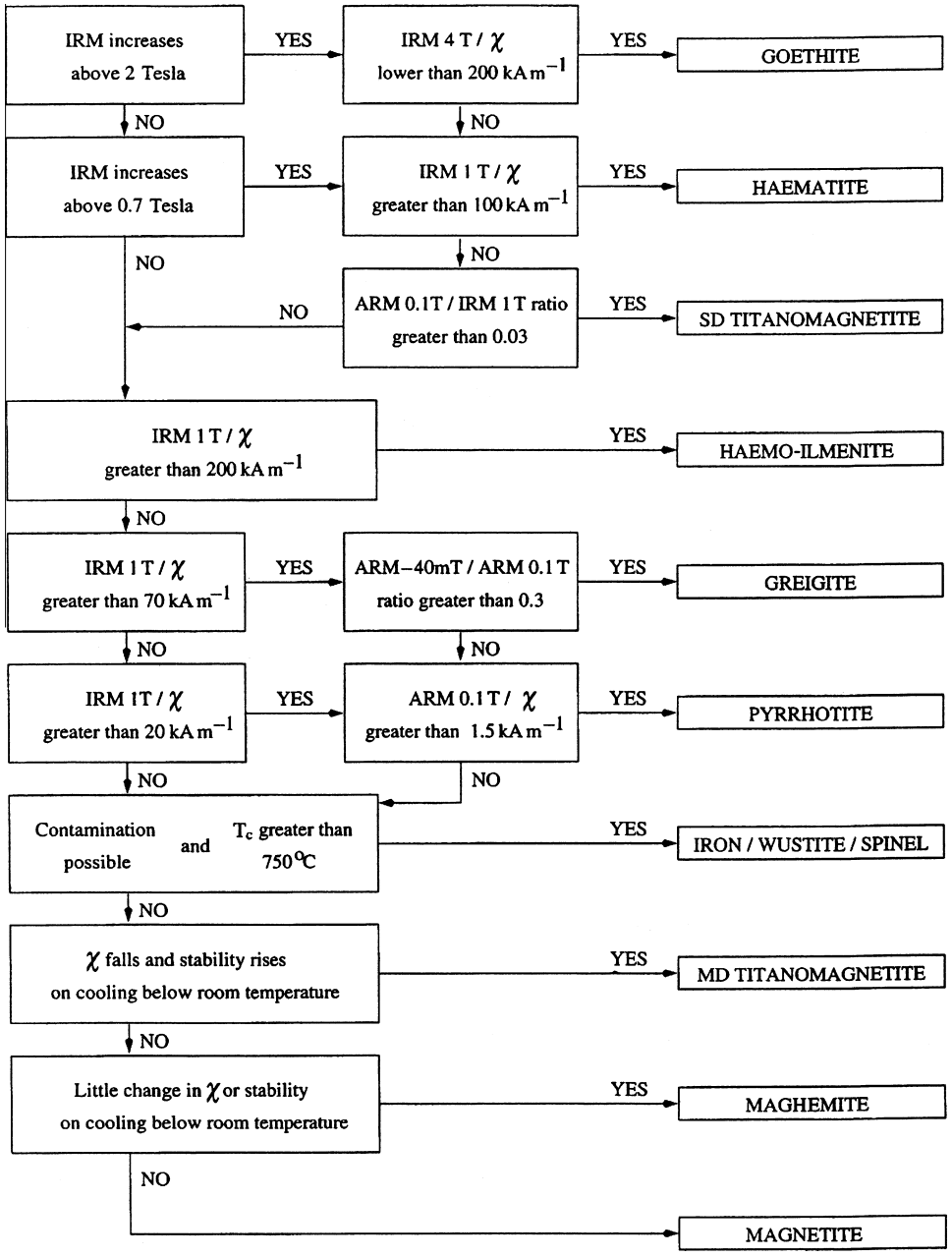


and with a range of grain sizes). Quantification and 'unmixing' of sample magnetic components can be achieved using a range of statistical techniques, mostly based on analysis of magnetisation curves. For example, Thompson (1986) used 'Simplex'-type optimisation to un-mix observations against model data. Subsequently, Egli (2004a,b,c) and Heslop et al. (2002a) and Heslop and Dillon (2007) have developed additional unmixing methods, whether against model functions or by mathematical decomposition without *a priori* knowledge of constituent minerals or domain states.

Measurement and analysis of first-order reversal curves (FORCs) provide an additional tool for identifying fine-grained magnetic minerals, their domain state and degree of interaction (Pike et al., 1999, 2001; Roberts et al., 2006). FORCs, descending partial hysteresis curves, require thousands of data points to produce magnetisation contours, providing in particular a more precise measure of particle magnetic interactions. Whilst FORC measurements can be made automatically (e.g. using the software controlling the Micromag vibrating sample magnetometer and the alternating gradient magnetometer), they are time-consuming, and thus will often be used to 'calibrate' more routine magnetic characterisation of large numbers of samples (Egli et al., 2010). A new raft of processing algorithms is being developed as application of FORCs to different environmental samples gathers pace (e.g. Harrison and Feinberg, 2008).

Sample affinities and provenance can also be examined statistically, in multidimensional, multi-magnetic parameter space, e.g. using cluster analysis of discriminatory (non-auto-correlated) magnetic properties of the sediment sample and of potential source materials. For example, fuzzy cluster analysis has been used in a range of environmental magnetic studies (e.g. Hanesch et al.,

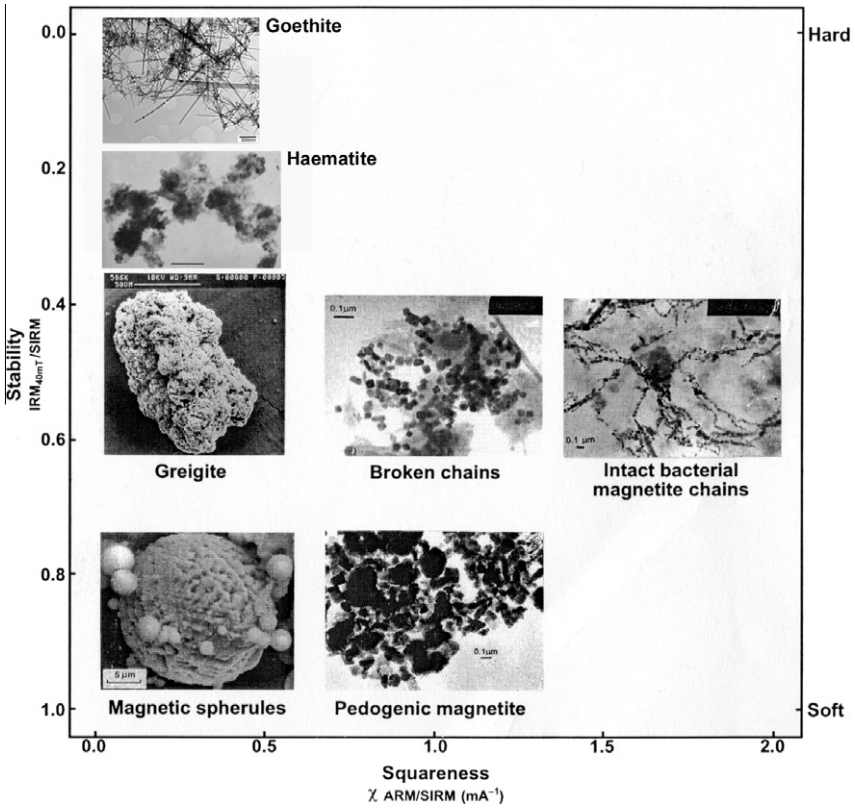


**Fig. 5.** Magnetic discrimination between seven examples of different magnetic minerals and grain sizes on a biplot of magnetic stability vs squareness. (Redrawn from Maher et al., 1999.)

2001; Watkins and Maher, 2003; Watkins et al., 2007; Hatfield and Maher, 2009). Clustering seeks to classify or group discrete but diverse sample magnetic properties without any a priori knowledge about any of the samples (e.g. geographic or temporal location). The 'fuzziness' of the analysis enables estimation of the degree of affinity of any one sample to all other clusters, rather than categorical assignment of the sample to one individual cluster (Minasny and McBratney, 2002). The optimal solution provides cluster statistics including centroids and a quantitative affinity of each sample to its own cluster, but also to all other clusters, ranging between zero (no affinity) and one (identical). This fuzziness is appropriate in many environmental contexts, where samples are likely to consist of mixtures of source materials. The possibility of spurious matches can be reduced by prior evaluation of sample magnetic properties by Spearman's Rank, for example, to ensure they show no auto-correlation.

## 3. Magnetic minerals in aeolian dusts and sediments

### 3.1. Introduction: dust mineralogy

Mineral dusts typically consist of a mixture of mineral species (and particle morphologies), often including quartz, clay minerals, calcium carbonate (Claquin et al., 1999), and a range of magnetically-ordered iron oxides and/or oxyhydroxides. The fraction of iron which is present within the iron oxides and oxyhydroxides is sometimes referred to as the 'free iron' (as opposed to structural iron, occurring as substituting ions within the aluminosilicates). This 'free iron' is responsible for absorption of light (e.g. Lafon et al., 2006). The mineralogy, concentration and grain size of the iron oxides and oxyhydroxides contained in atmospheric dusts are controlled primarily by the source soil mineralogy and water regime (Schwertmann and Taylor, 1987). Upon subsequent deflation from the ground surface, grain size changes (aggregation and/or disaggregation) can occur as a result of the erosional processes, such as 'sandblasting', i.e. impact-induced emission of finer dust grains from larger particles or aggregates (e.g. Grini and Zender, 2004). Finally, dust composition and particle size can change during transport, for example, by agglomeration with organic carbon or salt particles (e.g. Zhang and Iwasaka, 2004; Worobiec et al., 2007), and/or dissolution/re-precipitation reactions during cloud processing (Shi et al., 2009a,b).

Some dusts may be magnetically distinctive by dint of containing very little ferromagnetic material. For instance, the largest single dust source at the present day, the Bodélé depression, Chad, is reported to emit dust dominantly composed of diatomite (a siliceous, and thus diamagnetic, material), from erosion of Late Pleistocene and Holocene lake bed deposits of the palaeo-Lake Chad (Bristow et al., 2009). However, magnetic measurements (Maher, in prep.) show that even dust from this particular source contains abundant concentrations of the soil iron minerals, haematite ($\alpha Fe_2O_3$, i.e. the most oxidised of the iron minerals) and the iron oxyhydroxide, goethite ($\gamma$FeOOH).

Indeed, haematite and goethite occur on a global scale as trace to minor soil components (i.e. $\ll\sim$5% by mass), as a result of oxidative and hydrolytic weathering of $Fe^{2+}$-containing primary (lithogenic) minerals at the near-surface. As discussed below, these volumetrically-dominant minerals display distinctive magnetic properties, being magnetically both very weak and hard (i.e. difficult to magnetise and subsequently demagnetise). In contrast, the much more strongly magnetic minerals, magnetite and maghemite, occur at much lower concentrations in natural mineral dusts, but these trace minerals can readily indicate changes in dust mineralogy, source and depositional fate.

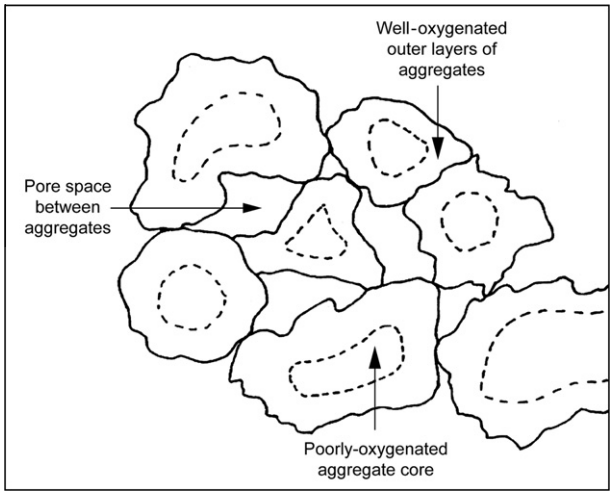


**Fig. 6.** Micro-environmental variations in redox environment in the soil ped and pore environment. From Maher (1984).

### 3.2. Haematite and goethite

#### 3.2.1. Introduction

Although the soil *micro*-environment (Fig. 6) controls finally the oxidation status of soil-formed iron minerals, haematite is prevalent in warmer and drier climatic regions; modern dusts from the arid and semi-arid zone (Claquin et al., 1999) contain measured haematite contents of ~0.6–3.4% (by volume). Goethite has a much larger geographic range than haematite; it may occur in (volumetrically) larger amounts even in soils and dusts visibly reddened by the presence of pedogenic, highly pigmenting, nano-scale haematite. The smaller the crystal size of haematite, the more saturated is its red colouration (Pailhe et al., 2008); caution is thus required when attempting to establish relationships between soil redness and haematite concentration (e.g. Torrent et al., 1983). Based on diffuse reflectance spectroscopy (DRS), goethite has been reported to be the dominant species (i.e. ~wt% 2–3 × higher than haematite) in reddened dust source (soil) samples from Niger and Tunisia (Lafon et al., 2004, 2006), and in the loess and palaeosols of the famous Chinese Loess Plateau (Ji et al., 2004; Balsam et al., 2004). Goethite (and magnetite and/or maghemite) is also suggested to occur in the red 'soils' of the Martian surface, again, critically, indicative of *hydrolytic* weathering processes (Morris et al., 2000).

The distinctive, hard magnetic properties of haematite and goethite (Section 3.4) provide a key tracer for modern and palaeofluxes of dusts emitted from the arid zone, especially from North Africa, the largest source of dust in the world (see Section 5.1.1).

#### 3.2.2. Haematite and goethite grain size: transport, radiative and biogeochemical effects

Haematite and goethite most commonly occur as discrete nanoscale particles (Fig. 7a–f), often associated with fine mineral fractions (≪10 μm, i.e. fine silt and clay-sized, e.g. Fig. 7c). They can also exist as surface coatings on larger particles, and as much larger, diagenetic overgrowths and/or replacements of original iron-bearing mineral grains (Fig. 5d).

Nanoscale iron mineral particles can achieve long atmospheric residence times (i.e. days) and long distance transport paths (>1000 km). Further, cloud processing reactions, involving large alternations in pH (~pH 2 to ~5–6) during transport, may generate neo-formed iron oxide nanoparticles from aeolian haematite and goethite particles, via dissolution and re-precipitation reactions (Shi et al., 2009a). These in-transport *chemical* mechanisms for nanoparticle neo-formation may account for the enhanced iron solubility of long range transport (LRT) dusts, observed in areas remote from major dust sources and associated with low dust concentrations (Baker et al., 2006; Shi et al., 2009b; Baker and Croot, 2010). It should be noted that such nanoscale particle fining will neither be identifiable nor measurable using conventional particle size distribution analysis of LRT dusts. (Conventional analyses indicate that the mode particle size of LRT dusts stabilises at ~2–3 μm (Maring et al., 2003.)

The nanoscale dimensions of these primary and neoformed iron mineral grains may be of key importance regarding dust interactions with the ocean biogeochemical cycle, via the transport of iron and other potentially limiting mineral species (e.g. Si) to high nutrient-low chlorophyll (HNLC) regions of the world ocean (e.g. Martin, 1990; Moore and Braucher, 2008; Boyd et al., 2010). Such particles have very high surface areas and potentially high reactivity, and may thus represent a bio-available form of iron for presently iron-limited marine organisms (Baker and Croot, 2010). The additional possible influence on iron mobilisation of organic ligands, and of surface adsorption and/or desorption of organic material, either during atmospheric dust transport and/or after ocean deposition, remains to be determined (Barbeau et al., 2001).

Even in minor concentrations, haematite and goethite can exert a disproportionate radiative effect. They display high absorptivity at shorter wavelengths (Sokolik and Toon, 1999; Balkanski et al., 2007), an effect maximised given the typically sub-micrometre grain size of these soil-sourced minerals, and the evenness of their distribution both in the source soil matrix, and in the dusts emitted from them. The atmospheric warming, and surface cooling, which result from dust absorptivity can occur on local or regional scales, especially over bright surfaces (e.g. Miller et al., 2004a, 2004b; Zhu et al., 2007; Balkanski et al., 2007). In turn, this can lead to other possible atmospheric dynamical effects, influencing, for example, monsoonal moisture transport and delivery (e.g. Lau et al., 2006; Huang et al., 2009) and surface albedo (e.g. Krinner et al., 2006).

.

#### 3.2.3. Magnetic properties of haematite and goethite

Because their magnetisations arise from crystal asymmetries, reflecting structural defects and/or substitutions (especially, in the soil environment, of aluminium), the magnetic behaviour of haematite and goethite can be variable (Dekkers, 1989; Liu et al., 2002; Maher et al., 2004; Rochette et al., 2005; Liu et al., 2006a). In general terms, their magnetic characteristics are similar (Table 1) in that both are magnetically weak and 'hard', that is, large magnetic fields (e.g. >300 mT up to ~10 T) are required both to magnetise and subsequently demagnetise them. They characteristically display rather low magnetic susceptibility (~60–70 × $10^{-8}$ $m^3$ $kg^{-1}$) and saturation remanence (SIRM, ~0.05 A $m^2$ $kg^{-1}$ for goethite, ~0.25 A $m^2$ $kg^{-1}$ for haematite), and high ratios of saturation remanence to susceptibility (SIRM/$\chi$ ~70 kA $m^{-1}$ for goethite, 400 kA $m^{-1}$ for haematite). More detailed magnetic and granulometric discrimination can be obtained for these minerals, even within the field range 100 mT–1 T, but also by using higher field and low temperature measurements (see Table 2). Measurements of frequency dependent $\chi$ ($\chi_{fd}$) and low temp (e.g. 77–300 K), high-field (e.g. >300 mT) remanence indicate the characteristic presence of SP-sized haematite and goethite in soils from the arid zone (Section 4). The fine size of these iron oxide and oxyhydroxide particles is independently attested by their highly pigmenting effect in such soils.

Compared with haematite, goethite is distinctively harder; for example, it acquires most (80–90%) of its isothermal remanent magnetisation (IRM) at applied fields greater than 2 T, whilst haematite acquires ~60–70% of its remanence at fields below 2 T (France and Oldfield, 2000; Maher et al., 2004). In many environmental laboratories, the maximum dc magnetic field which can

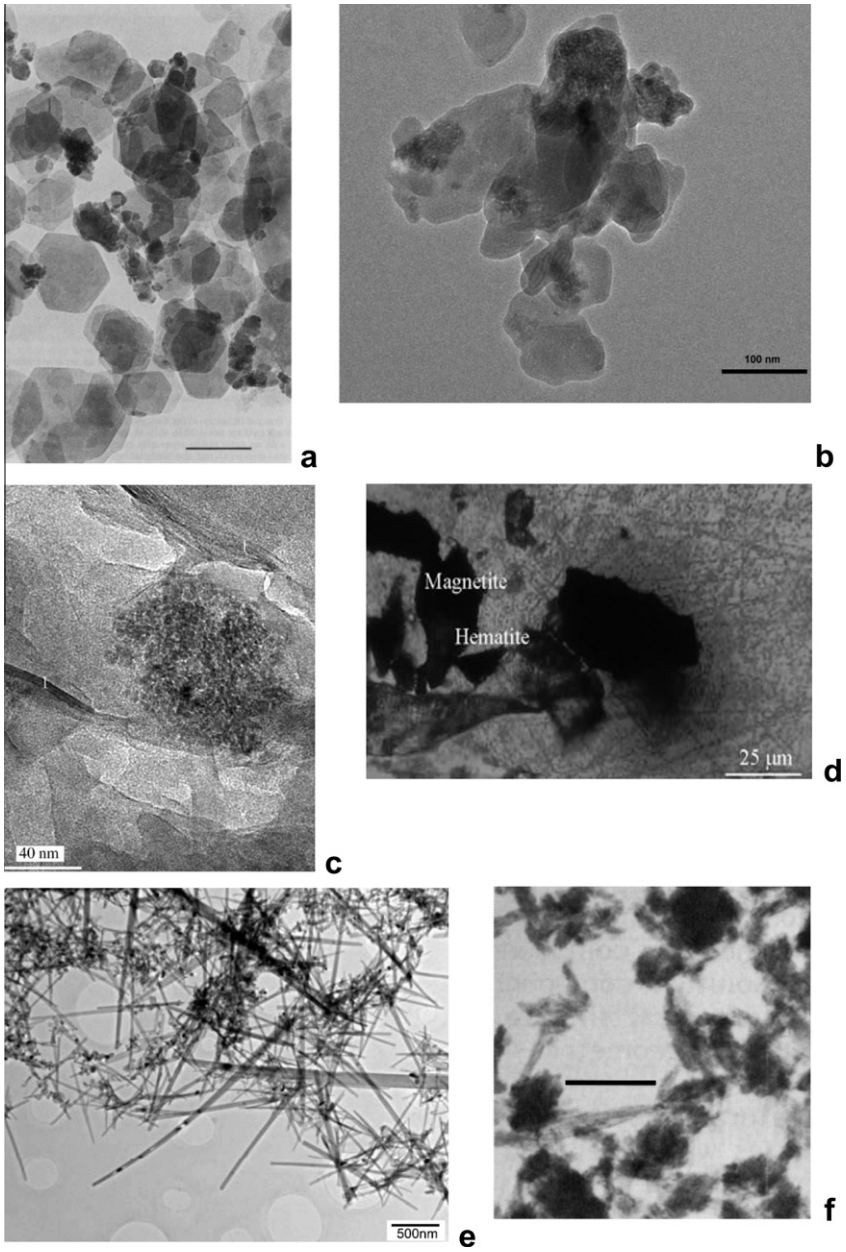


**Fig. 7.** Transmission electron micrographs showing a range of natural examples of haematite and goethite crystals; (a) ~ equidimensional particles of haematite ($\alpha Fe_2O_3$) appear here as the smaller, electron-opaque particles (i.e. essentially unassociated with the larger, clean flakes of kaolinite), scale bar = 1 μm; (b) ultrafine haematite crystallite, soil sample, Morocco, scale bar = 100 nm; (c) pedogenic haematite crystals formed within the interlayer space of a clay mineral, Chinese Loess Plateau; (d) red, oxidised rim of haematite around a lithogenic magnetite grain, Chinese Loess Plateau; (e) typically acicular grains of goethite, from North Atlantic sediments; (f) pedogenic goethites, from an oxisol, New Caledonia, scale bar = 0.1 μm. In order, micrographs from Jones (in Schwertmann, 1988), Lieke (pers. comm.), Chen et al. (2010), Xie et al. (2009a,b), Franke et al. (2007), and Schwertmann (1988).

be grown is ~1 T. Fortunately, the IRM acquisition and demagnetisation behaviour of goethite and haematite is distinctive even within the field range 100 mT–1 T. Whilst each displays acquisition of remanence at room temperature in dc fields beyond 100 and 300 mT, the response of each mineral to af demagnetisation of the resultant 'high-field' remanent magnetisation, 'HIRM', appears diagnostic. Irrespective of their grain size, goethites retain most (~90%) of their 'HIRM' in ac fields of 100 mT; for haematites, the 'HIRM' loss is as much as ~25%. Thus, the mass-normalised, af-demagnetised $HIRM_{0.1 \text{ or } 0.3 \text{ mT–1 T (100 mT af)}}$ may provide the simplest means of estimating the remanence contributed by these high-coercivity minerals.

Where larger dc fields are available, it is also possible to identify changes in goethite and haematite grain size in natural samples, through measurement of their remanence behaviour as the samples are cooled to low temperatures. Upon cooling in zero magnetic field to 77 K, synthetic goethites display large increases in their $HIRM_{2-7\ T}$ values, with the largest increases (+158%) shown by the smallest grain sizes (Fig. 8). In contrast, haematite grains larger than ~100 nm lose much of their remanence upon cooling through a Morin transition at the relatively low temperature of ~240 K, with no apparent dependence on grain size. Their $H_{cool}$ values range from −75% to −95% (Fig. 8). Ultrafine synthetic haematite grains, <~25 nm grain size, do not show the Morin transition in their $HIRM_{7-2\ T}$. Fig. 8 also shows the low-temperature, high-field behaviour of a number of natural goethite- and haematite-rich samples, including goethitic and haematitic soils, together with some redbeds (Triassic and Devonian), and two surface sediment

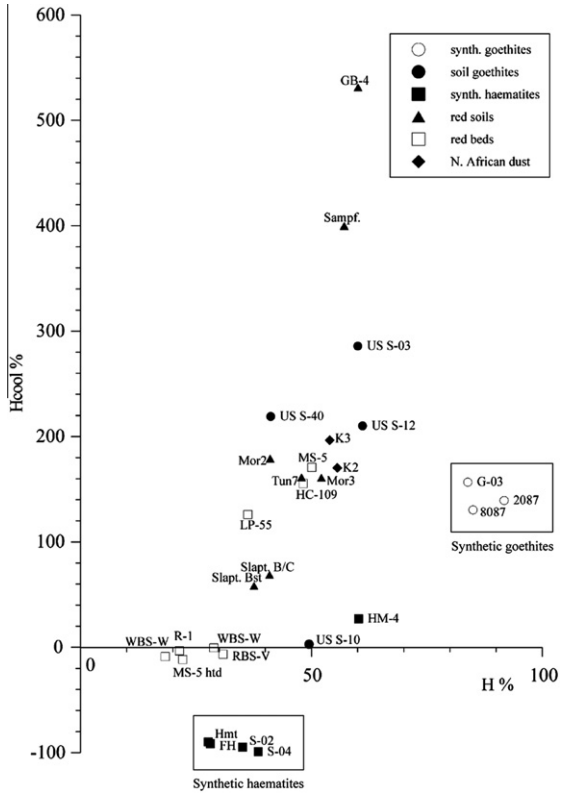


**Fig. 8.** Behaviour of synthetic goethites and haematites of differing grain sizes, and of a range of goethite- and haematite-rich natural samples, when subjected to measurement of their high-field remanence at room temperature, subsequently cooled to 77 K. H% = the proportion of the room temperature remanence acquired in fields from 2 T (T) up to 7 T and $H_{Cool\%}$ indicates the increase or decrease in high-field remanence upon cooling in zero field to 77 K (LT). From Maher et al. (2004).

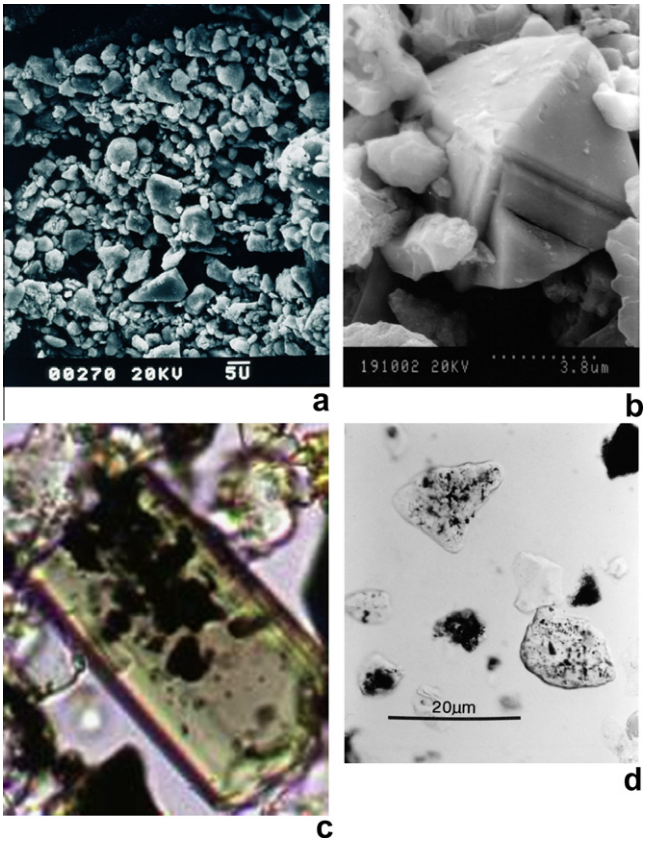


**Fig. 9.** Scanning electron micrographs of lithogenic magnetites, (a) an overview of the large (>∼1 μm), geometric detrital magnetites/maghemites extracted magnetically from a sample of Chinese Loess (L2SS1); (b) euhedral lithogenic magnetite crustal, from the same Chinese loess sample; (c) magnetite (?) inclusions within a tourmaline grain (width of micrograph = 5 μm, image provided by Mark Hounslow); (d) magnetite inclusions within quartz grains, Burdekin River sands.

samples from the North Atlantic, west of the North African dust plume (cores 12310-4, −18.72°W 23.5°N and 12328-4, −18.57°W 21.15°N).

In soils, substitution by aluminium of the octahedral $Fe^{3+}$ in haematite and goethite is common and (especially in goethite) often prolific, reflecting the abundance and similar dimensions of this cation (Norrish and Taylor, 1961). As a general observation, highly-substituted goethites (10–33 mole%) are prevalent in highly weathered, subtropical and tropical soils (e.g. oxisols), whilst lower substitution levels (<∼10 mole%) occur in weakly acid and gleyed soils (e.g. Schwertmann, 1988). However, long-weathered and often polygenetic soils characteristically display varied Al-substitution levels within their profiles, reflecting different stages of Fe mobilisation and precipitation. Al-substitution in haematite appears more limited, with maximum values of 15–18 mole% reported (Schwertmann, 1988).

One effect of increased Al-substitution in goethite is to reduce its crystal size, especially in the *z* direction. At 5 mole% Al substitution, synthetic goethites show ∼50% decrease in crystal length; at 20 mole%, a decrease by 90% (Schwertmann, 1988). Such changes lead to differences in magnetic remanence acquisition and demagnetisation (Liu et al., 2007), thus HIRM measurements must be carefully assessed in terms of possible changes in source mineralogy as well as in haematite or goethite concentrations.

### 3.3. Magnetite/maghemite

In contrast to the weak, hard magnetic minerals, even trace concentrations of the strongly magnetic, cubic spinel minerals, magnetite ($Fe_3O_4$) and maghemite ($\gamma Fe_2O_3$), can dominate the magnetic properties of sampled dusts, aeolian deposits and palaeosols. Magnetite and maghemite form a solid solution series, with gradual changes in the magnetic properties from one end-member composition to the other (Longworth et al., 1979).

#### 3.3.1. Lithogenic magnetite/maghemite

Magnetite/maghemite can occur as primary, lithogenic mineral, formed at high temperatures in the sub-crustal environment, and subsequently released by weathering from source rocks (Fig. 9a and b). Such detrital magnetite grains are often coarse-grained (>∼1 μm) and contain substituting cations (especially titanium) within their crystals lattices. Lithogenic (Ti-) magnetite can be abundant in soils developed on basic igneous lithologies. For example, spontaneous magnetisation is displayed by a significant percentage of subsoils across Brazil – up to 50% of the soil mantle across Parana State (da Silva et al., 2010). Primary magnetite grains also occur frequently as inclusions within host silicate minerals (Hounslow and Maher, 1996), displaying a range of possible morphologies (Fig. 9c and d). Because they are protected from weathering and/or post-depositional diagenesis by their host silicate grain, magnetite inclusions can contribute significantly to the magnetic properties of those sediments where discrete, lithogenic magnetites have been partially or completely removed by diagenesis (see Section 5.1.5).

#### 3.3.2. Low temperature magnetite/maghemite

In addition to these high-temperature forms of magnetite, field and laboratory evidence has demonstrated that magnetite forms

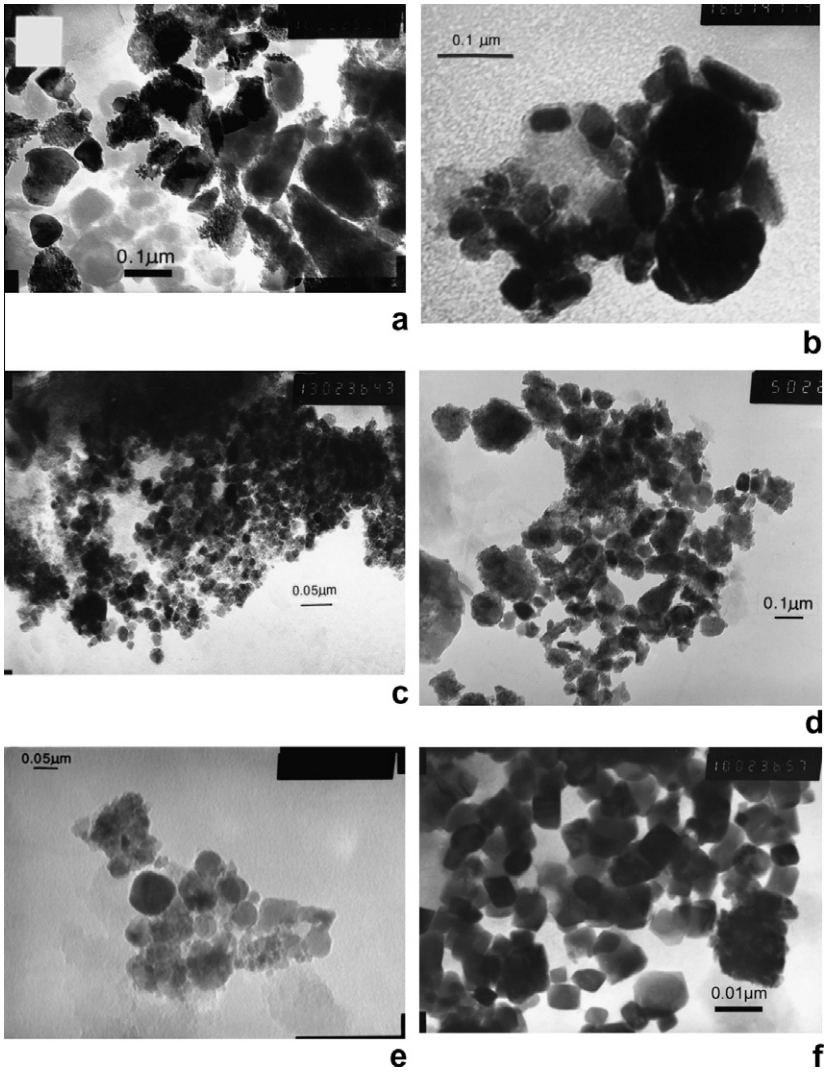


**Fig. 10.** Transmission electron micrographs of typical, well-crystalline, ultrafine-grained pedogenic magnetite (probably at least partly maghemitised), with grain size ranging from ~1 nm to 0.1 μm, magnetically extracted from: (a) palaeosol S1, Chinese Loess Plateau, (b) palaeosol S1, Chinese Loess Plateau (c) Exmoor, UK, cambisol; (d) palaeosol S1, Chinese Loess Plateau; (e) Cotswolds, UK, rendzina; (f) Cotswolds, UK, rendzina.

readily at near-surface temperatures and pressures. Two routes to such near-surface magnetite formation are currently documented: *extracellular* precipitation of magnetite, during pedogenesis, particularly in well-drained and -buffered soils; and *intracellular* precipitation of magnetite by magnetotactic bacteria.

Extracellular, pedogenic magnetite particles (Fig. 10a–f) are distinctively and variably nanosized (characteristically a mix of SP and SD particles) and commonly substitution-free. Notably, they are often Al-free, despite the abundant presence of this similar-sized cation (which can replace Fe in its octahedral position) in the soil environment (Schwertmann, 1988; Norrish and Taylor, 1961). These characteristics reflect the rapid precipitation of these magnetites within soil micro-site environments (e.g. in micropores, Fig. 6, and/or in association with clay–organic complexes), with crystal growth often restricted in the presence of interfering ions and/or organic matter (Taylor et al., 1987).

*In situ*, pedogenic formation of the mixed $Fe^{2+}/Fe^{3+}$ ferrimagnet, magnetite, requires production of some $Fe^{2+}$ within the generally oxic soil environment. Even in well-drained soils, such $Fe^{2+}$ production can occur frequently, during bacterial respiration of organic matter in soil micro-sites, made temporarily anoxic by wetting of the soil by rainfall (Fig. 6). Under such conditions, anaerobes utilise $Fe^{3+}$ species as an electron acceptor (Lovley et al., 1987), thus creating localised concentrations of $Fe^{2+}$. Release of reducing agents by plant roots may also contribute to this solubilisation of otherwise insoluble $Fe^{3+}$ species. As soils dry out after a rainfall event, redox conditions fluctuate across these micro-sites, and partial oxidation leads to precipitation of the mixed $Fe^{2+}/Fe^{3+}$ magnetite (Maher, 1988). Pedogenic magnetite formation is thus linked with the drying phase of a soil wetness event (Le Borgne, 1955). It has been suggested that magnetite precipitation occurs via an intermediate green rust phase (e.g. Lindsay, 1979); laboratory syntheses under analogous conditions indicate rapid transformation (minutes/hours) of any such unstable phase to magnetite (Taylor et al., 1987).

A distinctive feature of pedogenic magnetite in many modern soils and palaeosols is that although it typically displays quite a broad grain size distribution (e.g. in contrast to intracellularly-formed, biologically-controlled magnetite), this distribution demonstrates remarkable *constancy*, within the ultrafine (SP/SD, i.e. <~0.05–0.1 μm grain diameter) size range. In the laboratory, even small adjustments in the formation conditions, of initial Fe concentrations, pH, Eh, and oxidation rate, can lead to marked changes in the grain size distribution of the resultant synthetic magnetite (Taylor et al., 1987). The observed constancy of the grain size distribution of pedogenic magnetite strongly suggests that it precipi-

tates under a specific, repeated set of pH/Eh conditions. In turn, this indicates that pedogenic magnetite forms via the actions of specific Fe-reducing organisms, which 'activate' only at those set pH/Eh conditions. Hence, formation of pedogenic magnetite under this mediating, biological control, results in the observed specific and consistent grain size distribution (Fig. 11). The roles of climate and weathering processes in formation and dissolution of magnetite in soils are discussed in Section 9.5.2.

In contrast to the indirect role of Fe-reducing bacteria in pedogenic magnetite formation, magnetotactic bacteria form magnetite (and other ferrites) directly, actively and intracellularly (Blakemore, 1975). The resultant magnetosomes are similarly nanoscale and substitution-free, but they differ markedly from extracellular, pedogenic ferrites by dint of their unique crystal morphologies and rather narrow grain size distribution (Fig. 12a–c). These properties in turn reflect the controlled environment and dimensions of the *intracellular* environment in which bacterial magnetite particles are precipitated. Bacterial magnetosomes have been found in a wide range of environmental materials, including soils (Fig. 12c), but at population levels too low to account for the measured magnetisations of those soils (Dearing et al., 1996, 2001; Fassbinder et al., 1990).

Another source of nanoscale, biologically-formed magnetite is suggested to be botanical in origin (Gajdardziska-Josifovska et al., 2001). Reflecting their biological source, the magnetite nanocrystals extracted from grass plant cells are constrained in their morphology and grain size, often cubo-octahedral grains as small as 4 nm (i.e. an order of magnitude smaller than bacterial magnetosomes).

Unsurprisingly, given their high surface area, nanoscale magnetite particles readily undergo surface oxidation to maghemite, the degree of oxidation reflecting particle size. The smallest authigenic particles may transform completely to maghemite; slightly larger particles may retain a magnetite core (Maher, 1998). Many soil magnetite particles display a distinctively uneven or 'fluffy' appearance, reflecting the presence of a multitude of SP maghemite grains at and around their surfaces (e.g. see Fig. 10a and d). Largest, lithogenic particles may become oxidised at their surface to haematite (Fig. 7d; van Velzen and Dekkers, 1999; Chen et al., 2010).

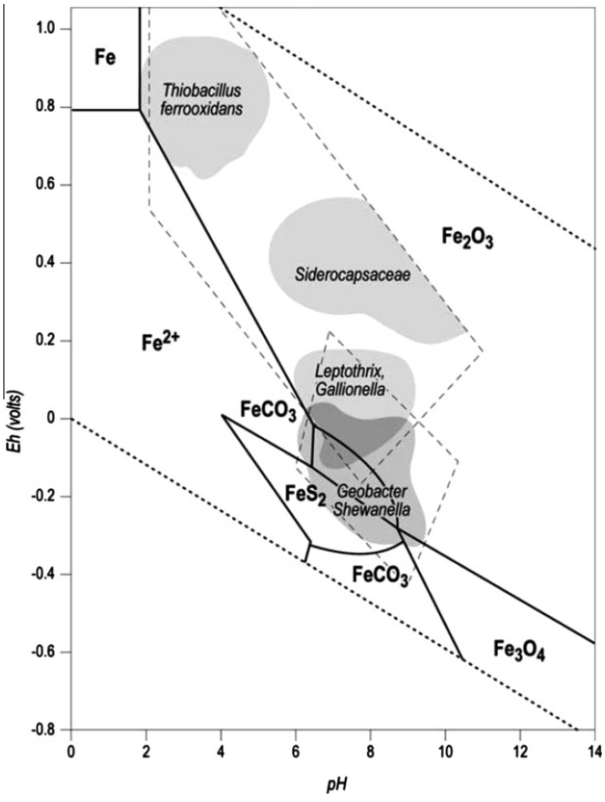


**Fig. 11.** Eh/pH stability fields for iron compounds, together with preferred redox/pH ranges for the major groups of iron-oxidising (e.g. Thiobacillus f., Leptothrix, Gallionella) and iron-reducing bacteria (e.g. Shewanella, Geobacter). After Zavarzina, 2001.

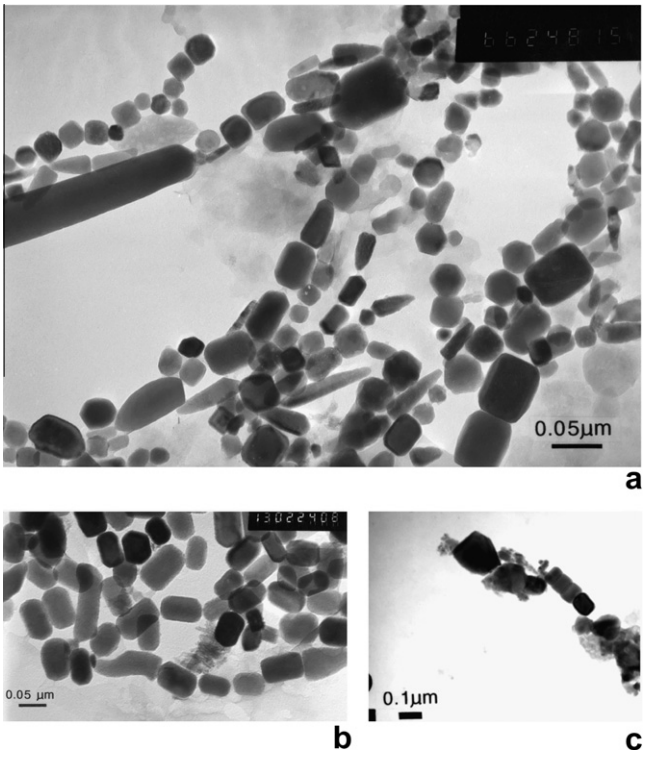


**Fig. 12.** Transmission electron micrographs of intracellular, bacterial magnetosomes, (a) a variety of the unique crystal shapes of bacterial magnetosomes are shown here, from four-sided, to eight-sided and bullet-shaped magnetosomes, and some unusual elongate, blade-shaped crystals (from ODP Site 1006D, the Bahamas); (b) Mostly eight-sided magnetosomes, and some bullet and boot-shaped crystals (from Cretaceous chalk, Culver Cliff, UK); (c) a possible bacterial magnetite chain, from a Chinese palaeosol (S1). Images from Hounslow (a and b) and Maher (c).

### 3.4. Other sedimentary magnetic minerals

Depending on location, and degree of oxidation, sediments can contain a range of additional allocthonous and authigenic magnetic components. Fig. 13a, for example, shows the typical spherule-type morphology of magnetic particles originating as cosmogenic micro-meteorites; volcanic pyroclasts can often adopt the same crystal morphology, and for the same reason, reflecting cooling from molten droplets. In sub-oxic post-depositional sedimentary environments, reductive diagenesis can operate to differing degrees and intensities, resulting in dissolution of detrital magnetic particles (in the order fine-grained ferrites → coarser-grained ferrites → fine-grained goethite and haematite → coarser-grained goethite and haematite), and authigenic formation of iron-bearing sulphides (Fig. 13b). Iron-reducing bacteria can also, under anoxic conditions, form bacterial magnetosomes composed of the ferrimagnetic iron sulphide, greigite (Stanjek et al., 1994).

The possibility of post-depositional diagenetic activity has always to be borne in mind when using sedimentary magnetic archives for palaeoclimatic and palaeo-environmental reconstruction.

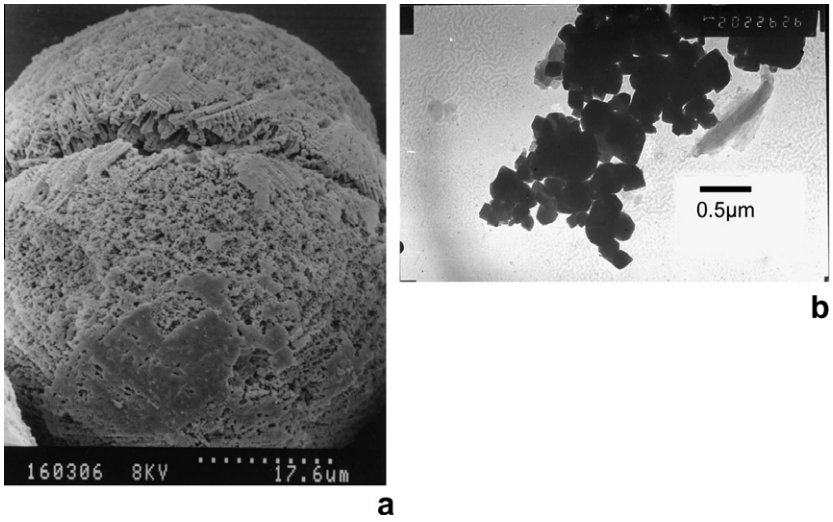


**Fig. 13.** Electron micrographs of (a) a magnetic micro-meteorite, extracted from the Chinese loess (SEM); (b) magnetic sulphide (greigite?) crystals, with typical rhomb-shaped grain outlines and grain sizes of 0.1–0.7 μm (TEM, width of micrograph = 4.5 μm), extracted from a Pleistocene estuarine sediment, East Anglia. Images from Maher.

To maximise accuracy and understanding of magnetic mineral grains and their specific origins, detailed magnetic characterisation (of at least a representative subset of samples) is desirable, together with complementary, independent mineralogical analyses. The latter might usefully include electron microscopy, to reveal diagnostic grain morphologies and compositions. If magnetic extractions are used in order to obtain magnetic concentrates from natural samples, the efficiency of the extraction process should be examined, to ensure that the extracts are representative of the initial sample (Hounslow and Maher, 1996, 1999).

## 4. Magnetic data for modern dusts

In comparison with studies of palaeo-dusts, magnetic analyses of modern dust samples are so far relatively rare, and certainly no examples exist of any long-term magnetic monitoring of natural dusts. Until now, mineral analysis of dusts has dominantly been attempted using X-ray diffraction (XRD), which is both phase-sensitive (rather than element-sensitive) and non-destructive. However, the limits of resolution of XRD (>∼1%) often preclude identification and quantification of iron oxide minerals, given their low concentrations in many soils and dusts. Magnetic analyses of dusts have the potential to provide phase-sensitive data to much lower levels of detection.

The current scarcity of magnetic analyses of modern dusts probably reflects two inertial factors: first, that dust sample masses are often both extremely low, and conventionally consumed by sample-destructive analyses (e.g. ICP-MS); and second, that some blank filter materials are variably magnetically contaminated (especially quartz fibre filters), and thus unsuitable for the trace-sensitivity of magnetic analyses. However, as magnetic instrumentation has developed, with sensitive superconducting quantum interference device (SQUID) magnetometers more widely available to environmental laboratories, low sample mass is increasingly less of an issue. For example, SQUID magnetometry can provide direct magnetisation data on polar ice samples, at much greater temporal resolution than isotopic analyses (see Section 7.1 and Lanci et al., 2004). With regard to filter materials, PTFE ('Teflon') filters, now widely used in modern dust sampling, are essentially magnetically 'clean'. Given that magnetic analyses are non-destructive, it is also possible that filters can be magnetically characterised prior to other types of analysis (with a key proviso that filters often need to be folded in order to be immobilized within suitable non-magnetic sample holders). Magnetic analyses of dusts can provide a sensitive, cost-effective and independent means of constraining dust provenance, either in addition to or in place of more costly means of analysis (e.g. strontium and neodymium isotopic analyses).

Arguably, John Murray was the first to examine magnetic particles from the atmosphere, reporting in 1876 his discovery of magnetic spherules (of cosmic origin) in marine red clays. More than a century later, Oldfield et al. (1985) reported that dust samples from a wide geographic range (including the Mediterranean, the North Atlantic, Barbados, and the Sea of Japan) could be magnetically differentiated, and attributed, at least qualitatively, to source. For the Barbadian samples, for example, 'summer' dusts – dominantly red-brown, Saharan/Sahelian-sourced – were magnetically harder (coercivity of ∼42 mT) than the grey, 'winter' dusts, of South American provenance (Oldfield et al., 1985).

These dust data can be compared with modern African soil samples, sampled as potential dust sources from Niger, Morocco and Tunisia (Watkins and Maher, 2003). These soils display distinctive magnetic behaviour; $\chi$ values vary between 2 and $190 \times 10^{-8}$ m$^3$ kg$^{-1}$, but frequency dependent susceptibility ($\chi_{fd}$) is consistently high, between 7% and 11%, and $HIRM_{100\ mT\ ac}$% between 8% and 32%. These HIRM values indicate volumetrically large concentrations of haematite/goethite, whilst the high $\chi_{fd}$% values identify the presence of ultrafine-grained magnetic particles, close to the room temperature SP/SD size boundary. Such fine magnetic particles probably occur as discrete, nanoscale grains (Fig. 7a–c), as well as coatings on other host particles. Soils sampled from north-south transects spanning the strong climatic gradients (hyper-arid to tropical) of Niger and Mali (Lyons et al., 2010) display increasing concentrations both of ultrafine-grained ferrites and defect antiferromagnets with increased rainfall. In Egypt, moving southwards in association with increasingly arid conditions (mean annual precipitation, MAP, < 5 to > 100 mm), the defect antiferromagnets become magnetically harder (reflected in increased coercivity of remanence, ($B_{0\ CR}$, values). These preliminary data identify some potential for magnetic discrimination between different North African dust source regions both at the present day, and for past dust fluxes to the North Atlantic Ocean (see Section 5.1.1).

For the North Pacific, modern dust samples collected along a longitudinal transect of North Pacific dust samples, during spring-

time dust maxima (1986 and 1987) on SEAREX (air–sea exchange programme) and ADIOS (Asian Dust Input to the Oceanic System) cruises, were magnetically analysed by Arnold et al. (1998). Samples were collected during rain-free periods on nylon meshes, positioned forward of any shipboard stack-derived contamination; thus, whilst sample size was reasonably large, atmospheric particulate concentrations could not be determined, and the particle size distribution may have been biased to the coarser fraction.

Air-mass trajectory analysis indicated shifts between rapid, and progressively longer Asian-sourced dust transport to rapid transport from the east, from the Aleutian/Alaskan land masses. These sources proved magnetically distinctive, with fine-grained haematite contributing to the Asian desert-sourced dusts, whilst higher concentrations of low-coercivity (magnetically-soft), multidomain magnetite were associated with the volcanogenic terrains of the eastern sources. Dust grain size and dust concentration showed little relationship, indicative of mixing of high concentrations of the fine-grained Asian dust source with lower concentrations of the coarse-grained eastern aerosol (Arnold et al., 1998).

Dust concentrations and mineralogy also varied with transport time/distance. For the <2 μ fraction, concentrations of dust and quartz, plagioclase and kaolinite decreased, whilst smectite, illite and chlorite concentrations increased, with increased transport time from Asia. Thus, the mineralogy, grain size and concentration of modern North Pacific dusts vary both with source area and transport-dependent fractionation processes.

On land, in addition to the large, international dust sampling campaigns (e.g. ACE-ASIA), atmospheric dust samples have been collected for magnetic analysis at a number of Asian sites, including the Chinese Loess Plateau (see Section 8.2), the city of Beijing (during and after the 2008 Olympic Games) and Korea. For the Loess Plateau, the $\chi$ values of the modern dusts exceed those of the glacial loess, and are seasonally higher in summer (Sun et al., 2003a). Dust fluxes are greatest during spring and early boreal summer.

The influence of human activity on modern dusts is evident in radiative terms; the carbonaceous aerosols that they contain have reduced the global annual average single scattering albedo. Present day dust is estimated to be approximately twice as absorbing as that in preindustrial conditions (Myhre, 2009). Magnetic comparison of Asian dust samples collected from Seoul, Korea (2002–2003) with natural potential source areas (the Asian deserts and the Chinese Loess) reveals significant addition of strongly magnetic, anthropogenic particles through the dust transport path (Kim et al., 2008). Anthropogenic, carbon-bearing magnetic iron oxides were confirmed as the magnetic additive by electron microscopy. Back-trajectories identify the likely magnetic pollution sources are the industrial areas of eastern China and western Korea.

Iron-rich anthropogenic particles may also exert a disproportionate effect upon iron solubility of atmospheric aerosols. Air masses from North America (measured in Bermuda, Sedwick et al., 2007) typically contain low concentrations of iron (~0.5 nmol Fe $m^{-3}$) but with high fractional solubility (19%). This can be compared with the high dust and iron concentrations of North African air masses (~28 nmol Fe $m^{-3}$), but which has much lower solubility (~0.5%). Close to the East Asian landmass, the modelled contribution of anthropogenic iron to total iron flux to the North Pacific is as high as ~30% (Luo et al., 2008). Magnetic

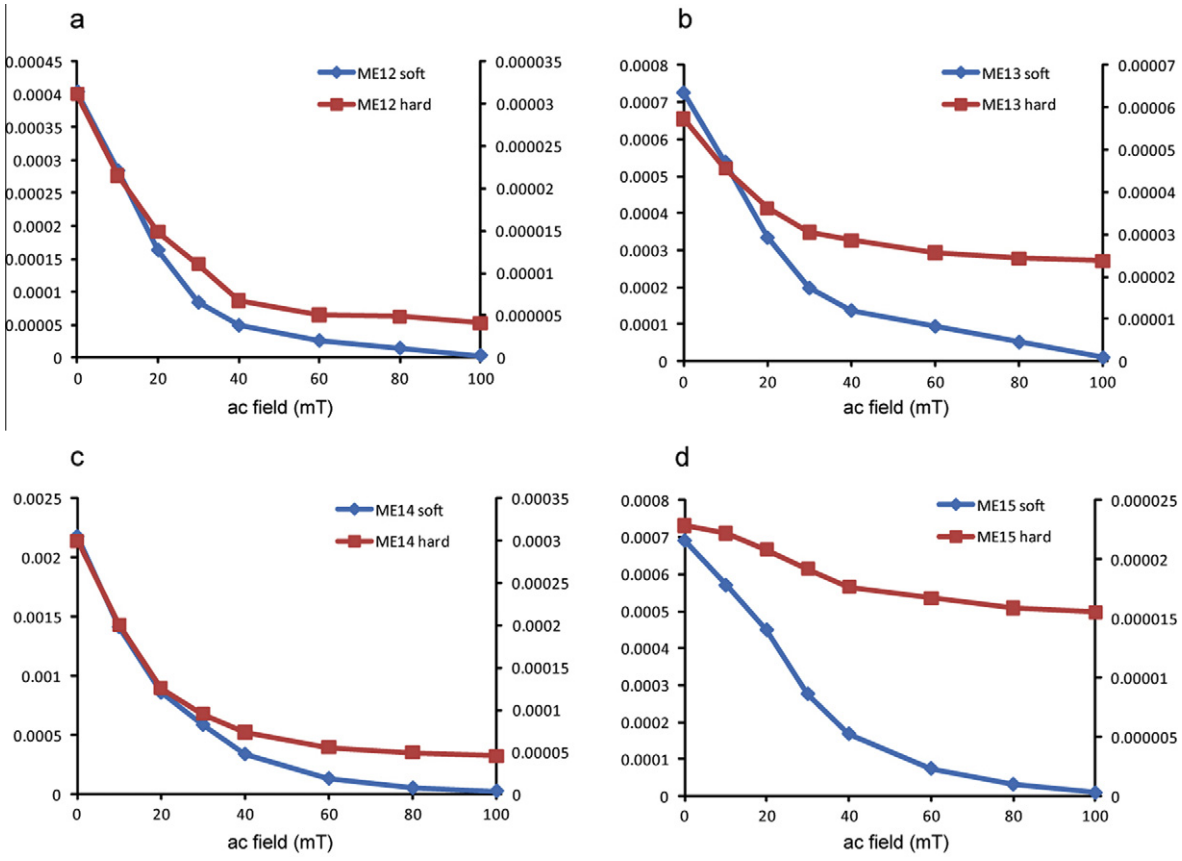


**Fig. 14.** AC demagnetisation behaviour of the soft remanence component (i.e. acquired in an applied dc field of 100 mT, $IRM_{100\ mT}$) on the left hand axis (diamonds) and the hard remanence component (i.e. acquired at applied dc fields of between 300 and 1000 mT, $IRM_{1\ T-300\ mT}$) on the right hand axis (squares), for dusts sampled in (a) northern, (b) central, (c) coastal and (d) southern Kuwait. For each *y* axis the units are IRM ($A\ m^2\ kg^{-1}$).

analyses of modern dusts can play an important role in both identifying dust sources and fluxes, and assessing temporal and spatial changes in flux in response to national and international mitigation strategies.

Compared with XRD, the sensitivity of dust/soil magnetic mineral analyses can be demonstrated with reference to a suite of modern surface soil and dust samples collected (during 2006) from sites across Kuwait (north, central, southern and coastal, Engelbrecht et al., 2009a, 2009b). From XRD of the local surface soils, all four of the Kuwaiti sites displayed similar mineralogies, comprising large amounts of quartz (between 27% and 54%, more than in adjacent Iraq), plagioclase feldspar (~21%), calcite (~10–20%) smaller amounts of clay minerals (palygorskite, illite-montmorillonite, and smaller amounts of kaolinite), and little, if any, dolomite. However, magnetic measurements of dust samples (collected on Nuclepore filters) show that the coastal Kuwait sample is 3–5× more magnetic than the other samples – although its soft demagnetisation behaviour is very similar to that of the N. Kuwait sample. The central and especially the southern sample are distinctive by their 'hard', haematite-like behaviour (Fig. 14b and d). These magnetic differences suggest distinctive variations in iron oxide mineralogy and thus dust source. Most Kuwaiti dust is transported from the Mesopotamian floodplain in southern Iraq (Fig. 15) but also from 'other parts of the Arabian peninsula' (Al-Awadhi, 2005, cited in Engelbrecht et al., 2009a).

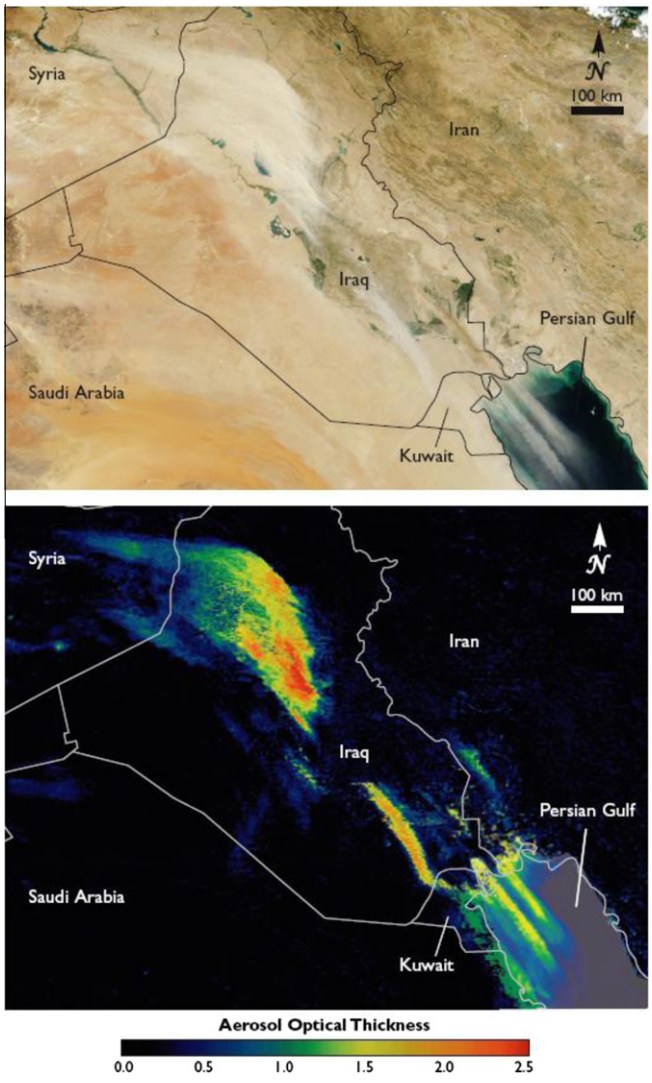


**Fig. 15.** Remotely-sensed images (visible, top, and optical thickness, below, from MODIS) of Middle East dust plumes over Iraq, Syria and Kuwait, on August 7, 2005. From Hsu et al. (2007).

Long range transport (LRT) of aeolian dust can be a key source of nutrients for long-weathered soils, otherwise deficient in micronutrients such as potassium and phosphorus. For example, these and other elements are entrained within boreal winter dust emissions from the Saharan/Sahelian region, lifted in storm events with surface winds stronger than ~14 $ms^{-1}$, and transported over 10 days and ~5000 km across the North Atlantic to the southwest (Ben-Ami et al., 2010). Upon arrival above the impoverished ferralsols of the Amazon Basin, the dust parcels increase atmospheric concentrations of crustal elements by an order of magnitude (Ben-Ami, op. cit.) and effectively replenish soil nutrient pools over timescales of ~500 years to 20 ka (Swap et al., 1992). Similarly, dust sourced from Asia, transported on a hemispheric scale via the westerlies, may contribute significant amounts of phosphorus to old, and heavily leached soils of the Hawaii'an Islands, the most remote archipelago in the world (Chadwick et al., 1999; Kurtz et al., 2001; Porder and Chadwick, 2009).

A number of analytical methods (isotopic, geochemical, mineralogical) exist for identifying and quantifying aeolian inputs to soils. A demonstrated advantage of magnetic methods is their relative speed and cost-effectiveness. This renders them applicable over large-scale arid-land regions, such as the central Colorado Plateau (Reynolds et al., 2001, 2006, 2010). The soils of this vast area, mostly developed on sandstone substrates, contain up to 40% fine (silt and clay-sized) particles. Moreover, they contain lithogenic Ti-magnetite grains, absent from the parent sandstones. The source both of the magnetite grains and the silt and finer particles is aeolian dust. Thus, the dust concentration ($dust_f$) can readily be estimated using magnetic measurements of magnetite concentration for the parent rock (here, the $IRM_{300\ mT}$ was used), the sampled surficial deposits/soil and modern dust (Reynolds et al., 2006):

$$dust_f = (IRM_{300\ mT}\ soil - IRM_{300\ mT}\ rock)/(IRM_{300\ mT}\ dust - IRM_{300\ mT}\ rock)$$

Whilst it has not yet been possible to magnetically discriminate active and past sources of dust for the Colorado Plateau, a likely source of magnetite-bearing dust is the Mojave Desert, from where dust has been observed reaching the Colorado Plateau during large wind events (Reynolds et al., 2006). The significance of the dust for the ecosystems and land management of this upland region is reflected in its contributions to the available nutrient pool (Fig. 16); dust contribution to soil phosphorus, for example, exceeds 40% (Reynolds et al., 2006).

Such links between dust transport and ecosystems extend, of course, to the marine realm. In the southern hemisphere, for example, aeolian transport of continental dust to the iron-deficient waters of the Southern Ocean may be significant both presently and for the past, with direct influence on ocean biogeochemistry and primary productivity. Recent observations show the importance of natural phytoplankton blooms in the Southern Ocean for drawdown of atmospheric $CO_2$. One observed natural event was prolonged (November 2004 to February 2005), and driven by iron supply not directly from dust but from upwelled bottom waters (Blain et al., 2007; Watson and LeFevre, 1999; Maher and Dennis, 2001). Compared to artificial Southern Ocean iron experiments, the mean $pCO_2$ drawdown associated with this natural event was 2–3× greater, and C sequestration efficiency estimated to be 10× higher (Blain et al., 2007).

Similarly, a dust-driven doubling of biomass in the North Pacific HNLC zone was recorded by Bishop et al. (2002), attributed to dust supplied directly from one dust storm event sourced from the Gobi Desert. These two sets of observations suggest that supply of iron-

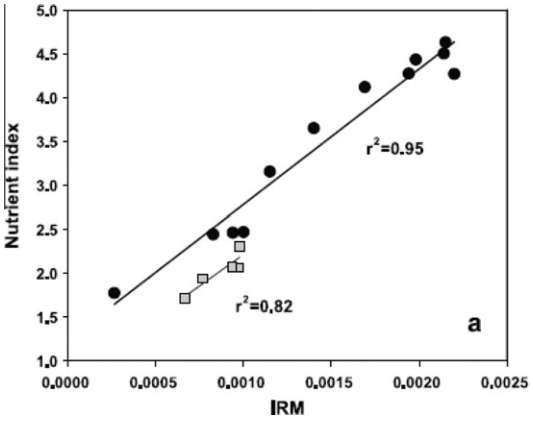


**Fig. 16.** Nutrient index (sum of abundances of K, Na, P, Mn, Zn) vs IRM (A $m^2$ $kg^{-1}$), in soils from the central Colorado Plateau. From Reynolds et al. (2006).

bearing dust to the HNLC ocean regions, whether directly and/or indirectly (i.e. dust deposited elsewhere and subsequently dissolved and transported), can be significant in ocean and atmospheric $CO_2$ changes. The ocean response also appears more sensitive to natural iron inputs compared with artificial iron enrichments. An example of the latter, the SOIREE experiment (Boyd et al., 2010), suggests the existence of a threshold value of iron supply required to produce a photosynthetic response. Only when the dissolved iron concentration doubled (to ~0.2 nM) in the treated Southern Ocean patch did phytoplankton productivity begin to increase. Thus, dust deposition can increase the iron inventory of ocean surface waters without stimulating a phytoplankton bloom (Boyd and Ellwood, 2010). Conversely, irrespective of enhanced dust supply, a bloom can only persist when other essential nutrients (e.g. silica) are also present in non-limiting concentrations. Attempts to identify palaeo-dust fluxes and sources, and their possible links to changes in palaeo-productivity, are discussed here in Section 5.1.4.

A final example of magnetic analysis of modern dusts draws on the volcanic context, with magnetic measurement of the leaves of chestnut trees distributed around the active volcano, Mount Etna, Sicily (Quayle et al., 2010). With the leaves acting as spatially-dense, passive particle collectors, their SIRM and $\chi$ values display strong correlation with the wind-influenced volcanic plume direction for the sample year (2008), with highest magnetic concentrations on the eastern flank of the volcano. These leaf magnetic data broadly agree with elemental analyses of the tree leaves (by ICP-MS). Magnetic granulometry indicates that the leaf magnetic particles are coarse MD (~5–15 μm). This new application suggests that magnetic biomonitoring can provide a new, sensitive and fast means of assessing the dispersion and health impacts of volcanic plumes over wide areas.

## 5. Sediment magnetic properties as palaeo-dust records: the marine record

### 5.1. The North African dust plume and the North Atlantic Ocean

The largest and most persistent source of mineral dust both at the present day, and during past Quaternary climate stages, is the Saharan/Sahelian region (Fig. 17a–c), which presently contributes ~40–60% of global dust emissions (e.g. Prospero, 1996a,1996b; Ginoux et al., 2001). With the exception of iceberg-rafted material, which has been identified in the Atlantic Ocean as far south as 39°N (Watkins and Maher, 2003), North African dust is the sole source of the mineral component of pelagic (abyssal plain) sediments in the central North Atlantic. Changes in dust flux

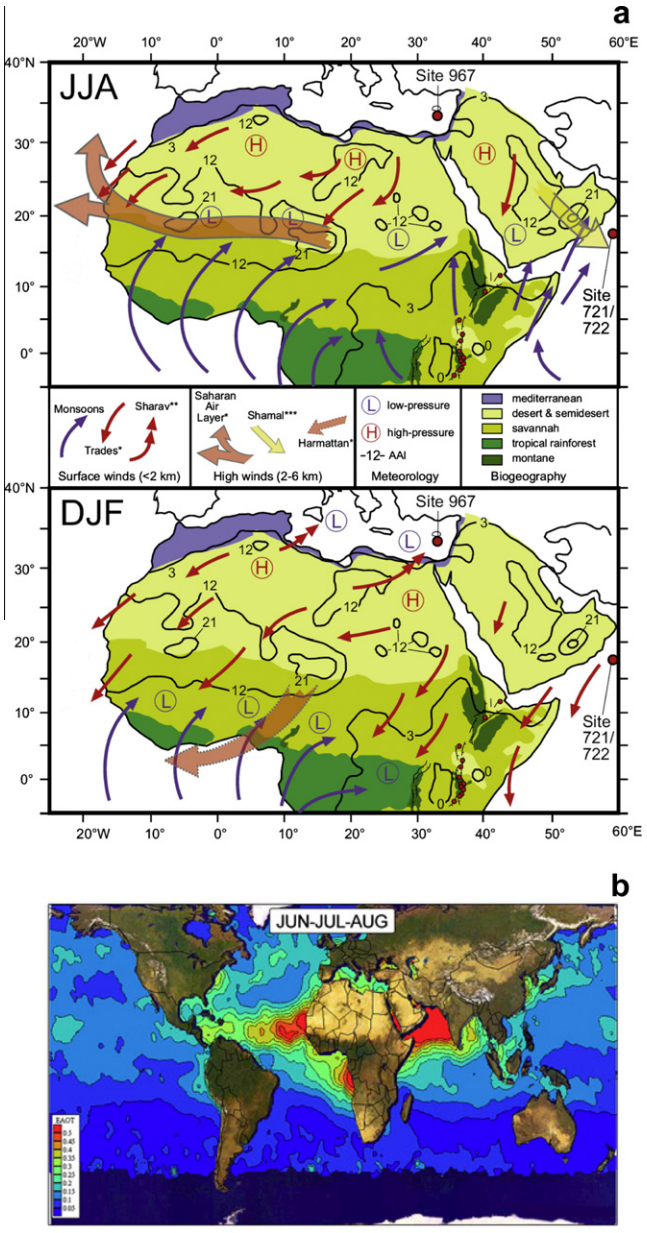


**Fig. 17.** (a) Maps of the N. African continent and Arabian peninsula, showing general patterns of summer (JJA, upper panel) and winter (DJF, lower panel) wind and pressure systems, biogeography (vegetation zones), and the location of 2 of the long (Plio-Pleistocene) magnetic dust proxy records discussed here (ODP sites 967, eastern Mediterranean, and 722, Arabian Sea. Dust-transporting wind systems are indicated by $*$ (over the Atlantic Ocean), $**$ (the Mediterranean, and $***$ the Arabian Sea; height of winds refers to the sea surface over which they blow. Annual aerosol index (AAI) contours indicating the main dust-source areas following Goudie and Middleton (2001). Adapted from Trauth et al. (2009). (b) Remotely-sensed aerosol optical depth measurements (Husar et al., 1997), EAOT = estimated aerosol optical thickness, TOMS = Total Ozone Mapping Satellite. The dust-bearing Saharan air layer (SAL) develops as a deep, well-mixed dry adiabatic layer over the Sahara and Sahel, which is undercut, as it moves westwards from the northwest African coast, by cool and moist low-level air. The Saharan dust plume takes a more southerly track across the Atlantic in the boreal winter (DJF) than in summer (JJA). For example, dust concentrations at Barbados are ~2.5× higher in summer than in winter.

over the observational timescale (i.e. the last few decades) have been related to changes in precipitation over the N. African region, with increased aridity linked to reduced vegetation cover and increased erosion of soils, dry lake beds and ephemeral stream deposits (e.g. Prospero and Nees, 1986; Prospero and Lamb, 2003; Sarnthein et al., 1981; Glaccum and Prospero, 1980; Mulitza

et al., 2010). Changes in the flux, particle size and provenance of North African dust have been identified over Quaternary timescales through examination of the terrigenous component of the North Atlantic pelagic and hemi-pelagic sedimentary record.

Conventionally, sediment samples are pre-treated in order to remove, sequentially, biogenic carbonate, iron oxides/oxyhydroxides and biogenic silica, and thus isolate the aeolian mineral fraction. X-ray diffraction can then be used to identify clay mineralogy and quartz content, coupled with particle size analysis (often via the Coulter principle, i.e. by electrical sensing of impedance changes caused by movement of differently-sized particles through an aperture) to identify size distributions, means and modes. Applying such mineralogical and grain size analyses to eastern tropical Atlantic sediments, for example, the LGM has been characterised as an interval of intensified meridional wind flow, with aeolian dust sourced from lateritic African desert zone soils (e.g. Sarnthein et al., 1981). Other sample-destructive analyses successively developed and applied to Atlantic sediments underlying the N. African dust plume include elemental ratio analysis (e.g. Bergametti et al., 1989), isotopic analysis (especially samarium and neodymium, e.g. Grousset et al., 1988), and analysis of the carbon isotopic composition of plant leaf waxes (as a proxy for $C_3$ and $C_4$ vegetation, e.g. Castaneda et al., 2009).

### *5.1.1. Magnetic records of North African dust flux to the tropical and equatorial North Atlantic*

Whilst non-destructive magnetic measurements (magnetic susceptibility and magnetic remanence) were made on mid-North Atlantic sediment cores as early as the mid-1970s (Freed and Watkins, 1975) – and related to aeolian transport of Azorean volcanic dust – the first detailed magnetic analysis of central North Atlantic sediment cores was carried out by Robinson (1986). The resultant data revealed the sensitivity of sediment magnetic properties to changes in Quaternary palaeoclimate (Fig. 18). The distinctive, nanoscale ferrimagnetic contribution by magnetotactic bacteria is evident during interglacial stages from increased ARM/SIRM ratios. Conversely, the glacial-stage sediments (Marine Isotope Stages (MIS) 2, 4 and 6) display strong peaks in coarser-grained, ferrimagnetic concentrations, reflecting lithic transport by iceberg-rafting, even at this latitude (~42°N). Superimposed on these ferrimagnetic signals, however, is a clear imprint of time-varying aeolian influx, carried by magnetically hard, defect antiferromagnets, particularly here the weakly magnetic iron oxyhydroxide, goethite. During glacial stages, the goethite-derived magnetic signal indicates strong increases in North African dust supply. Variable but diminished aeolian fluxes characterise interglacial stages.

Using Mossbauer analysis, Robinson (op. cit.) independently confirmed the identity and glacial-stage abundance of the high-coercivity mineral, goethite. XRD demonstrates strong association between the peak goethite concentrations and increased kaolinite/illite and kaolinite/chlorite ratios. Given a North African provenance for this aeolian material, and that Robinson's core sites presently lie some ~12°N of the present Saharan plume, these magnetic data strongly suggest a major change in glacial-stage wind trajectories. At least episodically, south-easterly, Harmattan-type winds must have been more intense, whilst the north-east trade winds were reduced in intensity compared with the present day.

Extending the spatial range of these North Atlantic magnetic studies, Bloemendal et al. (1988) examined sub-equatorial Atlantic sediment cores, from the Senegal continental slope and Sierra Leone Rise. Magnetic susceptibility measurements were used for core correlation and chronology transfer for 11 cores. Echoing Robinson's (1986) findings, glacial-age sediments are characterised by increased proportions of high-coercivity minerals and coarser magnetic grain size. In the temporal domain, variances in HIRM and $\chi$ were found to be concentrated at 120-kyr, with smaller spectral peaks at 42- and 23-kyr. In the spatial domain, the magnetic data indicate a range of sediment and magnetic sources. The proximal, Senegal continental slope sediments display a mixture of fluvial and aeolian sediment supply (and an additional *in situ* bacterial magnetite component), whilst the more distal Sierra Leone Rise sites appear dominated by aeolian magnetic influx (Bloemendal et al., 1988).

These high-resolution sediments of the Senegalese continental margin have recently been re-visited, with detailed magnetic and multi-proxy analysis of aeolian flux variations and drivers, at sub-millennial timescales over the last interglacial–glacial cycle, 0–130 ka BP (Itambi et al., 2009, 2010). Glacial and stadial stages are characterised by episodes of aeolian flux both of ferrimagnets (Fe-oxides and Fe–Ti oxides), and of goethite and haematite (Fig. 19), reflecting both stronger winds and drier source conditions, respectively. Increases in $\chi$ are strongly linked with increased redness of the sediments (Fig. 20). The presence of SP-

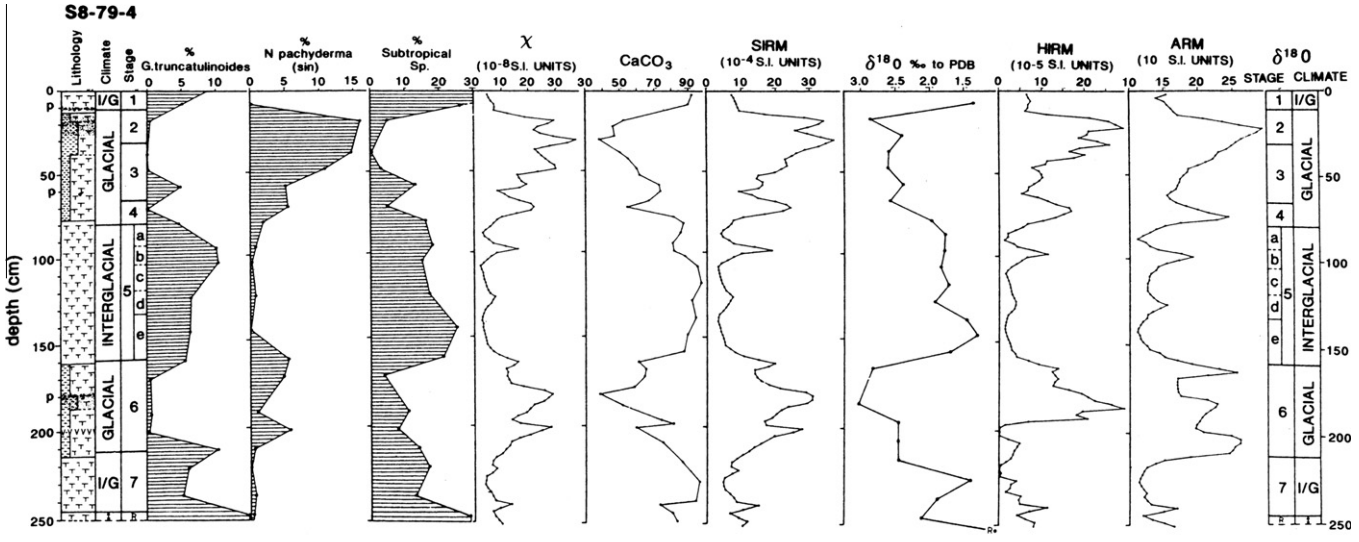


**Fig. 18.** The magnetic properties of core S8-79-4, and its late Pleistocene record of $\delta^{18}O$, carbonate content and planktic foraminifera. (From Robinson, 1986.)

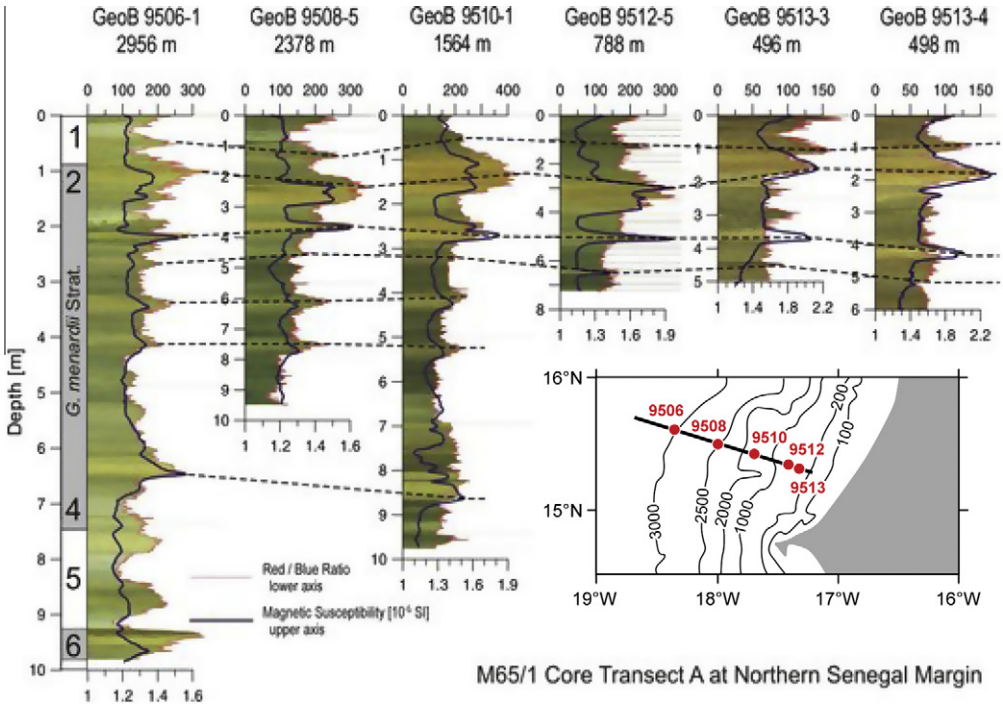


**Fig. 19.** Magnetic data for the late Pleistocene record of core GeoB 9516-5 off the Senegal coast, at 3500 m water depth (from Itambi et al., 2010). Sharp increases in magnetic susceptibility and in HIRM indicate enhanced aeolian influx of ferrimagnets and of haematite/goethite, respectively.

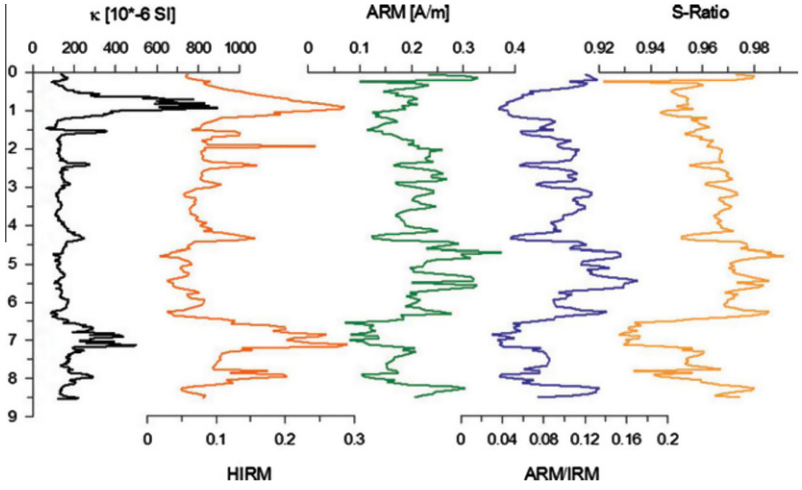


**Fig. 20.** The association between $\chi$ and sediment redness, Senegalese continental margin cores (Itambi et al., 2009).

sized haematite was also identified for glacial-stage sediments, in accord with the magnetic properties of potential source soils (Watkins and Maher, 2003; Lyons et al., 2010).

Additional, but magnetically insignificant, mineral components in these sediments include cosmogenic and volcanic spherules. During the higher-flux, glacial intervals, there is little evidence of diagenetic modification of the magnetic mineral assemblages. Conversely, interglacial sediments appear to have undergone significant reductive diagenesis, with resultant authigenic formation of pyrite.

A latitudinal transect of cores (Fig. 20) revealed dominance of aeolian flux north of 13°N, with periods of Sahelian drought pulsing in association with North Atlantic Heinrich events. Further south (~12°N), terrigenous flux has been fluvially-dominated, driven by the West African monsoon and co-varying with Dansgaard–Oeschger cycles. This study thus locates the glacial-stage position of the inter-tropical convergence zone (ITCZ) at between 12.26°N and 13.4°N, and indicates stronger association of drought phases with reduced Atlantic meridional overturning circulation rather than with southward shifts in the ITCZ (Mulitza et al., 2008; Itambi et al., 2009).

For the western sector of the central North Atlantic, the influence of African-sourced dust has been magnetically identified for sediments from the Ceará Rise (Bleil and von Dobeneck, 2004). Once again, the sediment magnetic properties are strongly modulated by climatically-controlled fluctuations in continental terrigenous flux and biogenic carbonate flux. Exhibiting strong coherence with precessional orbital forcing, the $\chi$ record could be used both to establish a high-resolution age model for the sediments, and, together with other measurements (especially HIRM), to identify the

mineralogy and contribution of African aeolian fluxes and South American fluvial fluxes. As for previous studies, the high proportion of haematite/goethite in the African dust distinguishes the Saharan/Sahelian aeolian material from the fluvial, Amazonian flux. Prominent maxima in aeolian supply to the core sites occurred during cold intervals of glacial stages. On average, over the last 200 kyr, 79% of the terrigenous material at the Ceará Rise has originated from the Amazonian hinterland, and 21% from North African dust flux.

The relative speed of magnetic analyses makes it possible to apply magnetic methods even at the whole-ocean scale. This approach was pioneered by Robinson (Robinson et al., 1995), with regard to iceberg-rafting and North Atlantic Ocean circulation at the LGM. Schmidt et al. (1999) examined Holocene sediment provenance across the South Atlantic (to ~40°S), newly combining sediment magnetic analyses with fuzzy cluster analysis to build an ocean-wide sediment classification tracing the major aeolian and fluvial fluxes, magnetite authigenesis, and effects of bottom water transport. Building upon these earlier studies, Watkins and Maher (2003) applied a room temperature suite of magnetic measurements (susceptibility, frequency dependent susceptibility, isothermal and anhysteretic remanence acquisition and demagnetisation) to 321 present day (surface) and 154 last glacial maximum (LGM) sediment samples from the North Atlantic. The resulting regional variations of sediment magnetic properties enable tracking of different particle fluxes, and their depositional areas, for both time slices. The spatial extent of deposition from the N. African dust plume is clearly identifiable, from its high and statistically distinctive values of both HIRM and $\chi_{fd}$ (Fig. 21a and b). Whilst the SP-sized particles contributing the high measured $\chi_{fd}$ values have been attributed to haematite occurring as surface grain coatings (e.g. Itambi et al., 2009), a significant contribution from discrete, nanoscale particles is probable (Fig. 7a–c).

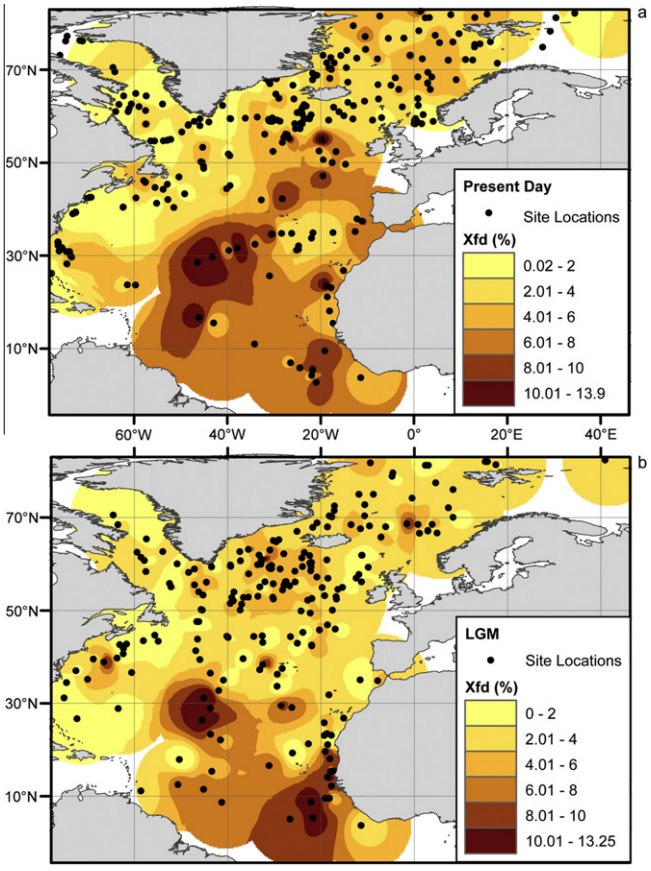


**Fig. 21.** Spatial distribution of frequency dependent susceptibility ($\chi_{fd}$%) for ocean-wide sediment samples, North Atlantic for (a) the present day and (b) the LGM. From Watkins and Maher (2003) and Watkins et al. (2007).

For the present day, in addition to delineating the westward extent of African dust deposition, the magnetic data indicate a secondary, northwestward-trending dust signal, extending to ~55°N (Fig. 21a). Compared with the westward dust signature, this northwesterly-trending plume displays the same high values of $\chi_{fd}$% but lower HIRM values (ave. 6% compared with ave. 10.6% for the westward sediments), indicating some possible differences in source and/or more mixing with other sediment magnetic components. For the LGM, large areas of the northern North Atlantic are magnetically dominated by iceberg-rafted debris (IRD), often of distinctive Scandinavian provenance, with more minor IRD contributions from the Laurentide ice sheet (Watkins et al., 2007). However, the low-latitude spatial extent of the LGM African dust plume is magnetically well-defined, despite the presence of (coarser-grained) haematite-rich, iceberg- or slope-derived debris issuing from the St. Lawrence region (Fig. 21b and Section 5.1.3). Comparing HIRM and $\chi_{fd}$% values for the present day with those at the LGM, enhanced LGM input of haematite is evident as far north as 30–40°N, indicating both a northward and westward expansion (by ~10°) of aeolian input across the North Atlantic. Such an expansion is consistent with intensified glacial-stage NE trade winds, resulting from an intensified winter subtropical high (e.g. Sarnthein et al., 1981; Ganopolski et al., 1998), and/or an expansion in the dust source areas (e.g. Goudie and Middleton, 2001), and/or enhanced gustiness (McGee et al., 2010). Conventional dust analyses indicate that whilst dust fluxes to the North Atlantic are higher presently than they were in the early Holocene, the LGM dust flux was higher than today by a factor of between 2 and 5 (e.g. Kohfeld and Harrison, 2001; Bradtmiller et al., 2007).

### *5.1.2. Magnetic records of North African dust flux to the Mediterranean Sea*

Even in the presence of volcanic ash layers and sapropels (organic-rich sediment layers associated with strong magnetic mineral diagenesis), magnetic analyses of Mediterranean sediments reveal a detailed Plio-Pleistocene record of aeolian flux from North Africa (Larrasoana et al., 2003, 2008). As with the North Atlantic dust flux archives, the key magnetic parameter is the HIRM (in this study, the remanence imparted at 0.9 T, subsequently subjected to an ac field of 120 mT), which records varying aeolian inputs of haematite. Flux minima are associated with precessionally-driven periods of African summer monsoon intensification; flux maxima with northern hemisphere insolation minima, and weakened monsoon intensity (Fig. 22). From the absence of goethite (in notable contrast to the southern Saharan dust plume, see Section 5.1.1), and the presence of palygorskite, the dust source region is suggested as the fossil lake, river and wadi deposits of eastern Algeria, Libya and western Egypt, between ~21 and 30°N. Over the 3 Ma time interval recorded by these eastern Mediterranean sediments (ODP Site 967, 34° 04'N, 32°43'E), high haematite fluxes also coincide with 400-kyr eccentricity minima, and, more weakly, with 100-kyr eccentricity cycles. These data strongly suggest that northward penetration of the African summer monsoon front beyond 21°N is modulated by total as well as by latitudinal distributions of insolation. The link between high dust fluxes and eccentricity minima for the northern Saharan-sourced dust contrasts with the equatorial Atlantic records of southern Saharan/Sahelian-sourced dust, where eccentricity minima coincide with low dust fluxes (Larrasoana et al., 2003; Tiedemann et al., 1989). Conversely, both the northern and the southern-sourced regions demonstrate a similar response on shorter, precessional timescales, with low dust fluxes during precession minima.

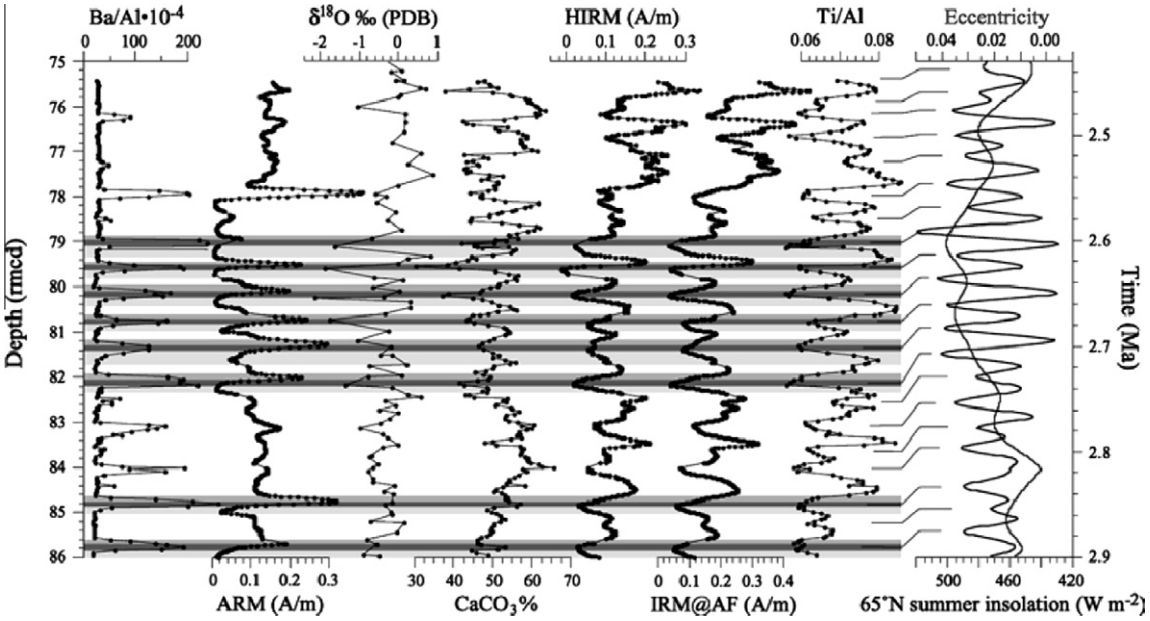


**Fig. 22.** Magnetic, geochemical and $\delta^{18}O$ data for ODP Site 967, for the time interval 2.4–2.9 Ma BP, shown plotted against northern hemisphere insolation and eccentricity (after Laskar et al., 2004). The dark grey bars identify the sapropels. Light grey shading above and below the sapropels indicates positions of oxidation fronts and magnetite dissolution, respectively. From Larrasoana et al. (2003).

*5.1.3. Magnetic identification of dust in the iceberg-rafted debris zone, North Atlantic*

Conventional methods for isolating the aeolian component of deep-sea sediments cannot be applied to sediments containing iceberg-rafted debris. Within the North Atlantic, maximum deposition of iceberg-rafted debris (IRD) occurred in a belt extending between ~40 and 65°N (Ruddiman, 1977). Thus, no quantitative estimates currently exist for dust deposition from the westerlies across the entire northern North Atlantic. Long-chain alkanes, derived from leaf waxes, have been used to identify terrigenous inputs to the northern North Atlantic through the last interglacial/glacial cycle. For example, Madureira et al. (1997) analysed a northeast Atlantic core (core T88-9P; 48°23′N, 25°05′W, 3193 m water depth, 790 cm core length); abundances of three land-derived biomarkers (long-chain compounds, LCC) were greater in glacial than in interglacial sediments. These authors attribute these biomarker variations at least partly to higher glacial-stage dust fluxes but cannot exclude enhanced particulate flux from either ice-rafted transport and/or bottom water transport.

Routine magnetic analyses made on the same northern North Atlantic core, T88-9P, show some associations between Heinrich ice-rafting events (e.g. H1-2, H3-H6) and increased sediment $\chi$ and SIRM values (Fig. 23). This is unsurprising given the strongly magnetic source rocks in the circum-Atlantic region, including the igneous provinces of Greenland and Iceland (Watkins and Maher, 2003). To isolate any SP haematite/goethite components, possibly indicative of aeolian rather than lithogenic source, low-temperature (77–293 K), high-field (2–7 T) analyses were additionally carried out (using Quantum Design's Magnetic Property Measurement System). Fig. 23 plots the down-core variations in the '$H_{Cool\%}$' parameter (Maher et al., 2004):

$$H_{Cool\%} = ((\text{HIRM 77 K}_{-2\,T} - \text{HIRM 293 K}_{-2\,T})/\text{HIRM 293K}_{-2\,T}) * 100$$

For comparison, the dust concentration in the NGRIP ice core is shown in Fig. 24, together with the total LCCs and $H_{Cool\%}$ values in T88-9P. Reasonably strong accord is evident between the $H_{Cool\%}$ and LCC records, and additionally for the NGRIP dust concentration record, whilst little relationship is evident between the $H_{Cool\%}$/LCCs and the record of *H* events.

These data suggest that the $H_{Cool\%}$ parameter might represent a sensitive proxy for aeolian dust even in sediments strongly dominated by IRD-derived ferrites. Since these magnetic measurements are relatively fast and non-sample destructive, they can precede, and corroborate, other sample-destructive approaches such as molecular biomarker analysis. One caveat regarding magnetic discrimination of aeolian dust in this context is that some Triassic red-bed samples contain sufficiently ultrafine haematite as to display significant $H_{Cool\%}$ values (Fig. 8). IRD derived from the Triassic sandstones of Spitsbergen, for example, could thus hamper aeolian flux estimation in the eastern sector of the northern North Atlantic (Fig. 21b, and Watkins and Maher, 2003).

*5.1.4. The role of North Atlantic dust in Southern Ocean iron fertilisation?*

Modern dust flux data for the presently HNLC Southern Ocean region are very sparse but recent observations indicate extremely low dust fluxes of ~0.14 (±0.005) g $m^{-2}$ $a^{-1}$, i.e. one or two orders of magnitude lower than modelled flux estimates (Wagener et al., 2008; Tagliabue et al., 2009a,b). Even if glacial-stage dust fluxes to the Southern Ocean were ~25× greater than at present day (i.e. equivalent to the dust increases seen in the Antarctic ice cores), the fluxes would still have been very low. Given that the North African region is the largest source of (iron-rich) dust in the world, it has been postulated to have provided an indirect supply of iron to the dust-deficient Southern Ocean HNLC region, via southward flow and subsequent circumpolar upwelling of the North Atlantic intermediate/deep water (Watson and LeFevre, 1999). This hypothesis suggests that aeolian-driven iron fertilisation of the Southern Ocean, and drawdown of atmospheric $CO_2$ (as recorded by the polar ice cores) might match more closely with Northern, rather than Southern, hemisphere dust fluxes (Watson and LeFevre, 1999).

This hypothesis has been tested by examining the timing of North Atlantic dust fluxes with regard to Southern Ocean $CO_2$ changes, for the time period spanning Termination II, through

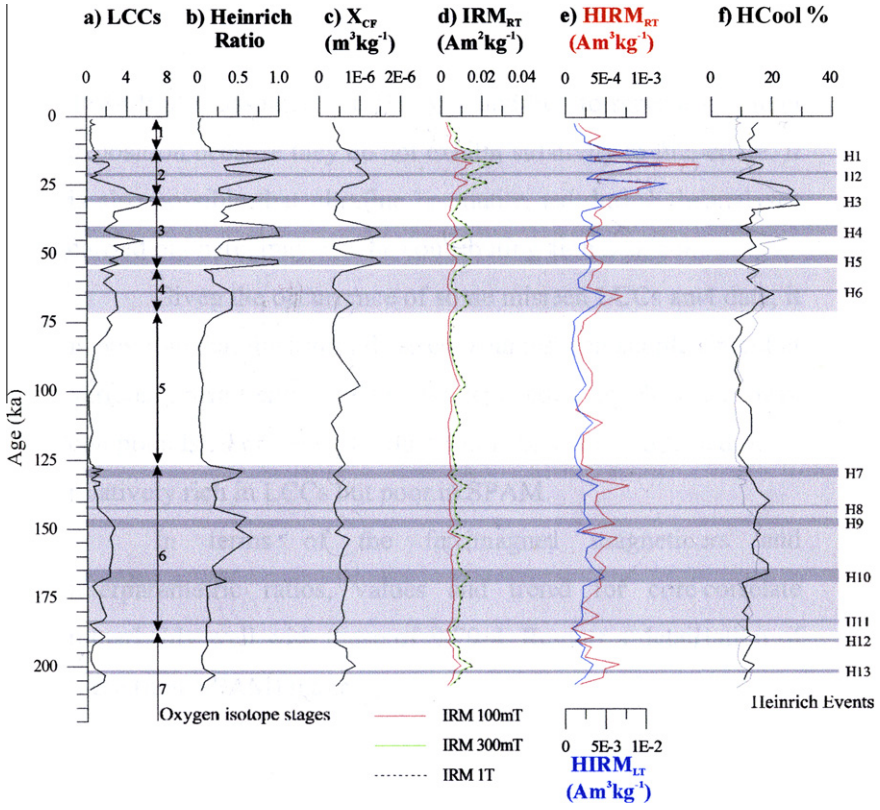


**Fig. 23.** (a) Long chain compounds (Σ LCCs, μg/gm dry weight), (b) Heinrich events as measured by IRD (>125 μm ice-rafted/total grains), and RT magnetic properties, (c) carbonate-free $\chi$, (d) SIRM, (e) HIRM) and (f) $H_{Cool\%}$ for Core T88-9P, northeastern North Atlantic, within the IRD belt (Maher and Mutch, in preparation).

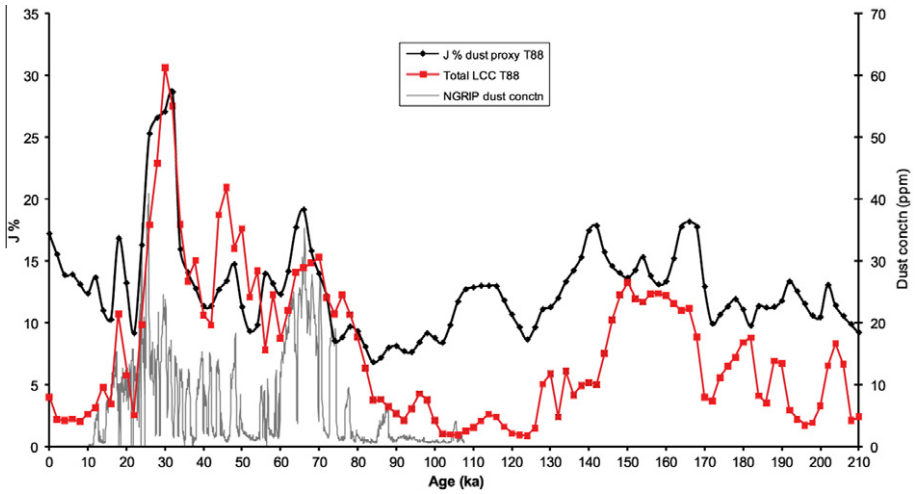


**Fig. 24.** Total LCCs and $H_{Cool\%}$ for core T88-9p, plotted with the dust concentration (ppb) at the GRIP ice core. (Maher and Mutch, in preparation).

high-resolution magnetic, oxygen isotope, and elemental analysis of core 82PCS01, from the abyssal plain NE of the Azores (Maher and Dennis, 2001). For glacial MIS 6, core 82PCS01 displays two peaks in HIRM, at ~155 ka and 130 ka BP. For the succeeding interglacial stage, from ~125 to 100 ka BP, HIRM values are low and less variable. Assuming goethite as the major contributor to the measured, carbonate-free HIRM values ($7–44 \times 10^{-4}$ A $m^2$ $kg^{-1}$), its sediment concentration ranges from 1.4 to 8.8 wt%. Strong, direct correlation between HIRM and the Fe content of the sediments enables calculation of the Fe flux and, assuming an average aerosol iron content of 3.5% (Duce et al., 1991a,b), the dust flux.

Fig. 25a shows the calculated dust fluxes for core 82PCS01, for the period spanning MIS 6, Termination II and interglacial MIS 5e. Dust flux was 3–5 times higher during two intervals: ~155 ka BP (~50 g $m^{-2}$ $a^{-1}$) and ~130 ka BP (~30 g $m^{-2}$ $a^{-1}$). During MIS 5e (from ~130 ka BP), dust fluxes decreased rapidly before steadying at about 1 g $m^{-2}$ $a^{-1}$. The fivefold increase in North Atlantic dust flux at ~155 ka BP coincides with a minor peak in dust flux (~2 mg $m^{-2}$ $a^{-1}$) recorded at Vostok (Fig. 25c). But this large rise in North Atlantic dust (and Fe) flux occurred entirely within MIS 6, with negligible apparent effect on either atmospheric $CO_2$ or oxygen isotope values, as recorded by the Vostok ice core. The sub-

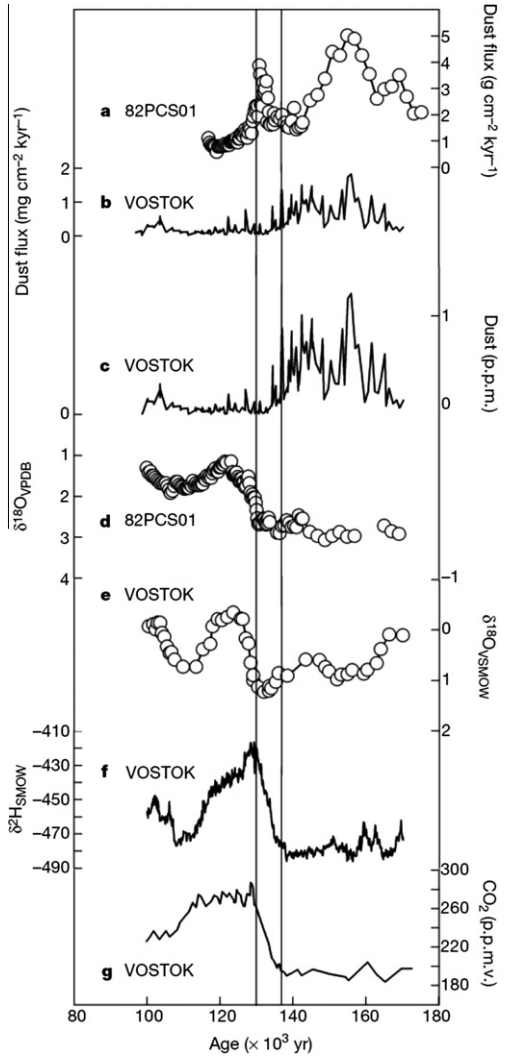


**Fig. 25.** Dust, $\delta^{18}O$ and $CO_2$ records from the North Atlantic (core 82PCS01) and the Vostok ice core. (a) Dust fluxes for core 82PCS01 (from HIRM/Fe correlation, and estimated average Fe content in aerosols of 3.5%); (b) dust fluxes for the Vostok ice core (Petit, pers. comm.); (c) dust concentration in the Vostok ice core (Petit et al., 1999); (d) $\delta^{18}O$ values for core 82PCS01; (e) $\delta^{18}O$ values for the Vostok ice core (Petit et al., 1999); (f) deuterium data for the Vostok ice core (Petit et al., 1999); (g) $CO_2$ data for the Vostok ice core (Petit et al., 1999). The vertical line at 137 kyr marks the onset of the $CO_2$ rise recorded at Vostok, and that at 130 kyr marks the Termination II boundary. From Maher and Dennis (2001).

sequent decline in North Atlantic dust flux substantially preceded (by ~7 kyr) the Termination II increase in atmospheric $CO_2$. Conversely, the second North Atlantic dust flux event, at ~130 ka BP, has no Vostok corollary and significantly post-dates (by ~7 kyr) the rise in $CO_2$ at Termination II. Rather than being linked with drawdown of atmospheric $CO_2$ and maintenance of glacial conditions, the peak flux of this later event coincides with a sharp, 1‰ shift to isotopically lighter $\delta^{18}O$ values, indicating either warming of North Atlantic sea surface temperatures and/or melting of the Northern hemisphere ice sheets (Maher and Dennis, 2001).

Thus, the high, glacial-stage fluxes of dust and Fe from the North African dust plume appear to display no causal relationship with changes in either atmospheric $CO_2$ or Southern Ocean temperature, as recorded at Vostok around Termination II.

In contrast, using $^{232}Th/^{230}Th$ ratios and biomarkers as dust flux proxies, Martinez-Garcia et al. (2009) report Southern Ocean dust fluxes as high as ~1 g m$^{-2}$ a$^{-1}$ during interglacial stages and 5–7 g m$^{-2}$ a$^{-1}$ during glacial stages. It is notable that these interglacial dust flux values are ~10× higher than recent data observations in the Southern Ocean (Wagener et al., 2008), and the glacial-stage dust fluxes are ~10× higher than modelled fluxes for this region (Mahowald et al., 2005). Martinez-Garcia et al. (2009) find a strong direct relationship between their dust flux estimates and biological carbon export, and suggest that this can account for ~40–50 ppmv drawdown of atmospheric $CO_2$ (i.e. as much as half of the total interglacial–glacial change of ~100 ppmv) during glacial maxima.

### 5.1.5. Magnetic records of dust flux to the Arabian Sea: dust and diagenesis

After North Africa and central/east Asia, the Arabian peninsular comprises the third largest dust source region at the present day (~10–20% of global emissions). High dust concentrations are prevalent over the Arabian Sea in late winter/early spring, transported by the winter monsoon and synoptic-scale northeasterlies (Verma et al., 2008). Providing readily-eroded sources of dust, coastal sabkhas and eroding wadis extend along the eastern Persian Gulf and Oman coast, respectively, whilst the lower Tigris-Euphrates basin also contributes a boreal summer peak in dust emissions, supplied from very large alluvial plains (Fig. 15).

Major development of magnetic methods as a dust proxy in marine sediments, and, critically, as a sediment property of key value in cyclostratigraphy, was achieved by analysis of a long, Plio-Pleistocene sequence of Arabian Sea sediments (Fig. 17), cored from the Owen Ridge during Ocean Drilling Program (ODP) Leg 117 (Bloemendal and deMenocal, 1989; Bloemendal et al., 1993). For the Owen Ridge sediments, the whole-core $\chi$ and $\delta^{18}O$ records show positive correlation, especially over the last ~200 kyr, when large-amplitude peaks in $\chi$ coincide with isotopically heavier, glacial-stage $\delta^{18}O$ values (Fig. 26). By calibrating the whole-core $\chi$ measurements with a subset of % terrigenous component values, Bloemendal and deMenocal (1989) and deMenocal et al. (1991) were able to use $\chi$ as a dust proxy for the >3.5 Myr-sedimentary record from the Owen Ridge. This core site lies in a pivotal position

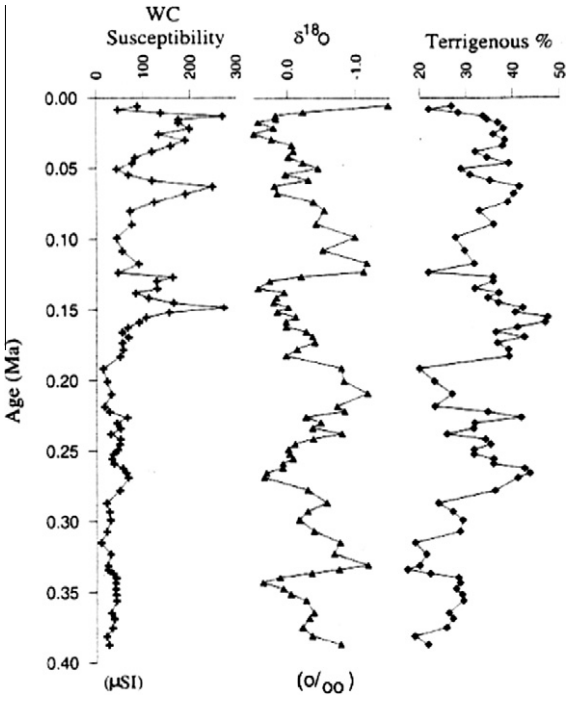


**Fig. 26.** Whole-core $\chi$, $\delta^{18}O$ and terrigenous % records for site ODP722, the Owen Ridge, Arabian Sea. From Hounslow and Maher (1999).

with regard to several major aeolian dust trajectories originating from Africa and Arabia, including boreal summer southwest and northwest monsoon winds, and winter northeasterlies (Fig. 17).

Spectral analysis of the whole-core $\chi$ record indicates that prior to ~2.4 Ma the proxy-recorded dust flux variations display precessional (23- and 19-kyr) periodicities,corresponding with indices of Arabian Sea upwelling, in turn interpreted as reflecting changes in the intensity of the Indian summer monsoon. After ~2.4 Ma, the $\chi$ record is dominated by 41-kyr cyclicity, possibly driven by growth and decay of the northern hemisphere ice sheets (Bloemendal and deMenocal, 1989). The $\chi$ peaks were attributed here not to fluxes of haematite/goethite but of lithogenic magnetite; higher Ti-magnetite concentrations associated with glacial stages (Bloemendal et al., 1992).

To understand the source of this 'outstanding proxy palaeoceanographic record' (Bloemendal and deMenocal, 1989), and demonstrating the multi-component nature of deep-sea magnetic records, it is necessary to decompose the $\chi$ record into its individual component contributions (Hounslow and Maher, 1999):

$$\chi_{\text{total}} = \chi_f + \chi_a + \chi_p + \chi_d$$

where $\chi_f$ = the $\chi$ contributed by ferrimagnetic minerals, like magnetite; $\chi_a$ = that contributed by the defect antiferromagnets, like haematite and goethite; $\chi_p$ = that from weakly magnetic paramagnets, like Fe-bearing silicates; and $\chi_d$ = the negative susceptibility carried by diamagnetic minerals, like quartz and calcium carbonate. The influence of the varying carbonate content can be seen by comparing the whole-core $\chi$ with the carbonate-free $\chi$ data (Fig. 27). The latter displays much lower amplitude $\chi$ variations. Thus, the whole-core $\chi$ record dominantly shows the effects of varying carbonate % (or, inversely, of varying terrigenous %). Second, the paramagnetic contribution to the measured $\chi$ can be quantified from low-temperature (77–300 K), low-field measurements of susceptibility. Above ~7 metres below sea floor (mbsf), the peaks in carbonate-free $\chi$ are associated with lower paramagnetic contributions (~30%), and troughs with slightly higher $\chi_p$ values (~45%). But below ~7 mbsf, the $\chi_p$ contribution to measured susceptibility increases to between 85% and 100% (Fig. 27b).

Thus, rather than representing a simple record of varying detrital flux of magnetite, the magnetic responses of the Leg 117 sediments to climate change reflect a variety of down-core mineral changes (Hounslow and Maher, 1999). Encapsulating even more detailed climatic and environmental information, the $\chi$ record arises from changes in: (a) the volume $\chi$ – primarily controlled by biogenic carbonate dilution; (b) the aeolian flux of ferrimagnetic grains (Fig. 27a and b – evident only in the upper 7 mbsf, and probably reflecting changes in source area aridity; and, critically, (c) the paramagnetic $\chi$ contribution, below 7 mbsf – which (unlike the aeolian magnetite and haematite component) has survived intense post-depositional diagenesis (Fig. 27c). An additional, authigenic ferrimagnetic component, bacterial magnetosomes, is also evident within just the upper 1.7 mbsf (Fig. 27a). Whilst this biogenic magnetite occurs in insufficient concentrations to influence $\chi$, its survival in the upper sediments indicates least intense diagenesis at this point in the sediment column.

Additional mineralogical, morphological and grain size data were obtained from quantitative magnetic extracts (Hounslow and Maher, 1999). The dominant, paramagnetic source of the $\chi$ variations is contributed by aeolian Fe-bearing clay minerals, ilmenite and other Fe-bearing silicates, and varies in phase with changes in lithogenic grain size (Clemens and Prell, 1991). This direct association between changes in paramagnetic $\chi$ and lithogenic grain size probably reflects changes not in wind speed but in sed-

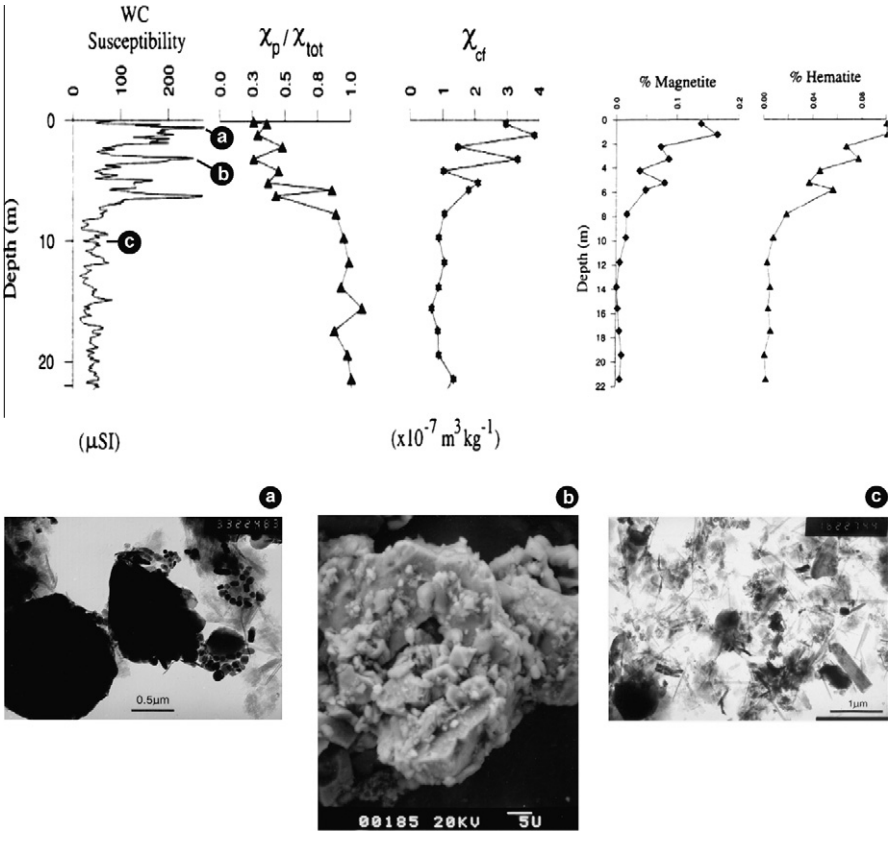


**Fig. 27.** Whole-core $\chi$, the paramagnetic contribution to $\chi$, the carbonate-free $\chi$, and the magnetite % and haematite % down-core, ODP Site 722, together with electron micrographs showing typical magnetic minerals at specified stratigraphic intervals (a = detrital lithogenic magnetites and *in situ* bacterial magnetosomes; b = detrital lithogenic magnetites; c = residual clay minerals and rare goethite needles). Adapted from Hounslow and Maher (1999).

iment source (possibly related to rainfall changes) and/or wind transport trajectories (Hounslow and Maher, 1999).

The Owen Ridge $\chi$ record demonstrates the importance of identifying the individual mineral components contributing to the magnetic record of palaeoclimate; detailed magnetic and mineralogical analyses are required in order to make robust use of the magnetic climate proxy. Despite intense diagenetic dissolution of the aeolian-sourced magnetite and haematite grains at the Owen Ridge, a record of changing dust flux survives, through the paramagnetic contribution of the iron-bearing silicate minerals. In order of vulnerability to diagenetic dissolution, magnetite and maghemite are most vulnerable (Karlin and Levi, 1983; Canfield and Berner, 1987; Canfield et al., 1992; Karlin, 1990; Tarduno, 1995), followed by goethite (Abrajevitch et al., 2009) and then by haematite. Within this sequence, finer-grained minerals will be removed preferentially compared with coarser grains. Thus, wherever diagenetic modification of the sediment record is suspected (and often detectable magnetically), the source of shifts in sediment magnetic mineralogy must be evaluated with care.

*5.1.6. Magnetic records of dust flux to the Northwest Pacific Ocean*

The North Pacific lies downwind from the major dust sources of the Asian deserts and the Chinese Loess Plateau, which together provide ~20% of global dust emissions at the present day (e.g. Tanaka and Chiba, 2006). Through upper level transport by the westerlies, Asian dust is transported right around the globe (Fig. 28). It contributes to dust samples across the Chinese mainland, to Japan and Korea (the 'kosa' dust storms), and is frequently observed at high concentrations at mid-ocean stations in the North Pacific (Duce et al., 1980; Prospero et al., 1989). Present day estimates of Asian dust flux to the central North Pacific range from ~6 to 12 $\times$ $10^6$ tons $a^{-1}$ (Uematsu et al., 1983, 1986, 2003). Distal transport extends even to the western United States (VanCuren and Cahill, 2002) and the Greenland ice caps (Biscaye et al., 1997; Bory et al., 2003a, 2003b). In addition to the major desert sources (the Taklimakan, the Gobi), the Chinese Loess Plateau is unique amongst the world's loess regions in that it is now a highly active source of dust, at least partly due to human agricultural activity (Wang et al., 2004).

The potential environmental significance of changes in dust flux to the North Pacific can be illustrated by recent iron enrichment experiments, which show that this large HNLC region of the world ocean responds particularly sensitively to iron fertilisation (Tsuda et al., 2003; de Baar et al., 2005). In order to achieve robust age models, based on oxygen isotope stratigraphies, records of Quaternary dust flux to the North Pacific have often been sought from seamount locations, i.e. from sites lying above the calcite compensation depth.

In addition to dating difficulties due to varying rates of carbonate dissolution and preservation, conventional analyses of dust flux have to contend with variable inputs of volcanic ash (e.g. Hovan et al., 1991; Urbat and Pletsch, 2003), and iceberg-rafting of debris into the North Pacific (e.g. Bigg et al., 2008; Fig. 29).

The Shatsky Rise (37.7°N 16°E), situated beneath the Asian dust plume, provides one of the best known aeolian flux records for the North Pacific, core V21-146 (Hovan et al., 1989, 1991). Glacial-age sediments in this core display increased dust fluxes, and can be linked directly with the low-$\chi$ loess units of the adjacent terrestrial record of the Chinese Loess Plateau (Fig. 30). Spectral analysis, however, indicates that the peaks in marine aeolian fluxes significantly lead the loess record of terrestrial deposition (by ~14 and ~7 kyr for the 100- and 41-kyr cycles, respectively). Neither does aeolian grain size show any simple correlation with climate stage; coarser grains (median diameter ~8 μm) show some association

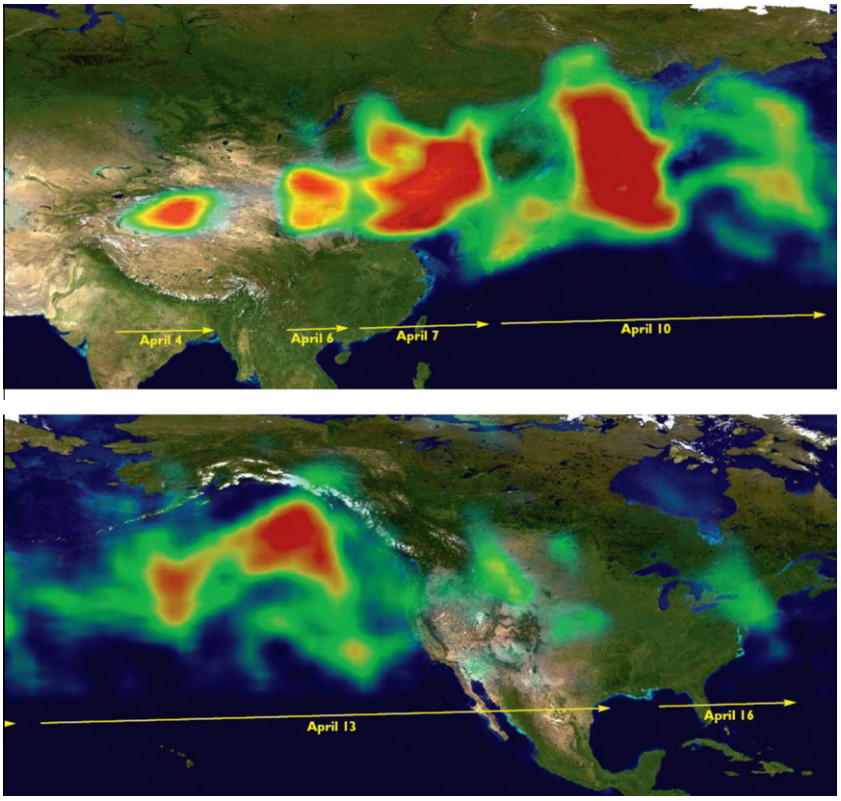


**Fig. 28.** A composite image of aerosol index (AI) measurements obtained from April 4 to 16 2001, showing the transport of Asian-sourced dust across the Pacific Ocean, North America and into the Atlantic Ocean. Red areas identify high AI values, yellows and greens are moderately high AI values. (Data from TOMS instrument on the Earth Probe satellite). From Hsu et al. (2007).

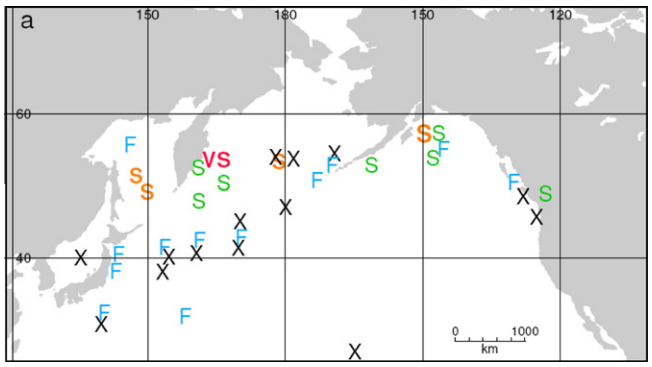


**Fig. 29.** Extent and relative abundance of LGM IRD in the North Pacific. 'X' indicates no evidence of IRD, 'F' indicates IRD concentrations of <0.5 g m$^2$ a$^{-1}$; 'S' ~0.5–2.5 g m$^2$ a$^{-1}$, '**S**' ~2.5–10 g m$^{-2}$ a$^{-1}$ and 'VS' ~>10 g m$^2$ a$^{-1}$. From Bigg et al. (2008).

both with interglacial and glacial stages (Rea and Hovan, 1995). These features of the Shatsky Rise dust record indicate likely changes in dust source and/or transport path through time, rather than any simple flux-related relationship with its upwind Loess Plateau neighbour.

Magnetic identification of coherent changes in haematite/goethite concentrations, linked to changes in aeolian sedimentation rate, has indicated that magnetic proxies of palaeoclimate could be used reliably even in palaeomagnetically unstable sections of the central Pacific pelagic red clays (Doh et al., 1988). However, as with the equatorial Pacific, some controversy has existed with regard to interpreted changes in North Pacific aeolian flux through Quaternary glacial and interglacial climate stages. For example, in a combined sedimentological, magnetic and mineralogical study (Core RC10-175), Wang et al. (2008) identified peaks of aeolian accumulation at a mid-Holocene climatic optimum and during the last interglacial stage (MIS 5e). In direct contrast, Yamazaki (2009), using first-order reversal curves (FORC analysis), S ratios and $\chi_{ARM/SIRM}$ ratios, infer increased aeolian flux (of both maghemite and haematite) during glacial stages. *In situ*, biogenic magnetite (produced intracellularly by magnetotactic bacteria) was characterised in this latter study as a non-interacting, low-coercivity component. In spatial terms, again based on HIRM and S ratios, enhanced aeolian influx to the central North Pacific has been suggested (Yamazaki and Ioka, 1997), particularly from ~2.5 Ma, in synchrony with the onset of Northern hemisphere glaciations, and deposition of the Chinese loess.

The relative influences of volcanic ash and episodic diagenesis on the magnetic properties of northwest Pacific sediments are demonstrated in ODP core 1149A. Here, the uppermost 32 m, spanning the Brunhes and extending into the Matuyama Chron, provide an expanded record of changes in Asian aeolian dust and volcanic ash input, interspersed with recurrent diagenetic intervals (Urbat and Pletsch, 2003). The magnetic signal in Hole 1149A is driven primarily by varying inputs of aeolian-dispersed ash and terrigenous dust (Fig. 31). Several intervals are characterised by rapid and large changes in rock magnetic parameters and adjacent enrichments in diagenetic minerals. These intervals correspond to palaeoredox boundaries, where suboxic conditions promoted post-depositional deletion of the detrital magnetic signal.

In contrast, and representing a cautionary note, the magnetic susceptibility record of the 6 Myr-long sediment record of ODP Hole 882 (NW Pacific, 50.3°N 167.6°E), in association with the siliciclastic fraction (>2 μm wt%), is reported as a Plio-Pleistocene record of IRD, with ice rafting initiated as early as ~2.75 Ma BP (Fig. 32; Haug et al., 1995). Even as far south as ~30°N (with the exception of the Sea of Japan), non-aeolian terrigenous fluxes may be significant, with IRD fluxes to the glacial North Pacific varying on the order of ~0.5–10 g m$^{-2}$ a$^{-1}$ (Fig. 29), based on available LGM data (Bigg et al., 2008).

Moving from the north to the south Pacific, fluxes of iron-rich dust from Australia to the Tasman Sea and beyond are poorly constrained both at the present day and in the past. For the present day, remote sensing by satellites (e.g. by the Nimbus-7 Total Ozone Mapping Spectrometer, TOMS) indicates some localised dust source activity (e.g. around Lake Eyre) but overall relatively little sustained emission of dust from the Antipodean region (Prospero et al., 2002). In contrast, dust cycle models often attribute very large dust plumes to Australia, comparable in scale to those from NW Africa (e.g. Li et al., 2008). In addition to Lake Eyre, the

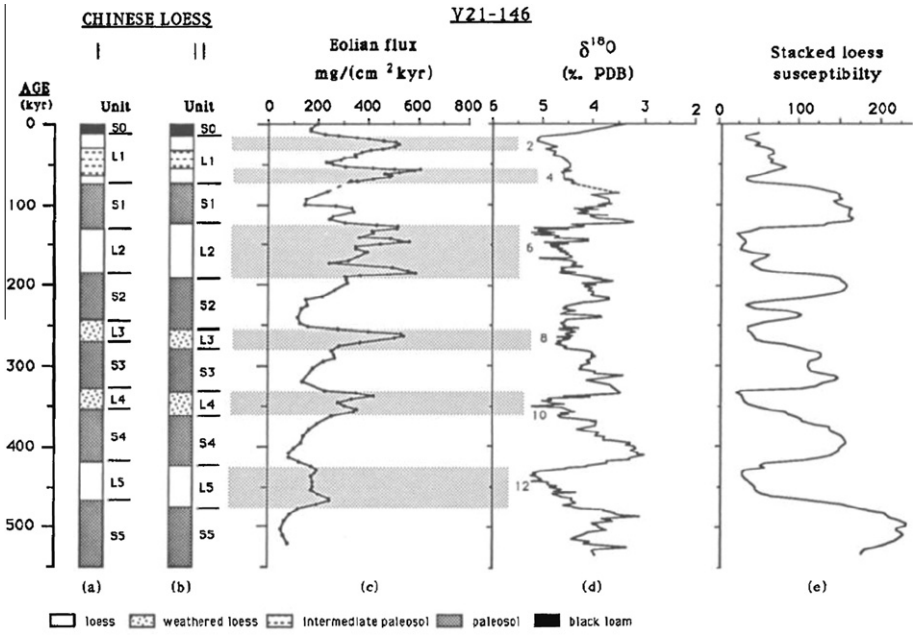


**Fig. 30.** Aeolian flux and $\delta^{18}O$ records for Pacific core V21-146, plotted with the stratigraphy of the Chinese loess and palaeosols and their stacked $\chi$ record. From Hovan et al. (1989).

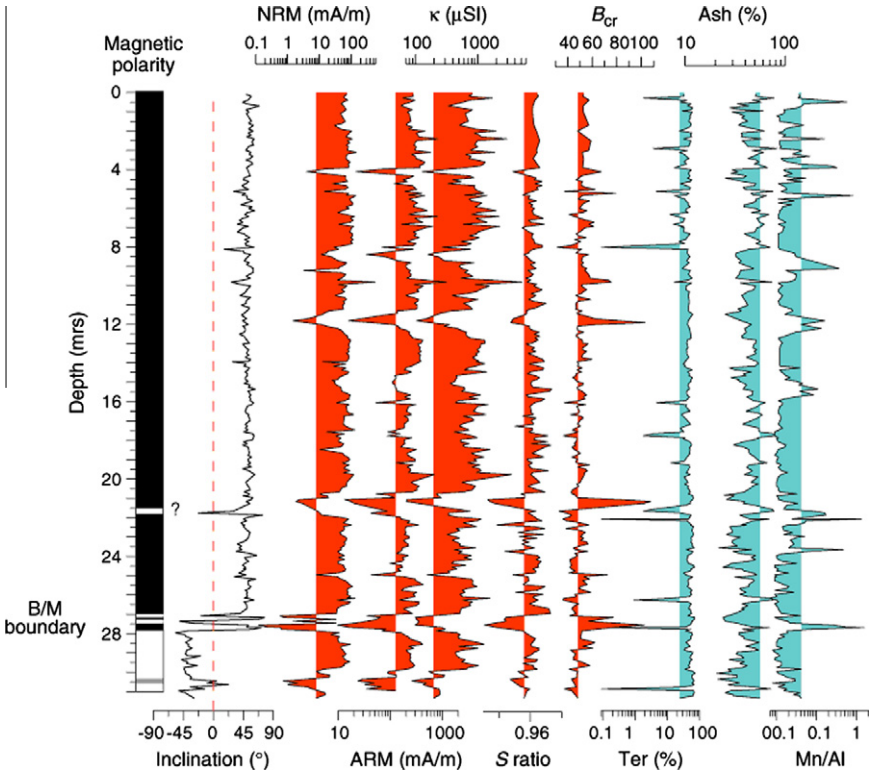


**Fig. 31.** Palaeomagnetic, magnetic and geochemical data for Hole 1149A (from the abyssal plain, Nadezhda Basin, 31.3°N 143.4°E). Sections strongly affected by diagenesis are highlighted by the Mn/Al ratio, and display large changes in magnetic mineralogy and composition. Minima in %Terr indicate the position of discrete layers of volcanic ash in the sediment sequence. (mrs = metres of recovered section; B/M = Brunhes–Matuyama boundary; K = volume susceptibility; $B_{cr}$ = coercivity of remanence; NRM = natural remanent magnetisation; ARM = anhystereric remanent magnetisation; Ter = terrigenous). From Urbat and Pletsch (2003).

increasingly desiccated floodplains and dunefields of the Murray-Darling basin provide a potential dust 'hot-spot'. Two main transport paths have been identified for Australian dust emissions. One trajectory is towards the south and/or southeast, crossing the Tasman Sea and possibly extending towards the southwest Pacific and the Southern Ocean (McTainsh et al., 2005; Shao et al., 2007). Indeed, isotopic evidence exists for the transport and deposition of Australian-sourced dust to the Antarctic region, especially during interglacial stages (e.g. Revel-Rolland et al., 2006, see Section 6.3). The second main dust trajectory is directed to the northwest (Bowler, 1976). An aeolian component has also been identified in the Quaternary sediments of the Coral Sea (Maher, in preparation).

Modern Australian dusts appear to be contaminated magnetically by ferrites sourced from agricultural soils (Hesse, 1997). In contrast, palaeo-dust contained within Tasman Sea sediments are often characterised by a fine-grained haematite/goethite fraction, which, in some locations, varies directly with the independently-measured concentration of mineral dust. However, as with the north Pacific sediments, detailed magnetic measurements are required in order to identify those cores where volcanic ash, bacterial magnetite and/or diagenetic mineral alteration have modified the sediment magnetic mineralogy. Again, this may represent a region where more detailed, low-temperature, high-field magnetic analyses might more robustly quantify the aeolian-sourced haematite and goethite sedimentary components.

*5.1.7. Summary, magnetic records of dust in marine sediments*

In summary, in oxic marine settings, the magnetic properties of sediments are frequently climatically controlled, whether by changes in carbonate content (by dilution or dissolution) and/or by changes in the flux and/or source of terrigenous magnetic particles. Hence, sediment magnetic properties can often be used as a high-resolution proxy for palaeoclimatic change (with care being required to account for any authigenic or post-depositional magnetic components). Further, the coherence exhibited by sediment magnetic properties with astronomical forcing frequencies, coupled with appropriate orbital tuning of the magnetic records, provides the opportunity for high-resolution chronological control. Magnetic cyclostratigraphy can thus assist in providing accurate age frameworks for climatic and environmental events and changes, a prerequisite for increased understanding of the causes and consequences of climate change. The relative sensitivity and speed of sediment magnetic measurements renders them both discriminatory and applicable over large (e.g. ocean-wide) spatial scales and high-resolution timescales. Statistical examination of the trends, rhythms and events recorded in two of the long (Plio-Pleistocene) magnetic dust flux records discussed here – the magnetic susceptibility record from the Arabian Sea (Section 5.1.5), and the eastern Mediterranean HIRM record (Section 5.1.2) – enables testing of postulated patterns and timings of change in tropical African climates (Trauth et al., 2009). Rather than showing a gradual increase in African aridity after intensification of northern hemisphere glaciation at ~3 Ma BP, or 100-kyr modulation of African dust fluxes only after ~1 Ma BP, or step-like increases in the amplitude of obliquity modulation of dust fluxes at ~2.8 and 1.7 Ma BP, these statistical results indicate that tropical African hydrology is dominantly and regionally controlled by low-latitude insolation mediated by monsoon dynamics. Key stages in hominin evolution, at ~2.6, 1.8 and 1 Ma BP, coincide with 400-kyr eccentricity maxima, suggesting that enhanced speciation and extinction events were associated with maximum climate variability but high moisture levels (Trauth et al., 2009).

For aeolian dusts sourced from arid regions, magnetic measurement of variations in the haematite and/or goethite content of sink sediments can provide a sensitive record of climatically-driven, of-

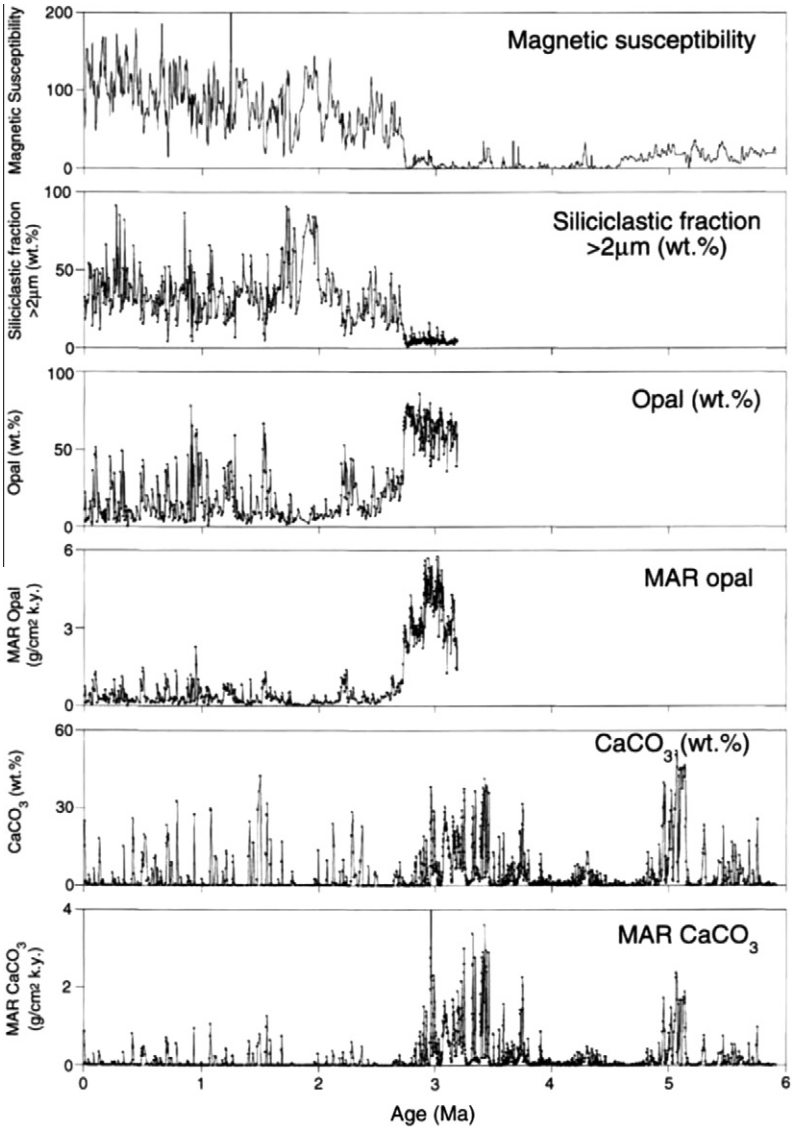


**Fig. 32.** Magnetic susceptibility, siliciclastic fraction (>2 μm wt%), opal (wt%), opal MAR, carbonate (wt%) and carbonate MAR for the 6 Myr-long sediment record of ODP Hole 882 (NW Pacific, 50.3°N 167.6°E). From Haug et al. (1995).

ten orbitally-forced, changes in aeolian flux. However, care is always needed in order to assess the degree of diagenetic overprinting of any sediment magnetic record, and the possibility of selective preservation of these minerals (at the expense of the ferrites) in response to post-depositional diagenetic attack.

## 6. Magnetic properties as palaeo-dust records: lake sediments

### 6.1. A North African case study

Lake basins, especially hydrologically-closed lake basins, provide land-based opportunities to examine palaeoclimatic changes as reflected by changes in the balance between precipitation and evapotranspiration, and changes in dust flux and deposition. Depending on location, such lake sediment-based studies can also provide a tie between the deep sea and continental records of climate change. Lake Bosumtwi (Ghana), for example, is located in the path of the dust-transporting, northeasterly Harmattan winds, and provides a 1-Ma record of regional changes in dust transport (Peck et al., 2004; King et al., 2008). As with the marine records, enhanced Saharan/Sahelian dust flux is identified during the last glacial stage, characterised here by high proportions of high-coercivity minerals (low S-ratios, Fig. 33). During the most arid intervals, coincident with Heinrich events 1 and 2, and the Younger Dryas, the proportion of such minerals was increased further, reflecting both increased dust flux and the in-lake effects of post-depositional reductive diagenesis, resulting from low lake levels and sulphate reduction. The diagenetic effects of diagenesis on the lake magnetic record include preferential removal of the fine-grained, detrital ferrimagnets and authigenic formation of the magnetic iron sulphide, greigite (Table 3, and see Section 5.1.5). The sharp magnetic transition at 12 ka BP indicates the end of the last glacial and the onset of the African Humid Period, with a very marked decline in dust fluxes to the lake. From ~3.2 ka BP, a return to increasingly arid conditions is indicated by steadily falling S-ratio values (Fig. 33).

The magnetic dust proxy archived within the ~290 m/1.07 Ma record of the Lake Bosumtwi sediments correlates readily with aeolian records from the deep sea and the polar ice cores. Peck

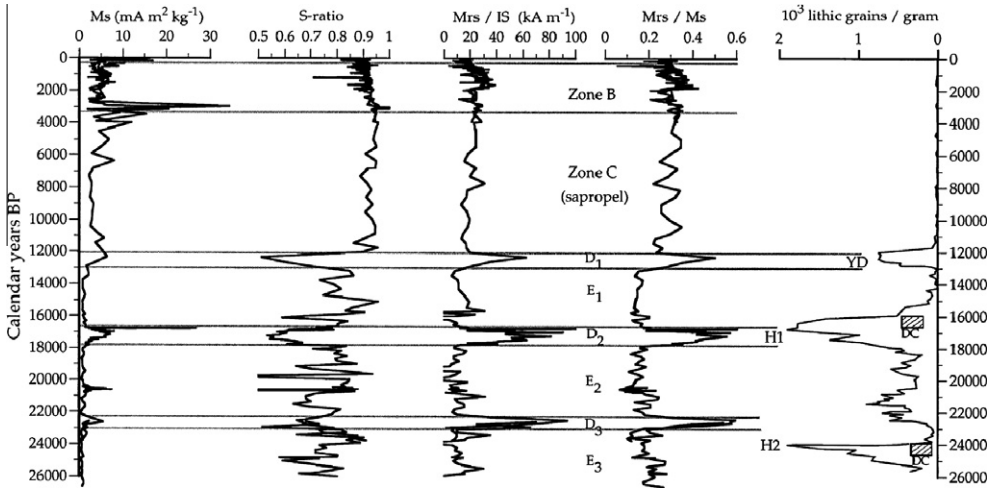


**Fig. 33.** Magnetic properties and lithic fraction, sediment core, Lake Bosumtwi, Ghana. From Peck et al. (2004).

**Table 3**
Magnetic zonation, grain size, mineralogy and palaeoclimatic interpretations for a lake sediment core from Lake Bosumtwi, Ghana. Generalized characteristics of the interglacial and glacial magnetic mineral sediment zones from Lake Bosumtwi. From Peck et al. (2004).

| Magnetic zone | Magnetic concentration (IS, $M_{rs}$, $M_s$) | Magnetic grain size (FORC, $M_{rs}/M_s$, $H_{cr}/H_c$) | Magnetic mineralogy ($M_{rs}$/IS, *S*-ratio, $H_{cr}$) | Paleoclimatic interpretation |
|---|---|---|---|---|
| *Interglacial* | | | | |
| A | High | SD and MD | High proportion of low-coercivity minerals | Interglacial conditions of reduced dust flux |
| B | Moderate to high | SD and MD | High proportion of low-coercivity minerals | Interglacial conditions of reduced dust flux |
| C | Moderate | SD and MD | Very high proportion of low-coercivity minerals | Very humid conditions; lake filled to overflowing |
| *Glacical* | | | | |
| D | Moderate to high | SD | Very high proportion of low-coercivity minerals | Correlative with Henrich events, arid, very low lake level |
| E | Very low | MD | High proportion of low-coercivity minerals | Arid glacial period charaterized by reductive diagenesis |

et al. (2004) suggest that the strong eccentricity and obliquity periodicities shown in the dust proxy record indicate that tropical climate responds to the presence of the mid- to high-latitude ice sheets. An alternative view is that the transfer of tropical heat to higher latitudes, the major driving force of the global climate, is also modulated by orbital forcing. Such forcing is abundantly evident at low latitudes, as changes in monsoon intensity, precipitation, vegetation feedbacks, wind speed/gustiness, and transport of dust. Thus, higher latitude climate changes are likely to be nearly synchronous with tropical changes, but need not be causally linked to them. Rather, changes in energy transfer from the tropics to higher latitudes may represent relatively under-estimated drivers in past climate change (see Section 5.1.7).

A number of other African lake-based studies report the use of $\chi$ records, often used for core correlation, and often interpreted as indicators of terrigenous input (e.g. Kropelin et al., 2008); additional magnetic analyses would be required in order to understand in detail the significance and reliability of these potential proxy records.

### 6.2. A South China case study

As with Lake Bosumtwi, a combination of changes in climate, lake level, erosion and the degree of diagenesis or preservation of detrital magnetic minerals provides an interesting context for possible re-interpretation of a lake sediment record, Lake Huguang Maar (Fig. 34), presented as a record of winter monsoon strength for the South China region (Yancheva et al., 2007).

Here, the high-resolution records of magnetic properties ($\chi$ and S-ratio) and sediment Ti content are used as proxies of winter monsoon wind strength. Specifically, the Ti content is assumed to represent the aeolian input into the lake, with the suggested dust sources including the Loess Plateau to the north. The $\chi$ data appear to record very large changes in magnetic content, e.g. from ~50 $'10^{-6}$ SI$'$ in the Bolling to ~5000 $'10^{-6}$ SI$'$ during the late Holocene. During cold intervals (the late Glacial, <~14.8 ka BP, the Younger Dryas, ~12.8–11.6 kyr BP) and the late Holocene (the last ~500 yr), $\chi$, Ti content and S-ratio are high (Fig. 34). These data suggest high detrital inputs of Ti-magnetites and little post-depositional dissolution. Conversely, during the Bolling and early Holocene (<~7.8 ka BP), $\chi$, Ti content and S-ratio all decline, indicative of reductive diagenesis and/or decreased detrital input of magnetite. Through the remainder of the Holocene, $\chi$ values increase markedly (x factor of 100), whilst Ti content and the S-ratio vary relatively little (Fig. 35).

Rather than representing far-travelled Chinese loessic dust, which contains volumetrically large proportions of haematite and goethite, it seems probable that the extremely large variations in $\chi$ reflect local erosional inputs of the strongly magnetic, Ti-magnetite-bearing basalts into this small crater lake. Episodes of reduc-

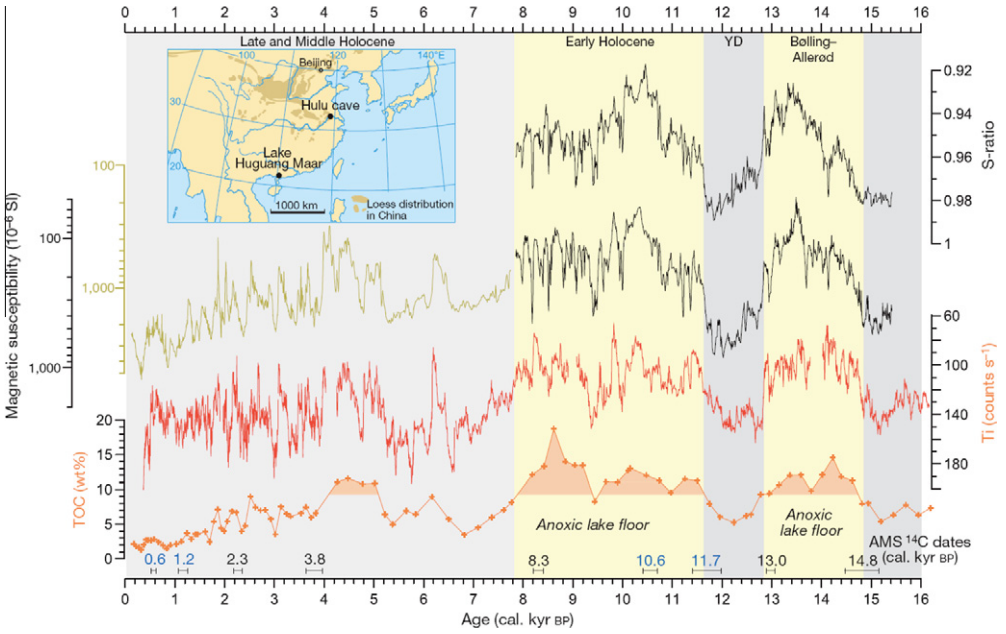


**Fig. 34.** Magnetic properties, Ti content and total organic carbon (TOC wt%), lake Huguang Maar (from Yancheva et al., 2007). YD = Younger Dryas, AMS = accelerator mass spectrometry.

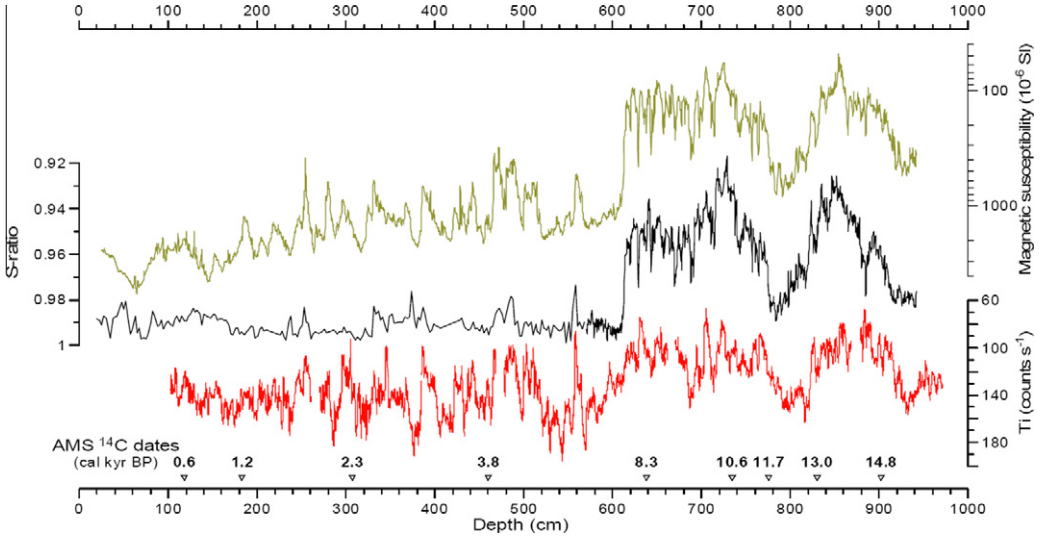


**Fig. 35.** Magnetic susceptibility, S-ratio and Ti content for Lake Huguang Maar, with depth in core. From Yancheva et al. (2007).

tive diagenesis are clearly a feature of the time interval from 16 to ~8 ka BP, with the exception of the cold periods noted above. It is possible that the Younger Dryas and Late Glacial were characterised by stronger winter monsoon winds and thus the lake was well-mixed, with little subsequent diagenesis. However, it is also possible that the lake level was lower during these drier intervals, maximising opportunities for overturning and mixing. From ~8.3 ka BP, the detrital input and/or preservation of magnetite increases markedly, with an apparent accompanying decline in total organic carbon (TOC) % (Fig. 34). Whilst the TOC% decline might indicate increasing lake mixing and oxygenation, it might equally reflect a relative increase in minerogenic input, as indicated by the increase in $\chi$. Thus, an alternative view of this record is that the Holocene interval is characterised by increased local runoff and erosion rates, possibly mediated by increased summer monsoonal rainfall.

### 6.3. A Patagonian case study

The transport of dust at high latitudes in the Southern hemisphere is of major scientific interest, given the possibility that aeolian supply of iron to the Southern Ocean might drive up marine productivity in this presently HNLC region, and alter marine and atmospheric $pCO_2$ concentrations as a result (Martinez-Garcia et al., 2009; Blain et al., 2007; Watson and LeFevre, 1999). Large shifts in aeolian dust flux over Quaternary glacial and interglacial stages are recorded in all of the Antarctic ice cores, with glacial stages characterised by up to 25× greater dust fluxes (e.g. Fischer et al., 2007a,b; Lambert et al., 2008)). Based on isotopic signatures (Nd and Sr), the major source of the dust deposited in the glacial-stage ice at Vostok and EPICA Dome C (EDC) is thought to be Patagonia (Grousset et al., 1992a; Gaiero, 2007; Delmonte et al., 2009; Sugden et al., 2009). Some isotopic overlap is also evident

between the ice and potential source areas in Australia (around Lake Eyre), more so during interglacial stages (Revel-Rolland et al., 2006; Marino et al., 2008; Delmonte et al., 2009). The only continental record of Quaternary dust accumulation currently reported from Patagonia is the lake sediment sequence cored in a maar lake, Laguna Potrok Aike (51.9°S 70.4°W), one of the few permanent lakes in the drylands of southern Patagonia (Haberzettl et al., 2009). So far, a composite sediment sequence (composed of three overlapping core sections) and covering the last ~55 kyr has been obtained, based on radiocarbon, OSL and tephrochronology techniques. Seeking to compare the independently-dated $\chi$ record from Laguna Potrok Aike with the non-sea salt calcium flux from the EDC record (Rothlisberger et al., 2002), these authors infer some similarities between these records (Fig. 36), finding therefore the first evidence for synchroneity of aeolian deposition both in the dust source (Patagonia) and sink area (Antarctica). The glacial-age lake sediments comprise well-sorted coarse silt and fine sand, in contrast to the interglacial sediments, which are more organic, less well sorted and richer in calcite. Using $\chi$ as a proxy for aeolian dust, glacial-stage aeolian deposition appears high ($\chi$ values are an order of magnitude higher than during Holocene times) and variable in the Patagonian record, indicating significant climatic and environmental change in southern South America. Without further information, it is difficult to ascribe the $\chi$ changes to differences in aeolian flux and/or dust source. More intense glacial activity during cold climate stages might activate additional or different dust sources compared with interglacial conditions (e.g. Sugden et al., 2009). The association between increased $\chi$ and clastic particle size during glacial stages might thus indicate increased wind speeds (e.g. stronger westerlies) and/or reduced vegetative cover and/or enhanced supply of coarse silt/fine sand particles for deflation and transport. More detailed magnetic and complementary analyses on this continental record, and on marine sediments from the Scotia Sea, lying between southern South America and the Antarctic ice (Pugh et al., 2009; Maher, 2008), will provide key information on sediment sources and fluxes in this critical region.

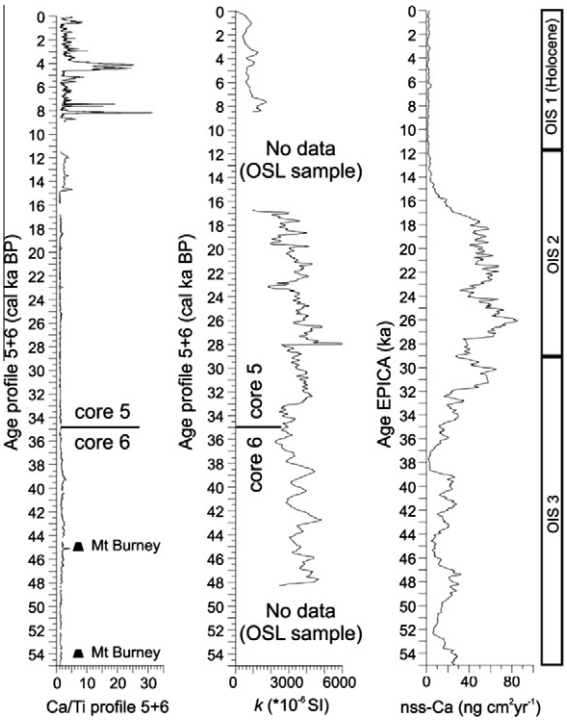


**Fig. 36.** Ca/Ti ratio and volume magnetic susceptibility for Laguna Potrok Aike (51.9°S 70.4°W) and the non-sea salt (nss) Ca flux, EDC (Rothlisberger et al., 2002). OSL = optically stimulated luminescence. From Haberzettl et al. (2009).

## 7. Magnetic properties as palaeo-dust records: the ice core record

### 7.1. Polar ice cores

Ice cores, whether from high latitudes or low latitude/high altitude sites, contain variable concentrations of terrestrial and extraterrestrial atmospheric particles. Long ice cores, spanning multiple glacial/interglacial cycles, from both Greenland and Antarctica exhibit large and rapid changes in dust flux, with increased fluxes (up to ~30× higher) during glacial stages (Figs. 24 and 37). For the eight glacial cycles recorded in Antarctica, the dust and temperature records are tightly and inversely coupled, especially during cold glacial-stage intervals (i.e. when $\delta D$ >~425‰, Lambert et al., 2008). Dust fluxes decreased synchronously with every warming interval, indicating rapid changes in either the dust source area (e.g. reduced dust supply and/or reduced wind speeds) and/or in the dust transport path (Fischer et al., 2007a,b; Lambert et al., 2008).

For the Greenland (North-Greenland Ice Core Project, NGRIP) core, isotopic evidence indicates a 'constant' source of dust, from

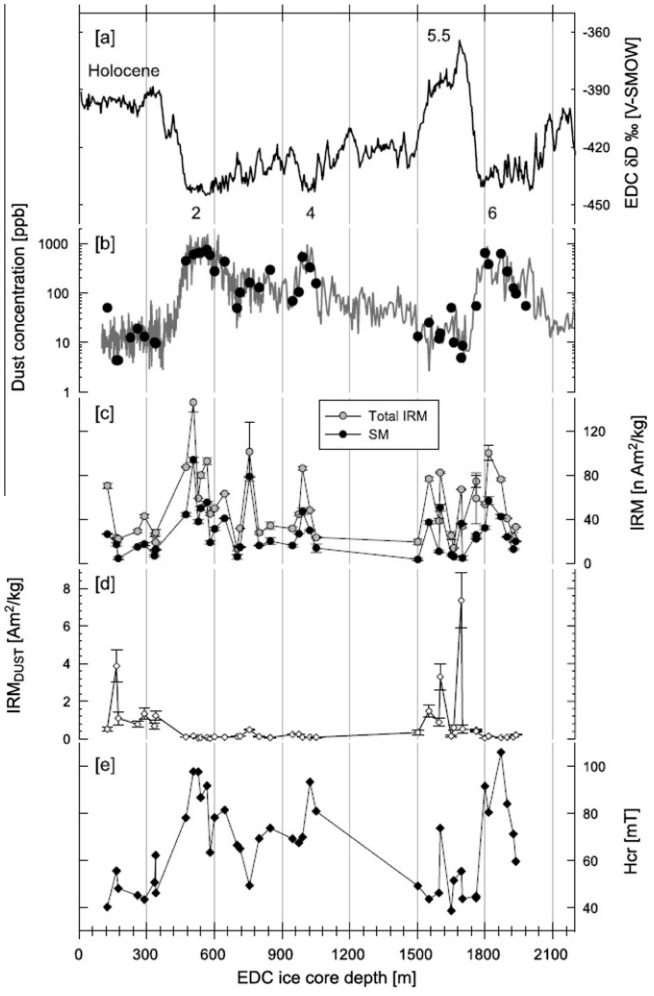


**Fig. 37.** Magnetic properties, $\delta D$ values and dust concentration (ppb) in the EDC ice core. The circles identify dust concentrations in samples measured here and for which magnetic properties have been measured on adjacent samples. SM = the stable magnetisation. From Lanci et al. (2008).

the Taklimakan and Tengger/MuUs deserts of China and Mongolia, respectively (e.g. Bory et al., 2003a,b). For Antarctica, the current consensus, again drawn from isotopic evidence, is that Patagonian sources dominated aeolian supply during glacial stages, with some subsidiary input from Australia during interglaciations (Marino et al., 2008; Revel-Rolland et al., 2006).

Initial attempts to apply magnetic measurements to ice core samples were hindered by use of room temperature fluxgate magnetometry, with inadequate sensitivity levels for the low concentrations of dust in the ice (Sahota et al., 1996). More recent work, using SQUID magnetometry, has identified measurable concentrations of dust-sourced magnetic minerals in polar ice cores and, in the case of Antarctic ice, climate-linked variations in ice magnetic mineralogy (Lanci et al., 2001, 2004, 2008; Lanci and Kent, 2006). The sensitivity of the magnetic analyses offers the potential for significantly improved temporal resolution of changes in dust mineralogy and provenance. Compared with isotopic analyses, ice magnetic measurements can be made on much smaller samples (e.g. ~5–7 cm long-samples from the EPICA-Dome C ice core, Lanci et al., 2008).

By making direct measurements of ice $IRM_{1\,T}$ at two different temperatures, 77 and 256 K, the respective IRM contributions of ultrafine (SP) and larger magnetic particles have been identified in polar ice samples. At 77 K, a proportion of the nanoscale, SP particles are magnetically 'blocked in' and provide a relatively large IRM contribution in the Vostok and EPICA cores, and a smaller 'background' contribution in the NGRIP ice. The size range of these SP grains is estimated to be ~7–17 nm, but possible variations in grain oxidation (Ozdemir et al., 1993) require that such estimates be treated with caution. At 256 K (i.e. freezer temperature), much of this IRM carried by the SP particles relaxes, due to thermal agitation. The source of the SP particles has been attributed to extra-terrestrial, micrometeoritic supply (Lanci and Kent, 2006, and see Fig. 13a). Larger (>SP) particles show much less change upon sample warming from 77 to 256 K. For the NGRIP ice samples, this 'stable' magnetic remanence is directly proportional to the measured dust concentration in the ice. For NGRIP samples, the mean IRM of the ice is higher by a factor of 3 in glacial compared with interglacial stages, with the notable exception of Holocene ice samples, which display higher magnetic concentrations (despite having much lower dust contents) than the few LGM ice samples measured thus far (Lanci et al., 2004). The magnetic mineralogy of the NGRIP samples seems relatively constant through glacial and interglacial stages, a mix of magnetite/maghemite and haematite, not dissimilar from pristine Chinese loess samples.

For the Antarctic ice samples, the situation is more complex. Whilst the total measured IRM is higher in glacial stage-ice (in association with increased dust concentrations), the 'stable' (non-SP) IRM, normalised for dust mass, appears both higher (10–40×) and more variable during interglaciations (Fig. 37). Several interglacial EPICA samples also display extremely high IRM values (up to ~8 A $m^2$ $kg^{-1}$), exceeding even the IRMs of possible volcanic source rocks. Caution is required given such high values, with the possibility of IRM errors arising from the extremely low interglacial dust mass, and/or from contamination, e.g. from drilling fluids. The coercivity of remanence of the ice +dust also varies with climate stage.

Interglacial samples display lower $(B_0)_{CR}$ values (~40–60 mT) than glacial samples (~50–100 mT). These data consistently suggest variations in dust magnetic mineralogy, and thus in Antarctic dust source.

### 7.2. Sub-polar ice cores

In addition to the polar ice cores, low-latitude, high-altitude ice caps provide an additional, sensitive archive of climate and of dust (Thompson et al., 1997, 2006). On the Tibetan Plateau, in the Qilian Shan on the north-central margin of the Plateau (38°6′ N, 92°24′ E), lies the ~138-m thick Dunde ice cap, with an area of 60 $km^2$ and a summit elevation of 5325 m. The ice cap survives in a presently arid environment, lying between the Qaidam Basin (the highest desert in China) and the Gobi Desert. Three cores to bedrock were recovered from the ice cap summit in 1987: Core D-1 (139.8 m), Core D-2 (136.6 m) and Core D-3 (138.4 m) and microparticle and calcium concentration data reported (Thompson et al., 1990). The upper parts of the ice core have been dated using a combination of $\delta^{18}O$ seasonal variations and their relationship with dirt layers in the ice. Microparticle counts show that dust concentrations in the ice were highest (×10) during the LGM, in association with colder, wetter conditions, and diminished in the Holocene. The morphological properties of the particles in the LGM ice match those of the central Chinese Loess Plateau, which accumulated episodically and most rapidly during the deglacial phases of the Pleistocene glacial stages (e.g. at ~16 ka BP for the last glacial stage).

Magnetic measurements on a pilot set of Dunde ice samples (Holocene and LGM, melted and Millipore-filtered) reveal clear differences in magnetic particle concentration and mineralogy between climate stages, and offer some preliminary indication of dust source changes. The Holocene ice core samples display lower $\chi$ values, indicating (together with the microparticle counts) lower dust concentrations, and higher Hcr/Hc values (Fig. 38), indicating coarse magnetic grain size (>~20 μm). For the LGM samples, the $\chi$ values are variable but up to 10× higher (in tandem with the particle counts) and most fall within the finer, PSD size range on the Day plot. For comparison, data are also shown for some modern desert (the Taklimakan) and LGM Chinese loess samples (spanning the Plateau). The Holocene samples from Dunde occupy a similar range of values as the coarse-grained Taklimakan samples. In contrast, the LGM ice contains dust of finer size, resembling the finer Taklimakan samples and the well-mixed, Chinese loess samples (see Section 8.2).

These preliminary data identify the potential for magnetic measurements to identify dust fluxes, mineralogy and grain size in ice core samples, and to examine possible source areas for provenancing of the dust through space and time.

## 8. Magnetic properties as palaeo-dust records: desert sediments

### 8.1. Dune sand redness

For desert sediments, the environmental significance of iron oxide-induced variations in colour has long been debated, with regard to dune provenance, age, and movement (e.g. Lancaster and Ollier, 1983; Pye, 1981, 1989). The Namib Sand Sea, for example, displays strong increases in sand redness from the western coastal to the eastern inland zone, attributed to increasing concentrations of haematite, as surface coatings on quartz grains (Lancaster, 1989). Using very high-field magnetic remanence measurements (i.e. in dc fields of up to 9 T), Walden et al. (2000) were able to show the additional presence of goethite in the sands. Thus, environmental interpretations based on haematite genesis alone are no longer valid. They also demonstrated, however, a clear geographic and lithological split in goethite concentrations; samples to the west, overlying the Karpfencliff Conglomerate, having higher goethite contents than the more reddened samples to the east (overlying the Tsondab Sandstone). The latter also contain more ferrimagnetic (magnetite-like) minerals. Recently-obtained data on a range of haematite and goethite samples of known grain size and degree of substitution (Liu et al., 2002, 2006b; Maher et al., 2004) may enable more detailed, *post hoc* analysis of these miner-

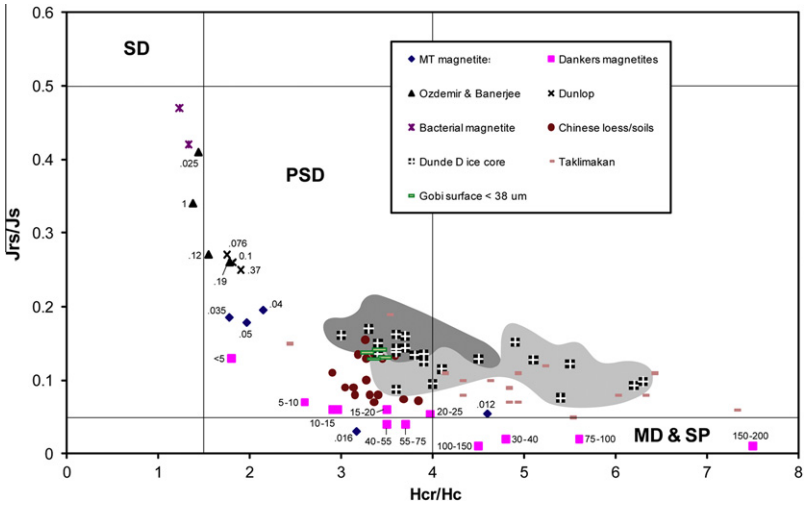


**Fig. 38.** A Day plot (Day et al., 1977) for samples from the Dunde D ice core, plotted with magnetites of known grain sizes (grain size in μm shown for each point), and potential source samples (the Chinese Loess, Taklimakan Desert, the Gobi Desert). Dunde samples in the light grey data envelope are Holocene-age samples (core depths 44–128 m); samples in the dark grey data envelope are Last Glacial-age (core depths 134–139 m). Ice core samples kindly provided by Lonnie Thompson. Taklimakan data from Torii et al. (2001).

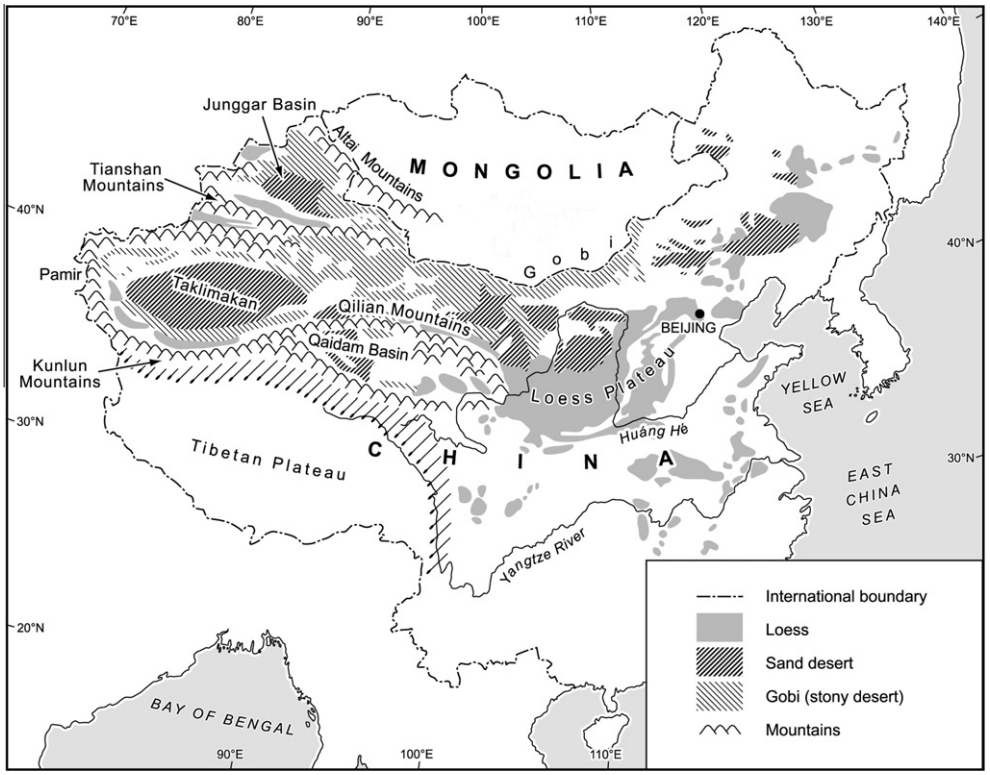


**Fig. 39.** Location of the Chinese Loess Plateau and its potential desert source regions.

alogical variations, with the aim of disentangling the respective roles of climate, geology and time in this desert context.

### 8.2. The desert sources of the Chinese Loess Plateau

Vast arid areas surround the loess sequences of the famous Chinese Loess Plateau (Fig. 39). The source of this, the world's most extensive deposit of Quaternary loess, has long been held to be the northern deserts (especially the Gobi Desert), since the loess sequences display increasing thicknesses, accumulation rates and clastic particle size from southeast to northwest across the Plateau (e.g. Sun et al., 2008; An et al., 1990, 2000b; An, 2000). Geochemical analyses of last glacial stage loesses across the Plateau also indicate north-south variations in zirconium/rubidium ratios, but little west-to-east variability (Chen et al., 2003, 2006). Use of electron spin resonance measurements for characterisation (rather than dating) of quartz grains (Sun et al., 2008) has further suggested that the Gobi, and two other sandy northern deserts (the Tengger and Badain Juran), have been the dominant loess source during the last climatic cycle.

However, as noted by Mahowald et al. (1999), no potential source area can be either confirmed or discounted until it has been

sampled and characterised – preferably using independent and multiple methods of analysis, rather than any single technique, in order to avoid spurious or non-unique source identification (Maher et al., 2009a, 2009b). Given that mineralogical, isotopic and elemental signatures can vary widely with particle size, it is also preferable that analyses are performed on a particle size-specific basis.

To the north and west of the Loess Plateau lie vast, arid areas, $\sim 350–400 \times 10^4$ km$^2$ (Liu, 1988), all of which constitute potential source areas for the Quaternary wedge of loess sediment contained within the Loess Plateau. These source areas include more than twelve desert regions, including the Tengger, Mu Us, Junggar, Qaidam, Badain Jaran and the Gobi of Inner Mongolia (Fig. 39). Critically, however, whilst most atmospheric dust particles are <50 μm in diameter, >90% of particles present in most Chinese deserts exceed this size range (Tsoar and Pye, 1987). Just three desert areas contain sediments with sufficiently fine particle size distributions to contribute effectively to dust deflation: the Gobi of the western Inner Mongolia Plateau, the Gobi of the central Inner Mongolia Plateau, and the western Taklimakan (e.g. Wang et al., 2004). Of these, the Taklimakan Desert is the largest ($\sim 3.5 \times 10^3$ km$^2$), and subjected to severe and high-frequency dust storm activity (Pye and Zhou, 1989), but most distal from the Loess Plateau, which lies ~2000 km to the east.

Magnetic and elemental analyses have been applied to surface samples from the northern and central Gobi, from an area spanning ~12,000 km, within dune fields and alluvial fan sediments subjected to wind erosion (Maher et al., 2009a, 2009b). Magnetic measurements, X-ray powder diffraction and X-ray fluorescence were applied to sized clastic fractions (> and <38 μm), and the resulting data compared with least weathered loess samples from the last glacial stage, spanning the Loess Plateau.

The Gobi sediments show little if any magnetic, elemental or mineralogical overlap with the Chinese loesses (Fig. 40). Not only are the Gobi sediments more magnetic (~0.2–0.6 wt% magnetite) than the unweathered loess (~0.05 wt% magnetite), they have lower $SiO_2$ contents, higher $Fe_2O_3/TiO_2$ and lower $Al_2O_3/TiO_2$ ratios. Given their respective $\chi$ values, the Gobi sediments could only contribute to the Chinese loess if they were admixed with very large volumes of diamagnetic material (e.g. 1 part Gobi with 80 parts $CaCO_3$).

The rather variable mineralogy of the Gobi sediments also contrasts starkly with the remarkably homogenous nature of the Chinese loess (Fig. 40), despite samples spanning the marked west-east rainfall and weathering gradient across the Loess Plateau. This homogeneity indicates that the loess has been extremely well mixed prior to deposition downwind from its source(s), a finding independently corroborated by rather uniform REE patterns and restricted Nd isotopic compositions (Jahn et al., 2001).

Given the observed mineralogical mismatches between the Gobi surface sediments and the Chinese loess, the distal but appropriately fine-grained Taklimakan Desert requires evaluation as a possible major dust source for the Chinese Loess Plateau. Magnetic analysis of surface samples from the Taklimakan desert (Torii et al., 2001) reveals similarities with the unweathered Chinese loess. The Taklimakan sediments have $\chi$ values in the range 20–$40 \times 10^{-8}$ m$^3$ kg$^{-1}$, they contain only slightly oxidised, lithogenic magnetite (not Ti-magnetite), with an average grain size of ~5 μm, and minor amounts of haematite/possibly goethite. Comparison of magnetite grain size from the Taklimakan surface sediments to the west, with unweathered loess from Shajinping (western Loess Plateau) and from Luochuan (central Loess Plateau) indicates progressively finer magnetite grain size, compatible with increased distance along a dust transport path from the western desert region (Torii et al., 2001). If, as these data suggest, the Taklimakan has been a significant dust source and/or 'mixing area' for the Chinese Loess Plateau, then wind directions would have been different from those of the present day, with stronger near-surface westerlies during the winter/early spring seasons.

As noted by Maher and Thompson (1999), an additional clue to the provenance of the Chinese loess arises from its relatively high beryllium-10 loadings ($\sim 0.5–5.5 \times 10^8$ atoms g$^{-1}$; e.g. Beer et al., 1993), in combination with its low $\chi$ ($\sim 20–30 \times 10^{-8}$ m$^3$ kg$^{-1}$). Given average $^{10}$Be fluxes (Pavich et al., 1986), prolonged exposure (>1 million years) in a humid but cold environment is required to account (a) for the loess $^{10}$Be concentrations but (b) the absence of any pedogenic-derived increases in loess magnetic content. The $^{10}$Be/magnetic data thus indicate the tectonically-rising Himalayan/Tibetan regions as a major possible loess source; thick beds of periglacial and/or glaciogenic silt occur on the Tibetan Plateau (Fig. 41). Southwesterly winter winds blow from the Himalayas and Tibet towards the deserts north and west of the Loess Plateau (Fig. 42). These surface winter winds may have formed the first of a two-stage transport path for Tibetan/Himalayan dust. In a second transport step, intensified springtime (north)westerlies may have subsequently carried the dust to the southeast, across the Loess Plateau.

## 9. Quaternary loess/palaeosol sequences

Magnetic studies of loess sequences have proliferated over the last 20 years; more than 2000 papers having been published on their palaeomagnetic and/or environmental magnetic properties.

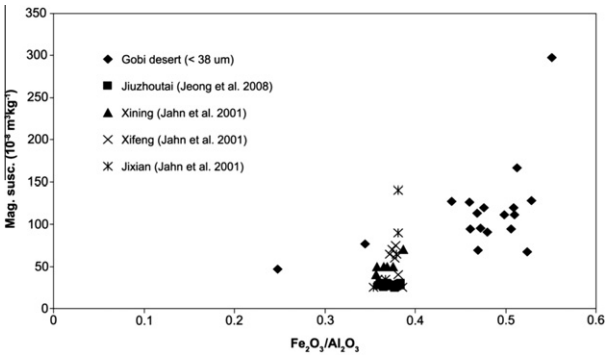


**Fig. 40.** Magnetic susceptibility ($10^{-8}$ m$^3$ kg$^{-1}$) vs $Fe_2O_3/Al_2O_3$ for LGM loess units across the Chinese Loess Plateau and potential source samples (<38 μm) from the Gobi Desert. From Maher et al. (2009a,b).

**Fig. 41.** Outcrop of glacigenic silt, Tibetan Plateau.

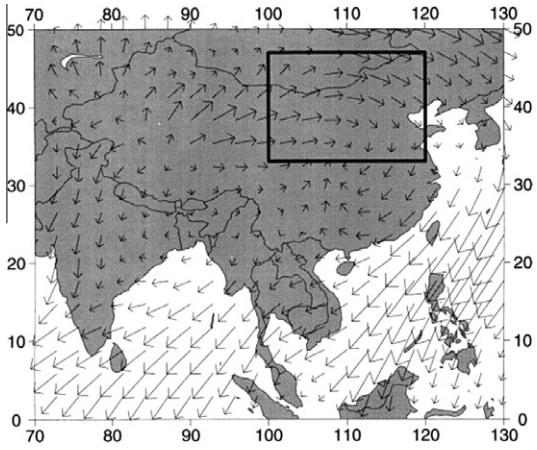


**Fig. 42.** GCM-modelled surface wind directions and intensity, for the LGM. The box outline denotes the area of the Chinese Loess Plateau. From Maher and Thompson (1999).

This rich record of scientific investigation reflects the intersection between the widespread, climate-dependent occurrences of loess, and the sensitivity (and speed) of magnetic analyses.

### 9.1. The environmental significance of loess

Sequences of loess comprise accumulations of windblown, clastic sediments, often interbedded with fossil soils (palaeosols). Loess sediments provide not only a key agricultural resource but also represent key aeolian archives on every continent (Fig. 43). High-resolution loess/palaeosol sequences can provide quantitative information on the interactions between aerosols and climate. They can be dated (e.g. by luminescence, Roberts, 2008), to provide a record of changing rates of dust transport and accumulation over large continental areas. Loess sequences incorporate mineralogical, physical and chemical information on the nature of the transported dust (e.g. Prins et al., 2007; Sun et al., 2008), of potential significance for climate radiative and/or cloud forcing, and/or for iron supply and biogeochemical cycling in the ocean.

Loess sequences girdle the planet, reaching $\gg$10 s of metres vertical thickness, often reflecting enhanced glacial-stage production (and transport) of fine particles – not only by glacial comminution and freeze-thaw, but also by surface desiccation, aided by vegetation loss and wind-driven 'sand-blasting' from inter-particle collisions (e.g. Alfaro et al., 1997; Grini and Zender, 2004). In North America, for instance, loess sequences in Nebraska, which display some of the highest sediment accumulation rates so far recorded in loess (>6700 g $m^{-2}$ $a^{-1}$, Roberts et al., 2003), result from desiccation and expansion of the Great Plains area, rather than from glacial production of silt-sized particles (Aleinikoff et al., 2008). For the Eurasian region of the northern hemisphere, loess almost continuously spans Eurasia from west to east at mid-latitudes (~30–50°N), reflecting dust supply both from arid/semi-arid and glacigenic sources (e.g. Frechen et al., 2003).

Extensive loess sequences can act not only as dust sinks but as dust sources. The world's most extensive Cenozoic accumulation of loess, the Chinese Loess Plateau, comprises $\sim 2 \times 10^5$ $km^3$ of extremely well-mixed, windblown dust, but has itself been a major dust source for the ocean sediments of the northwestern and equatorial Pacific (Rea and Hovan, 1995; Shigemitsu et al., 2007), the volcanic soils of Hawai'i (Chadwick et al., 1999), and the accumulating ice caps of Greenland (Bory et al., 2003a,b). Emissions of iron-bearing dust from the Loess Plateau may have influenced past atmospheric $CO_2$ concentrations via changes in productivity of the HNLC region of the northwest Pacific. Dust emitted from palaeosol surfaces (see below) may have been particularly reactive in biogeochemical terms; it will have contained a range of nanoscale iron oxides and hydroxides (spanning the mineral spectrum from magnetite, slightly oxidised magnetite and maghemite, to haematite and goethite, see Section 9.5.2 below), in close association with soil organic matter (Maher and Thompson, 1995).

Magnetic methods have played two key roles in loess studies; first, in determining the chronology of loess/palaeosol sequences; and second, in identifying their post-depositional response to the range of climates to which they have been subjected through the late-Cenozoic.

### 9.2. Palaeomagnetic dating of loess/palaeosol sequences

For many loess sequences, palaeomagnetic dating has been the fundamental plank upon which age models have been erected. For example, Bidegain et al. (2005, 2007) identified the Matuyama–Brunhes boundary (MBB) in the Pampean loessic deposits of the Buenos Aires province. Loess deposition in Alaska (the Gold Hill sequence) has been shown to date back to ~3 Ma BP (Westgate et al.,

**Fig. 43.** The global distribution of loess deposits (modified from Pye, 1989, and http://serc.carleton.edu/vignettes/collection/25463.html).

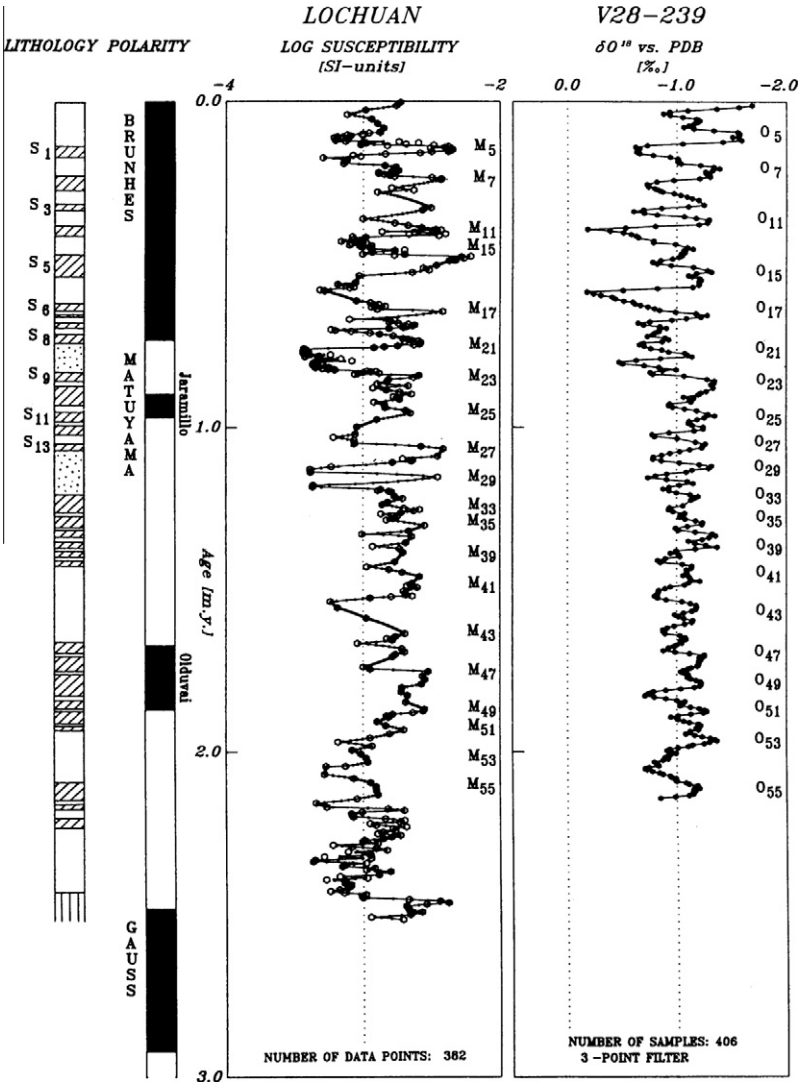


**Fig. 44.** Reversal magnetostratigraphy for the loess/palaeosol sequences of the central Chinese Loess Plateau, Luochuan (from Heller and Liu, 1982). $S_n$ = palaeosol$_n$.

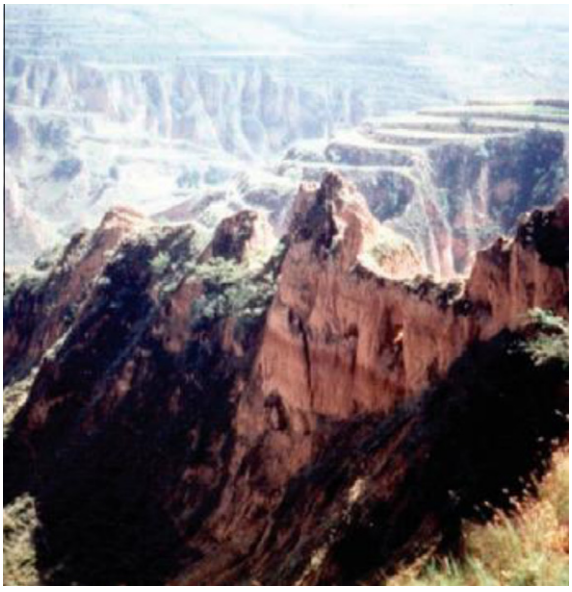

**Fig. 45.** The interbedded loess and palaeosols of the Chinese Loess Plateau at Luochaun (central Loess Plateau), photo by Maher.

1990). Other complete Plio/Pleistocene loess/soil sequences include the Karamaidan site, Tajikistan (Forster and Heller, 1994; Ding et al., 2002a). For the Chinese Loess Plateau, the long sequences of the central region, for example, at Luochuan and Baoji, provide the 'classic' and complete Pleistocene loess magnetostratigraphies (Fig. 44). Conversely, sites in the western Chinese Loess Plateau provide the high MARs and lowest intensity of pedogenic magnetic overprinting to optimise recording of geomagnetic excursions like the Blake event (~120 kyr BP).

Regarding the >30 interbedded loess and palaeosol units of the Chinese Loess Plateau (Fig. 45), the basal age was thought to be ~1 Ma BP, until the 1980s, when collaboration between Friedrich Heller and Liu Tung-Sheng enabled isolation (by thermal demagnetisation) of the loess depositional remanence, and conclusive evidence that the loess records some 2.5 Myrof Earth and climate history (Fig. 44; Heller and Liu, 1982, 1984; Heller and Tungsheng, 1986). Critically, not only were Heller and Liu able to show the unambiguous recording of all six major geomagnetic polarity reversals from this time period. They also demonstrated that the loess/palaeosol $\chi$ record showed strong coherence with the deep sea oxygen isotope record (Fig. 44). Correlation of these two independent proxies provided a much more detailed chronology than gained from the reversal magnetostratigraphy alone. Since these

early days, higher-resolution palaeomagnetic dating has been sought for the Chinese sequences using geomagnetic events, especially the Blake (e.g. Zhu et al., 1994, 1998, 1999; Fang et al., 1997), excursions (Zhu et al., 1999; Pan et al., 2002) and reversal transition features, allied with improved mathematical correlation and interpolation techniques (e.g. Ding et al., 1994, 2002b; Guo et al., 2002; Thompson and Maher, 1995; Heslop et al., 2000, 2002b). The variable effects of pedogenic magnetic 'overprinting' caused the observed discrepancy in reversal boundaries, with the Matuyama–Brunhes boundary (MBB), for example, apparently located within a glacial-stage loess (e.g. Sun et al., 1993), rather than MIS 19 (Tauxe et al., 1996). The palaeomagnetic 'lock-in' depth in the Chinese loess/palaeosols has been estimated to be as much as 2 m, or equivalent to a time delay of $\sim 10^3$–$10^4$ years (Zhou and Shackleton, 1999; Spassov et al., 2003a, 2003b; Liu et al., 2008).

### 9.3. The palaeoclimatic significance of loess/palaeosol magnetic properties

It was evident from the early palaeomagnetic studies that the loess and the interbedded, reddish-brown palaeosol units of the Chinese Loess Plateau display different magnetic properties. The palaeosols display higher values of natural remanent magnetisation (NRM) and $\chi$, the latter up to 3–5× higher than the parent loesses. Palaeosols to the south and east of the Plateau demonstrate increasingly high values, e.g. up to $\sim 400 \times 10^{-8}$ m$^3$ kg$^{-1}$ at Baoji, compared with the unweathered western loess, with a $\chi$ of $\sim 25 \times 10^{-8}$ m$^3$ kg$^{-1}$ (Fig. 46).

The palaeosols also required extensive thermal demagnetisation to remove unstable remanences carried by 'over-printing', post-depositional magnetic components. Heller and Liu (1984,1991) concluded that these palaeosol magnetic properties indicated climatically-controlled chemical alteration from the parent loess, with decalcification and soil compaction causing relative enrichment of the aeolian, detrital magnetic minerals in the interglacial palaeosol horizons. In contrast, Kukla and colleagues suggested that a constant rate of subaerial magnetic dustfall was diluted during glacial stages by large volumes of low $\chi$-dust (Kukla, 1987; Kukla et al., 1988, 1990). These hypotheses did not consider the possibility of *in situ*, pedogenic formation of magnetite, a process observed in well-drained modern soils in the temperate zone (Mullins, 1977; Longworth et al., 1979; Maher, 1986; Maher and Taylor, 1988; see Section 3.3.2).

Thence began the increasingly detailed magnetic analysis of loess and palaeosols around the world, with the aim of using palaeosol magnetic properties to make quantitative reconstructions of climate (especially of rainfall) right through the timespan of these natural Quaternary archives. For good reasons, this aim has been achieved most successfully in the homogenous, low-$\chi$ loesses of China (Heller et al., 1993; Maher et al., 1994; Lie et al., 1995; Sun et al., 1996; Hao and Guo, 2005) and Russia (Alekseeva et al., 2007). Attempts to apply the climate/magnetism relationship displayed at *these* sites to other locations worldwide have met, predictably, with mixed results. As shown by modern soil analogues, 'interpretation of palaeosol magnetic properties must be done on a *site-specific basis*, taking into account the possibilities of *pedogenic enhancement, pedogenic dilution or depletion, and allochthonous inputs of magnetic minerals*. Excessively arid, wet or acid soils are unable to form significant amounts of pedogenic ferrimagnets' (Maher, 1998, *italics added for emphasis*).

### 9.4. Loess/palaeosol magnetic properties around the world

For any sedimentary pile of windblown loess and palaeosols, their magnetic properties will depend on (a) the magnetic content and characteristics of the source material (reflecting sediment provenance), and (b) post-depositional weathering/soil formation processes. As defined classically by Jenny (1941), a soil, or soil property (including, here, any soil magnetic property) is a function of parent material, climate, relief, organisms and soil-forming duration:

$$\text{Soil or soil (magnetic) property} = f(\text{pm, cl, r, o, t})$$

In terms of parent material, the magnetic properties of loess around the world vary widely (Fig. 47). Even within the area of the Chinese Loess Plateau (*sensu lato*), some differences in loess provenance and mineralogy can be seen (Fig. 48).

In notable contrast to the loesses of China and the Russian steppe, many loesses are sourced from adjacent igneous rocks and are thus very strongly magnetic. The least weathered Siberian

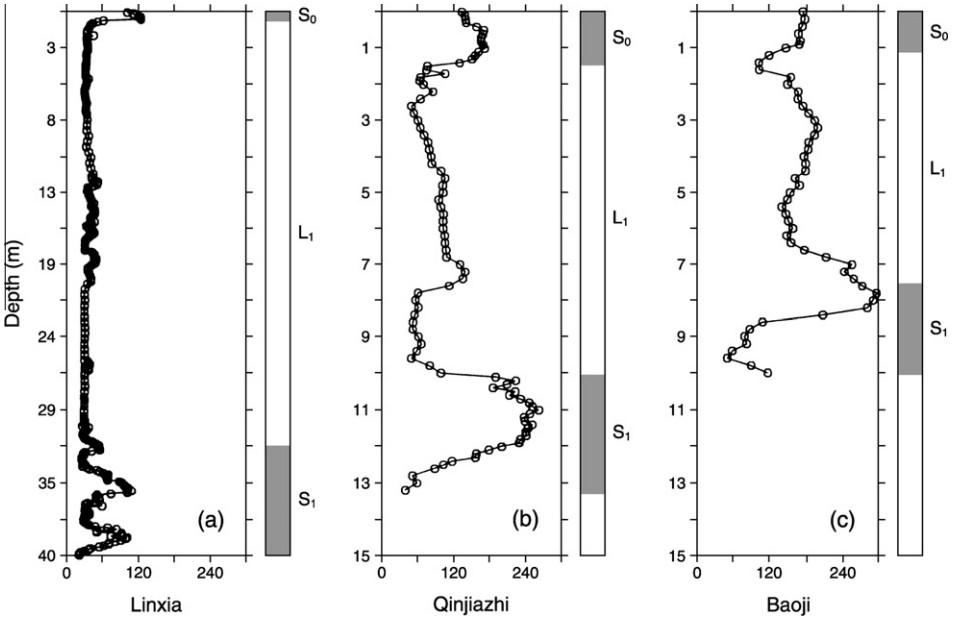


**Fig. 46.** Variations in lithology, sediment thickness and $\chi$ from west (Linxia) to central (Qinjiazhai near Luochuan) and southeast (Baoji) across the Chinese Loess Plateau. From Maher (2005).

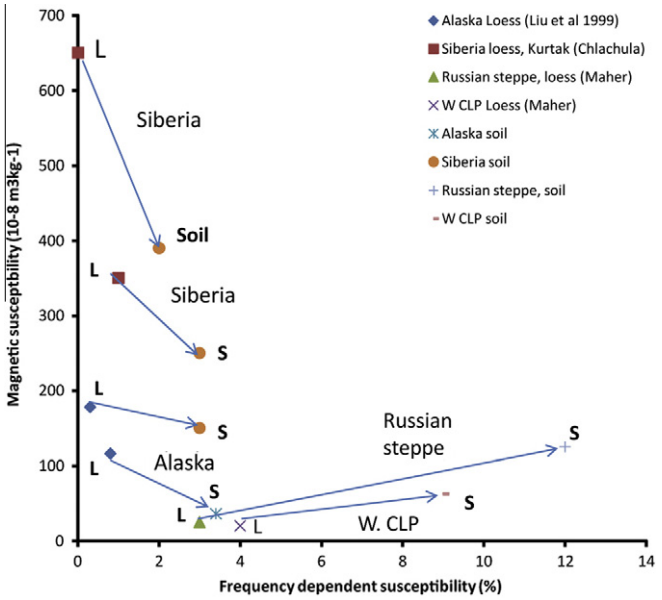


**Fig. 47.** Magnetic susceptibility ($10^{-8}$ m$^3$ kg$^{-1}$) vs $\chi_{fd}$% for unweathered loesses around the world, and of the palaeosols which have developed from these parent materials. L = parent loess, S = palaeosol, W CLP = western Chinese Loess Plateau.

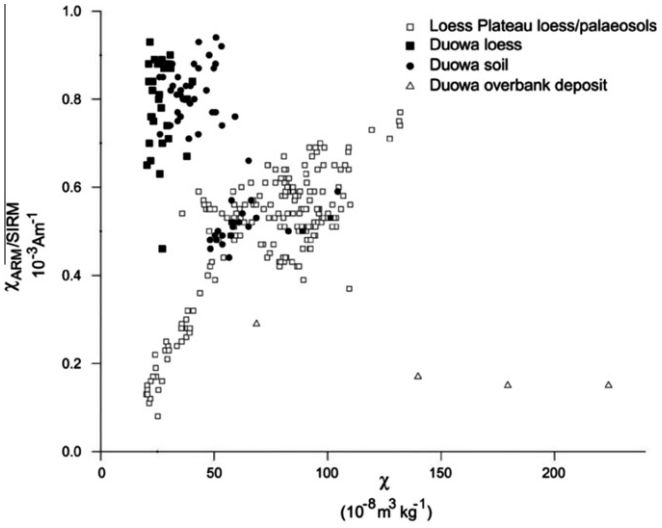


**Fig. 48.** Differences in loess magnetic properties from the western margins of the Loess Plateau (Duowa, close to the China/Qinghai boundary) and the central Loess Plateau. From Maher et al. (2003).

loesses, for example, display $\chi$ values of ~350–650 × $10^{-8}$ m$^3$ kg$^{-1}$ (Chlachula et al., 1998; Matasova et al., 2001) – i.e. 17–32× higher than the Chinese loess. This high magnetic content of the Siberian loess derives from glacially-supplied, detrital, MD ferrimagnets inherited from igneous and metamorphic rocks from the south Siberian mountains (the Altai, Sayan and N. Baikal). In South America, Argentinian loesses display variable but moderately high values, ~200 × $10^{-8}$ m$^3$ kg$^{-1}$ (e.g. Bidegain et al., 2005, 2007), again reflecting proximal supply of volcanogenic material, including volcanic glass. Similarly, Alaskan loesses commonly derive from aeolian transport of volcanic tephra, with pristine loess units displaying $\chi$ values of >~100 × $10^{-8}$ m$^3$ kg$^{-1}$ (Liu et al., 2001).

When strongly magnetic parent materials are subjected to post-depositional soil formation, physical and biogeochemical breakdown of the primary ferrites frequently ensues, leading to diminished soil $\chi$ values (Fig. 47). This process can readily be observed in analogous modern soils (Fig. 49a). The impacts of weathering can be seen most clearly from magnetic measurements on particle-sized soil fractions (Fig. 49b). Comparing the basal soil with the topsoil, each of the coarser particle size fractions (coarse sand – coarse silt) displays a reduction in its % contribution and in its measured $\chi$. The medium silt fraction % contribution increases very slightly, but its $\chi$ also decreases. In contrast, the fine silt and, especially, the clay-sized fractions both increase in terms of their % particle size distribution, and display increased $\chi$ values. The *in situ* formation of characteristically ultrafine-grained soil magnetite is further evidenced by the rise in $\chi_{fd}$% values, from 0 at the soil base to ~5% in the topsoil. Overall, however, the impact of weathering on this strongly magnetic bedrock is to reduce soil $\chi$ values, since the rate of pedogenic magnetite formation is exceeded by the rate of detrital magnetite breakdown.

Whether or not neoformation of ultrafine-grained (<~0.1 μm), substitution-free pedogenic ferrites takes place (countering to some extent the loss of primary detrital grains) depends on the soil-forming conditions at the site. Fig. 50 shows a toposequence of modern soils developed on uniform, metasedimentary parent material (slate): a low-relief, poorly-drained stagnogley at the upland plateau; an excessively-drained acid podsol on the slope shoulder; a well-drained and -buffered cambisol close to the mid-slope; and a seasonally-wet cambisol close to the valley floor. Each soil displays distinctive magnetic characteristics, reflecting their drainage, topographic position, micro-climate and organic activity (parent material and time being constants for each profile). The plateau gley and podsol display little/no evidence of pedogenic ferrite formation; they are too wet or too acidic, respectively (Maher, 1986, 1998).

The mid-slope and toe-slope soils, generally well-drained (and buffered by receipt of bases leached from the upslope soils), both display obvious magnetic enhancement (pedogenic ferrite formation) in their A and B horizons. Such enhancement is evident here from increased values of $\chi$ and $\chi_{fd}$% (but see Maher, 1998 for additional magnetic, XRD, and electron microscopic data on these soil magnetic minerals).

By analogy, Quaternary palaeosols formed under rather harsh (wet/freezing) climates – for example, in Siberia and Alaska – often show both depletion of detrital ferrites and very little ferrite neoformation, reflecting gleying and/or cold-temperature soil formation processes (Fig. 51). Palaeosols in these high latitude locations thus display lower $\chi$ values than the parent loess units. This signal is (a) opposite to the magnetism/palaeosol relationship in China and Russia, and (b) as expected, given the modern soil analogue data. It is additionally possible that these loess/palaeosol magnetic contrasts (Virina et al., 2000; Liu et al., 2001) can be affected by reduced aeolian transport of ferrite-bearing dust during the soil-forming intervals (Vlag et al., 1999).

Given the high initial magnetic content of the parent loess in these locations, it is difficult, if not impossible, to use $\chi$ to identify any pedogenic ferrite formation; any such $\chi$ signal would be relatively extremely small. However, other magnetic parameters, sensitive to the distinctive SP/SD size of pedogenic ferrites (Fig. 10a–f) can instead be used to identify any magnetic enhancement in such soils. Suitable magnetic parameters may include the $\chi_{fd}$ (Forster et al., 1994) and/or anhysteretic susceptibility, normalised for the saturation remanence ($\chi_{ARM/SIRM}$) and the median destructive field of the ARM ($MDF_{ARM}$), all of which discriminate well between MD, SD and SP ferrite grain sizes (Fig. 52). For the Kurtak site (Siberia), minor increases in $\chi_{fd}$ were recorded by Kravchinsky et al. (2008) for the palaeosol horizons, indicative of low concentrations of pedogenic, SP ferrites. For the Halfway House loess and palaeosols of Central Alaska, selected, SP-sensitive hysteresis measurements (ferromagnetic susceptibility/saturation magnetisation) were used

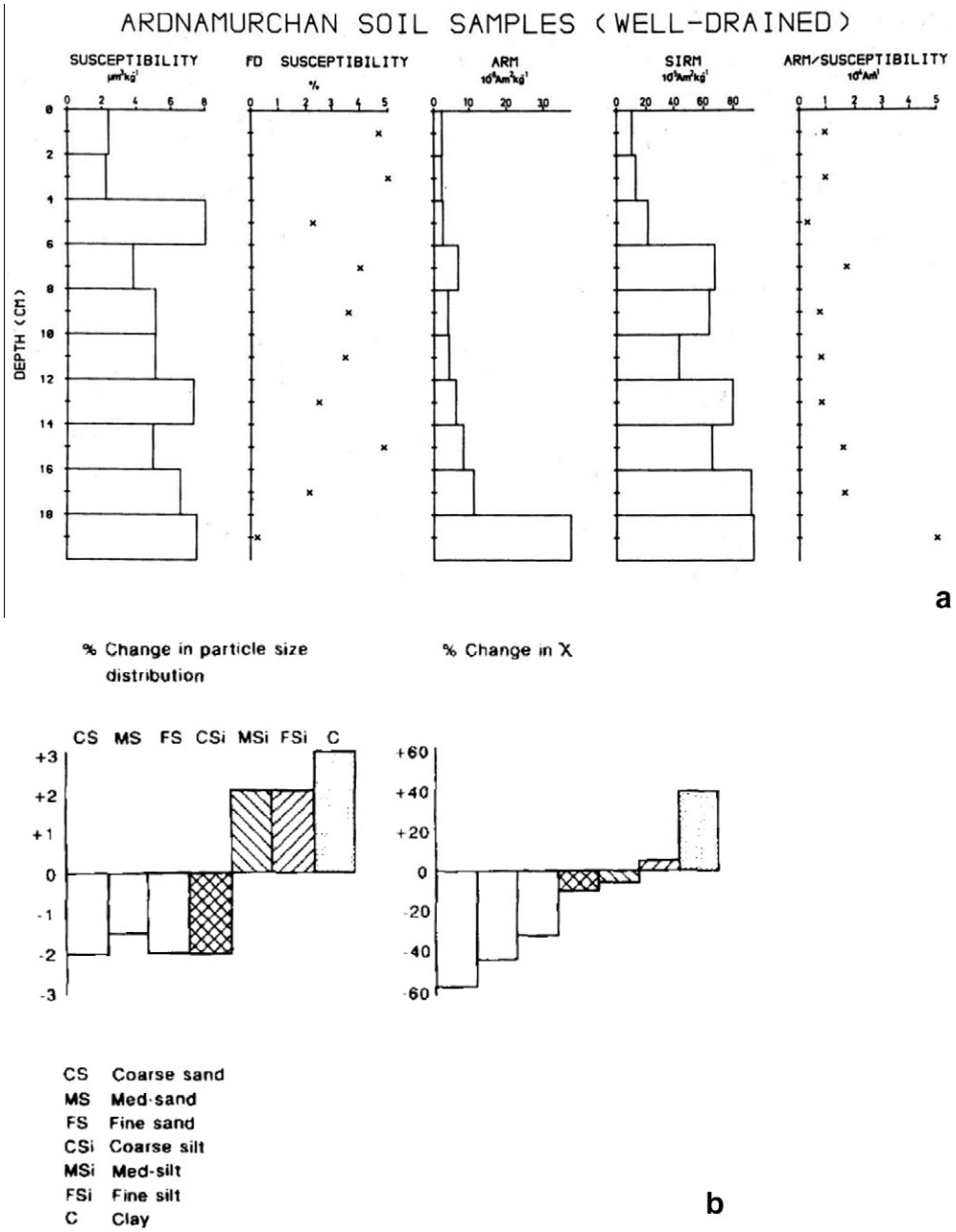


**Fig. 49.** (a) Down-profile magnetic properties for a modern cambisol, developed on strongly magnetic rhyolite, Ardnamurchan, NW Scotland (from Maher, 1988). (b) Down-profile changes in particle size distribution and magnetic susceptibility of each particle size fraction, Ardnamurchan cambisol.

to identify some *in situ* ferrite formation (magnetite oxidised to maghemite), against a spatially varying background of lithogenic magnetites, Ti-magnetites and Ti-haematites inherited from the rhyolitic Old Crow tephra (Lagroix et al., 2004).

For the loess/palaeosol sequences of South America, deciphering of pedogenic magnetic signals has been a thorny process, given spatially variable parent materials (pre- and post-Andean), containing a range of volcanic and pyroclastic magnetic materials, including volcanic glass (e.g. Schellenberger and Veit, 2006). Typical Pampean loess contains abundant plagioclase (up to 65%) and volcanic glass shards and pyroclasts (up to 25%). As with the Alaskan and Siberian sequences, the $\chi$ of many of the Argentinian Pampean palaeosols is lower than in the parent loess (e.g. Orgeira et al., 2009). At the 50-m thick Las Carreras loess/palaeosol sequence, in NW Argentina, for example, palaeomagnetic analysis revealed the MBB at 26.7 m, associated with a soil horizon (MIS 19), and the Jaramillo between ~40 and 50 m depth. The NRMs displayed little viscous overprinting, $\chi_{fd}$% values were generally low (<5%), and $\chi$ maxima ($\sim 300 \times 10^{-8}$ m$^3$ kg$^{-1}$) associated with loessic rather than palaeosol horizons (Schellenberger and Veit, 2006). Exceptionally, some high $\chi$ values were seen in the modern soil and the palaeosol Ah horizons.

The rather weak evidence of pedogenic formation of ferrites in the Pampean palaeosols has been attributed by these authors to the spatial and temporal variability of the magnetic mineralogy of the parent loess, together with quasi-continuous weathering of the loess as it accreted. However, noting that soil magnetic enhancement is evident in modern Pampean soils to the northwest of Buenos Aires but lacking for similar loessic soils to the southeast, Orgeira et al. (2009) also postulate climatic control via differences

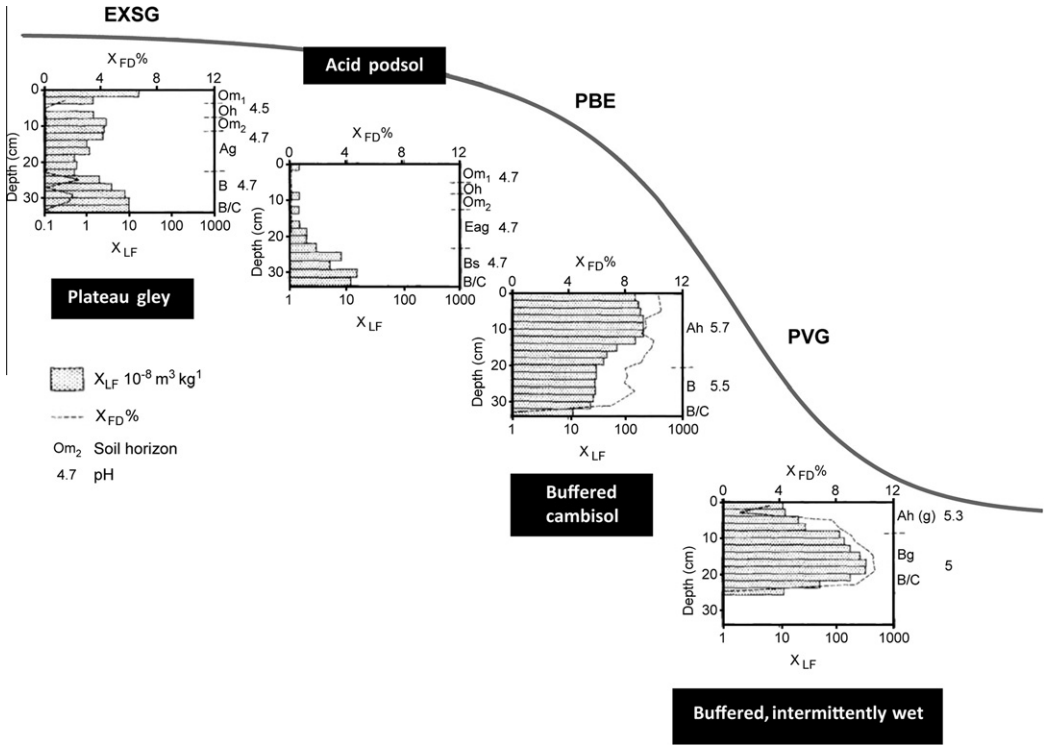


**Fig. 50.** Magnetic susceptibility ($\chi$) and frequency dependent susceptibility ($\chi_{fd}$%) for a toposequence of modern soils, developed on uniform, metasedimentary parent material (slate). From Maher (1998).

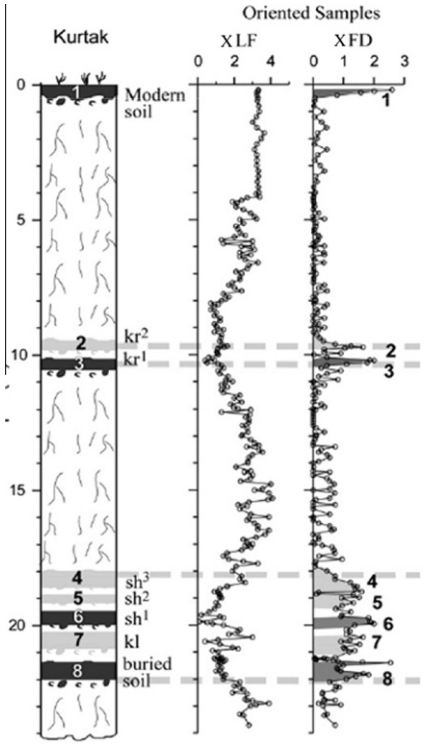


**Fig. 51.** Magnetic susceptibility ($\chi$) and frequency dependent susceptibility ($\chi_{fd}$%) for a loessic palaeosol at Kurtak, Siberia. From Kravchinsky et al. (2008).

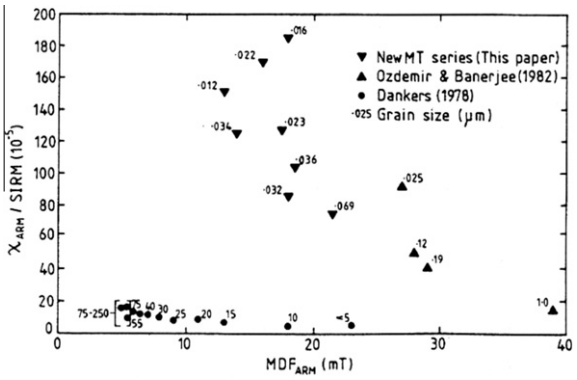


**Fig. 52.** Magnetic granulometry based on $\chi_{ARM/SIRM}$ and the median destructive field of the ARM ($MDF_{ARM}$) for magnetite powders of known grain size. From Maher (1988).

in effective rainfall (i.e. precipitation – potential evapotranspiration). For the NW site (Zarate), they suggest that negative effective rainfall values (precipitation – potential evapotranspiration) result in formation and preservation of pedogenic ferrites, in contrast to the SE site (Veronica) where positive effective rainfall incurs excess soil wetness and dissolution of SP ferrites (Maher, 1986, 1998; Hanesch and Scholger, 2005). Such an approach attempts to refine the soil magnetism/rainfall relationship, as developed in the context of the Chinese Loess Plateau (see Section 9.5.1).

Similarly, a detailed magnetic study of 6 palaeosol units from a ~1.9 Myr-long loess record in the central eastern Pampas (Buenos Aires Province) reveals consistently low levels of ultrafine (pedogenic) ferrites, with little enhancement of $\chi$ and low values (<4%) of $\chi_{fd}$% (Heil et al., 2010). Again, the Pampas magnetic signature seems to reflect changes in magnetic input by aeolian transport (supplemented episodically by rather meager pedogenic enhancement), and *in situ* magnetic loss, by dissolution of ferrites in gleyed palaeosol horizons. Alternation between periods of landscape stability – associated with clearly developed soil horizonation – and periods of increased sedimentation, leading to superimposed,

welded soils, appears to be a feature of Plio-Pleistocene loess/soil development in this region (Kemp et al., 2006). Such cyclicity renders differentiation of individual soil profiles and palaeoclimate response difficult at anything other than long wave-length resolution. Potential may exist for use of pedogenic haematite, rather than magnetite, as a palaeoclimatic indicator for these soils (Carter-Stiglitz et al., 2006).

For the North American mid-continent, loessic modern soils spanning the Great Plains demonstrate soil magnetic enhancement in tandem with a mean annual precipitation (MAP) gradient of <500 mm in southwestern Nebraska to ~1000 mm in central Missouri (Geiss and Zanner, 2006, 2007). These authors calculate dimensionless magnetic enhancement ratios ($M_{enhanced}/M_{parent\ material}$) using several different parameters ($\chi$, IRM, ARM), and find highest correlation between MAP and ARM enhancement. These Midwestern North American soils display less magnetic enhancement per unit of precipitation than do the modern soils of the Chinese Loess Plateau and the Russian steppe (see Section 9.5.1). This disparity is attributed by these authors to differences in parent material and resultant availability of iron for weathering and conversion into pedogenic ferrites (Geiss et al., 2008). Additionally, however, as suggested by Orgeira et al. (2009, in press), regional differences in the effective rainfall (taking into account soil moisture as controlled both by precipitation and evapotranspiration) may play a role in varying magnetic enhancement rates (see Section 9.5).

The loess and loessic sequences of the North African region potentially provide a record of changes in precipitation and wind direction in this climatically vulnerable region. In mainland North Africa, loess occurs in sequences up to ~20 m thick, in the peridesert area to the north of the Sahara. The most well-known loess area lies on the Matmata Plateau, southern Tunisia (Coude-Gaussen et al., 1987; Grousset et al., 1992b). Luminescence dating suggests that these loess sequences span the time interval from ~100 to 245 ka BP (Dearing et al., 1999). Within these sediments, four or five distinct palaeosols occur, characterised by rubification, leaching of carbonate and variable degrees of ped development. As with the loess and palaeosols of the Chinese Loess Plateau (Section 9.5.1), each of the Tunisian palaeosols displays enhancement of its ultrafine-grained ferrimagnetic content, with $\chi$ values 2–3× higher (30–40 $10^{-8}$ $m^3$ $kg^{-1}$) than the parent loess, and $\chi_{fd}$% reaching values as high as 10%. Comparison between the $\chi$ and $\chi_{fd}$% of modern surface soils in the area with modern climate variables shows that peak soil magnetic values occur in association with MAP values of 400–500 mm. All effective precipitation in this area falls during the winter period, December to March. MAP values of ~350–400 mm appear to represent rainfall thresholds for intense pedogenesis. Based on a chronology derived from thermoluminescence methods, the palaeosols and their inferred increases in winter rainfall are linked with interglacial and interstadial stages (Fig. 53). In detail, the S1 and S3 palaeosols (at the Techine site) appear to correlate with MIS 5.5 (123 ka BP) and MIS 7.1 (193 ka BP), respectively, and the less well-developed soils S2 and S4 with MIS 6.5 (175 ka BP) and MIS 7.5 (240 ka BP). Dearing et al. (1999) draw on marine palynological data (Van Andel and Tzedakis, 1996) which indicate southward migration of the subtropical high during glacial stages, and resultant northward expansion of arid conditions. Conversely, interglacial stages appear characterised by enhanced humidity and southward expansion of Mediterranean woodland or steppe. To identify broader connections and, specifically, the role of the African monsoon in driving these observed MAP variations, the Tunisian (Techine) loess/soil sequence and chronology can be compared with the precession-forced record of sapropels in the eastern Mediterranean. The majority of Quaternary sapropels (from the Greek *sapros*, putrefaction, and *pelos*, mud) are not only rich in organic matter but also exhibit isotopically light $\delta^{18}O$ values, both attributed to increased Nile run-off during intense African monsoons accompanying precession minima (Rossignol-Strick, 1983). Even lighter $\delta^{18}O$ values have been recorded for sapropels located between Libya and southwest Crete (e.g. Rohling et al., 2002), indicating simultaneous northern penetration of the African monsoon beyond the central Saharan watershed (at ~21°N). Over the Techine time interval, whilst interglacial-age sapropels appear to coincide with palaeosol S1, and possibly also with soils S3 and S4, the glacial/stadial-stage sapropels (dated to MIS 6 and 7.4) have no obvious palaeosol counterparts. Dearing et al. (1999) thus suggest that palaeosols required interglacial temperatures as well as higher MAP rates and/or that the African monsoon exerted little influence on this Tunisian region.

Beguilingly, at the only other reported loessic/colluvial sequence in the North African zone (Lanzarote, Canary Islands), an opposite magnetism/climate signal has been reported; enhanced moisture during glacial and interstadial stages of the last ~180 kyr (Fig. 53; von Suchodoletz et al., 2010). Using clay content and $\chi_{fd}$% of aeolian sediments (trapped in volcanically-dammed valleys) as palaeo-indicators of humidity, these authors identify direct correlation of their proxies with trade wind strength off northwest Africa and inverse correlations both with SSTs in the NE Atlantic and the extent of Mediterranean vegetation (Fig. 54). They suggest as key drivers either glacial enhancement of precipitation from westerly depressions (e.g. Ganopolski et al., 1998) and/or increases in relative humidity due to decreased air temperatures.

If this discrepancy is real, then the climatic influences on the two sets of records must differ significantly. It seems possible that the Tunisian record reflects both African monsoonal rainfall and interglacial temperatures, whilst the Lanzarote record reflects reduced glacial-stage temperatures (linked to cooled North Atlantic SSTs), leading to increased soil moisture. Another possibly key factor in interpretation of these proxy records is changes in seasonality, and the distribution of rainfall and vegetative response. However, in each location, improved age control is critical for identifying more precisely any correlations, leads or lags with other climate proxies both regionally and more globally.

### 9.5. The Chinese Loess Plateau

#### 9.5.1. The Chinese loess and palaeosols as magnetic proxies of climate

Arguably, the most favourable location for magnetic recording of palaeoclimate by loessic palaeosols is the famous Chinese Loess Plateau (followed, probably, by the Russian steppe). Here, the special characteristics of the Loess Plateau are identified with direct regard to Jenny's (1941) soil-forming equation:

$$\text{Soil or soil (magnetic) property} = f(\text{pm},\ \text{r},\ \text{t},\ \text{cl(o)})$$

First, in terms of parent material, the Chinese Loess Plateau comprises remarkably well-mixed, homogenous and weakly magnetic material (Fig. 40 and Section 8.2). The relative magnitude of any pedogenic $\chi$ signal is thus optimised, and readily and robustly measurable. Second, in terms of topography, the loess and palaeosol units mostly occur as wide-reaching (i.e. 100 km), quasi-horizontal layers (Fig. 45). Third, in terms of time, magnetic enhancement in both the modern soils and palaeosols of the Loess Plateau appears to develop very quickly, in parallel with rapid (~100–100 yrs) evolution of soil organic carbon (Thompson and Maher, 1995; Maher et al., 2003). Thus, the maximum value of soil $\chi$ equilibrates with ambient climate and is not time-dependent (unlike the cumulative soil $\chi$, which is likely to increase with soil-forming duration, especially in accreting soils). Fourth, for the Loess Plateau, climate (co-associated with soil organic activity) is therefore isolated as the key soil-forming factor for the magnetic properties of the soils and palaeosols.

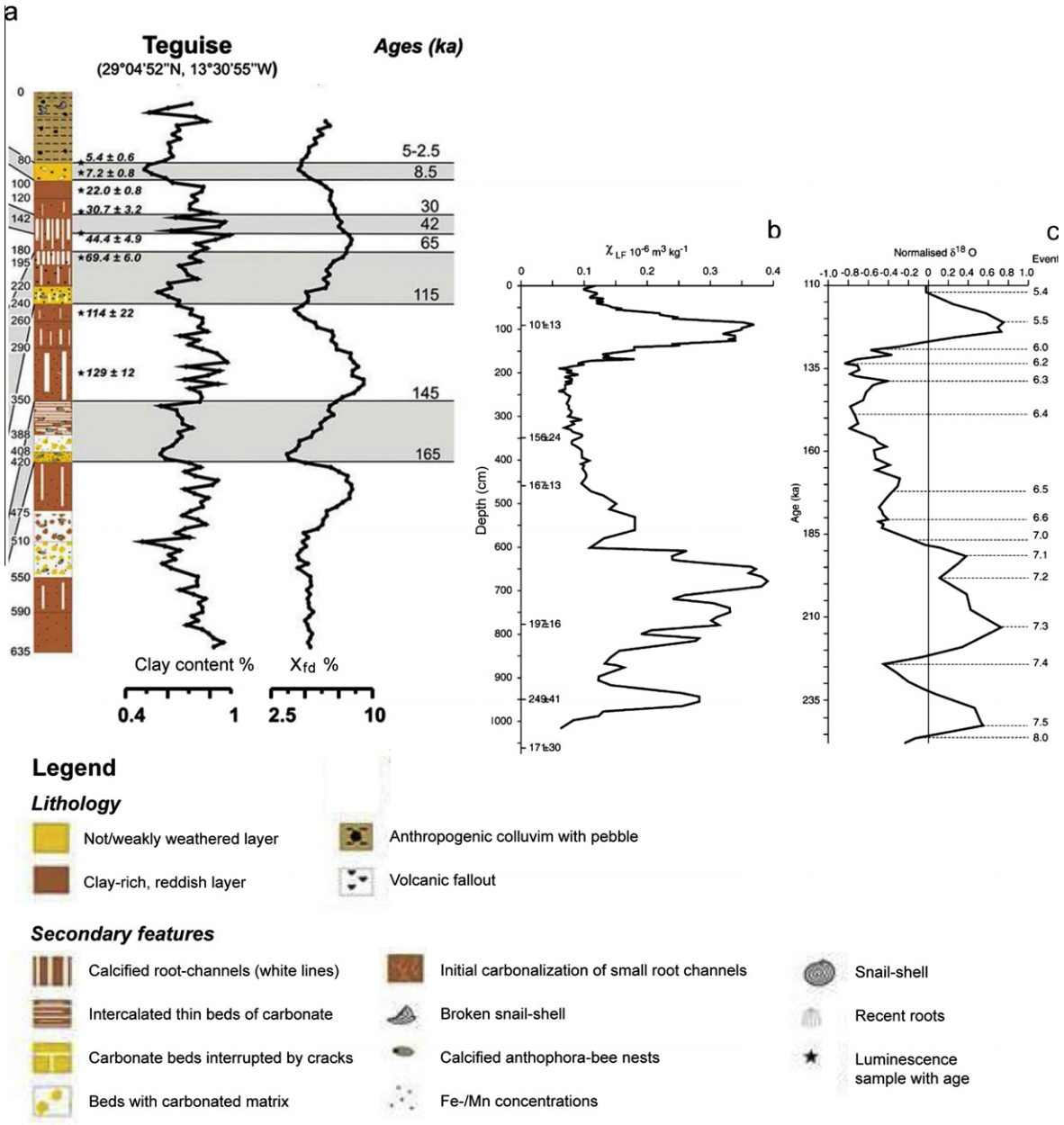


**Fig. 53.** (a) Stratigraphy, clay content (%) and $\chi_{fd}$% for a loessic colluvium, Lanzarote (from von Schudoletz et al., 2010); (b) magnetic susceptibility for the Techine loess/palaeosol sequence from southern Tunisia, correlated with (c) the MIS timescale (from Dearing et al., 2001).

Across monsoonal areas like China, precipitation shows larger variability than does temperature. Examination of the correlation matrix obtained for the pedogenic $\chi$ of modern soils from across the Loess Plateau and the wider northern hemisphere temperate zone, and various temperature parameters and rainfall, shows that a weak but significant positive correlation exists between winter temperature and susceptibility enhancement. However, the dominant explanatory variable is annual rainfall. Because the *in situ*, pedogenic susceptibility signal in the Loess Plateau is large (up to $\sim 350 \times 10^{-8}$ m$^3$ kg$^{-1}$) compared with the weakly magnetic parent loess ($\sim 20 \times 10^{-8}$ m$^3$ kg$^{-1}$), it is sensitive to "pedogenic formation of magnetite, as controlled by regional temperature and rainfall variations" (Maher and Thompson, 1992).

Other magnetic parameters are even more sensitive to the ultrafine SP/SD ferrite fractions which arise from rainfall variations (such as $\chi_{ARM/SIRM}$ and $\chi_{fd}$, Fig. 46). However, because pedogenic susceptibility is demonstrably a reasonably sensitive indicator of annual rainfall across this extensive area ($\sim 440 \times 10^3$ km$^2$), and because $\chi$ is quick and easy to measure, it can be used in order to generate the large spatial and temporal datasets required for palaeorainfall reconstruction across this region (Maher et al., 1994; Sun et al., 1996; Hao and Guo, 2005; Section 9.5.3), and others like it, such as the Russian steppe.

### 9.5.2. The soil magnetism/rainfall linkages in the Chinese Loess Plateau

Given the importance of changes in monsoonal rainfall for the populous East Asian region, the underlying mechanisms for this soil magnetism/rainfall linkage warrant close examination.

In modern soils, extracellular pedogenic ferrites appear to form most efficiently in iron-bearing (but not necessarily iron-rich), well-buffered, generally well-drained soils, affected by intermittent soil wetting and drying episodes (Le Borgne, 1955; Mullins,

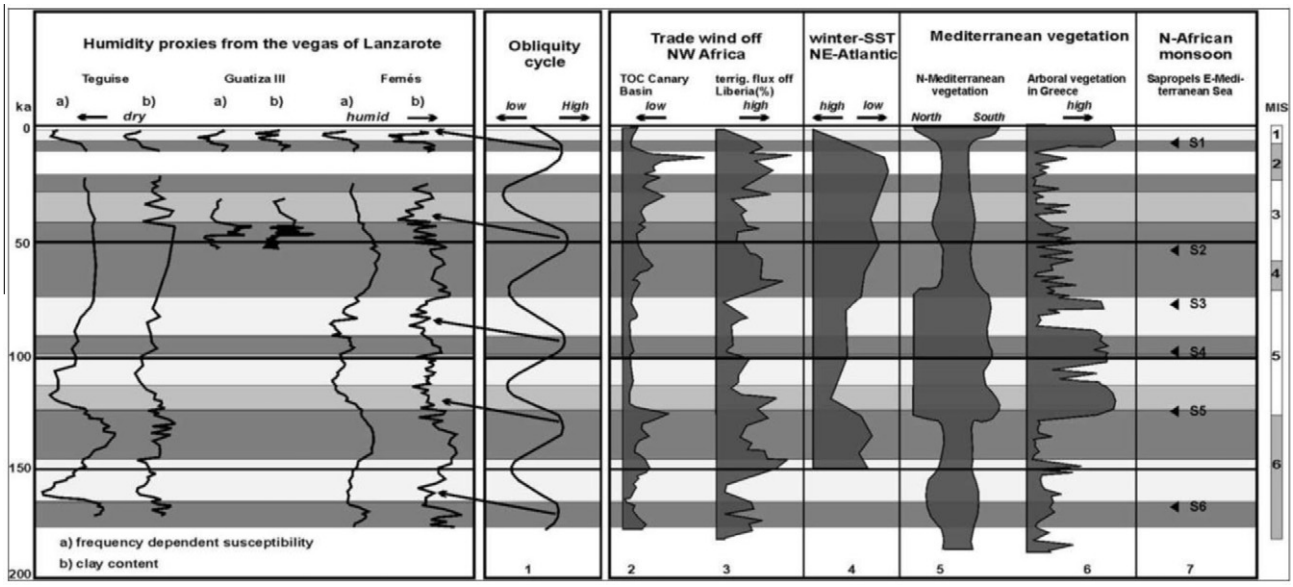


**Fig. 54.** Comparison of the Lanzarote magnetic/humidity proxy data with orbital forcing and other regional climate change parameters. From von Schudoletz et al. (2010).

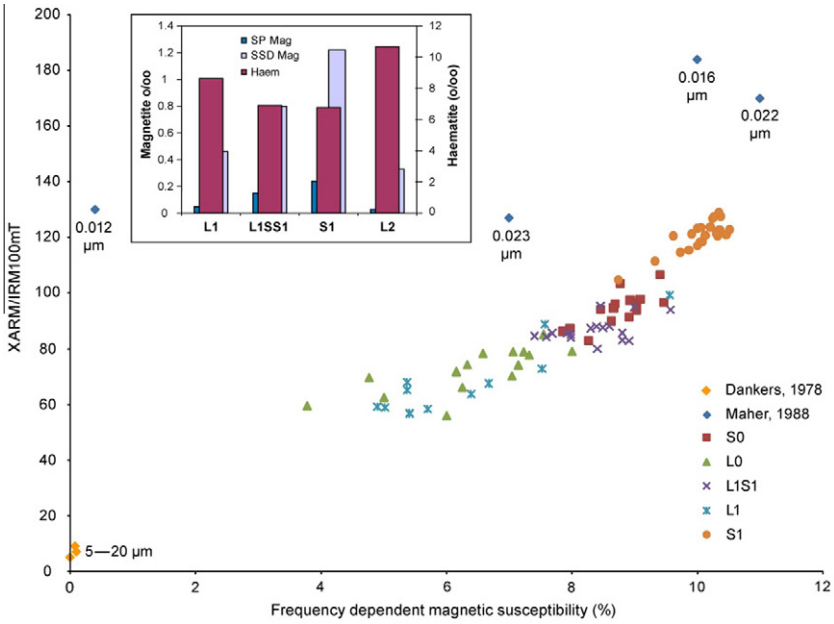


**Fig. 55.** Magnetic granulometry for loess and palaeosol samples from the central Chinese Loess Plateau, based on $\chi_{ARM/SIRM}$ and $\chi_{fd}$%; data for sized magnetites also shown. The inset diagram shows the quantitative estimation of the loess/palaeosol magnetic components (‰, SP and SSD magnetite, and haematite). Adapted from Maher and Thompson (1992).

1977; Maher, 1986, 1998). In such soils, not only will respiration of oxidisable organic matter operate at a reasonably fast rate, but it will be combined with frequent temporary redox fluctuations at soil micro-sites. Thus, opportunities for $Fe^{3+}$ solubilisation and magnetite precipitation and survival will be maximised. It is *not* the case that $Fe^{3+}$ reduction 'requires the soil to be water-saturated for significant periods' (Michel et al., 2009). Indeed, permanently wet, anoxic soils do not display magnetite formation (Maher, 1986), since the iron remains in reduced, $Fe^{2+}$ form; even lithogenic magnetite particles are actively dissolved under such soil conditions (Maher, 1986, 1998; Hanesch and Scholger, 2005). Pedogenic ferrite formation occurs not at the soil wetting stage but upon soil drying (Le Borgne, 1955), with subsequent re-oxidation at the soil micro-sites, and precipitation of the mixed $Fe^{2+}/Fe^{3+}$ ferrite, magnetite (see Section 3.5.2).

In modern, weatherable, well-drained, near-neutral soils, direct correlation is observed between the amount of pedogenic magnetite formed in the soil and mean annual precipitation (MAP), within the range ~200–2000 mm (Maher et al., 1994; Han et al., 1996). At lower rainfall totals, bacterial production within the soil microenvironment (Fig. 6) of $Fe^{2+}$, the essential precursor for soil magnetite, is minimal. Soils thus accumulate only the more oxic iron minerals, goethite and/or haematite. At higher rainfall levels, soils become excessively wet, leached, poorly buffered and thus inimical to ferrimagnet formation (Maher, 1986; Maher and Thompson, 1992, 1995; Maher et al., 1994). Between these rainfall extremes,

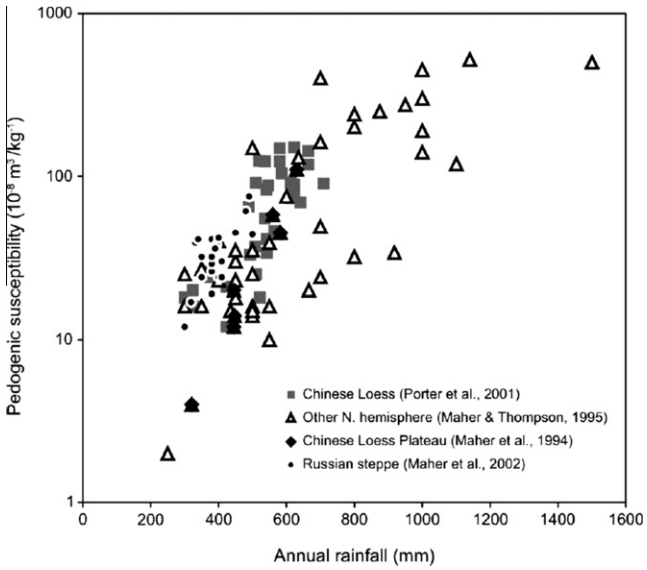


**Fig. 56.** Soil magnetic enhancement vs MAP, northern hemisphere temperate zone soils. Adapted from Maher and Thompson (1995) and Maher et al. (2002).

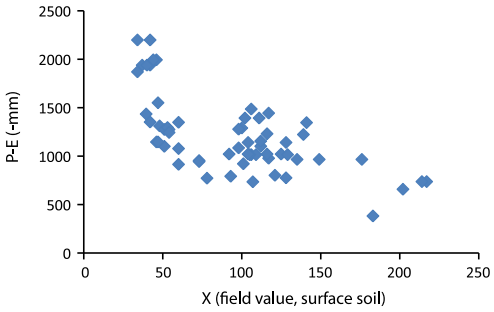


**Fig. 57.** Magnetic susceptibility of modern soils (surface, field measurements) plotted against soil moisture (precipitation – potential evapotranspiration), using data from Porter et al. (2001).

soil magnetic enhancement (i.e. measurable *in situ* formation of magnetite) is evident across the northern temperate zone, in 'suitable' soils (Fig. 56).

Correlation is evident between soil magnetic enhancement and organic carbon and cation exchange capacity (Maher, 1998; Maher et al., 2003), and with an independent palaeoprecipitation indicator, $^{10}$Be (Beer et al., 1993). Magnetic enhancement appears to proceed rapidly to equilibrium with ambient rainfall, and in association with organic matter decomposition, as shown for example by soils developing rapidly (i.e. within 100s of years) on unconsolidated, easily-weathered loess (Thompson and Maher, 1995; Maher and Hu, 2006; Alekseeva et al., 2007; Nie et al., 2010). Care is needed when examining older palaeosols, where soil welding may blur the soil magnetism/climate record. Some authors propose that sedimentation rates influence soil magnetic enhancement (e.g. Porter et al., 2001; Vidic et al., 2004).

For modern loessic soils, pedogenic susceptibility shows no additional increase beyond a MAP value of ~2000 mm, and at MAP values of ~3000 mm, begins to decline (for reasons outlined above). Hence, for the Chinese Loess Plateau, pedogenic susceptibility can only record MAP variations within the range ~200–2000 mm. If MAP has varied in the past to values outside this range, it cannot be estimated from the pedogenic susceptibility proxy.

As noted previously, MAP may be an insensitive measure of soil moisture, and intensity and degree of pedogenesis may, in turn, not be a simple function of MAP (Maher, 1998). Soil moisture may more realistically be represented by the soil moisture parameters, precipitation – potential evapotranspiration (P – PET).

Fig. 57 shows the relationship between P – PET and the field-measured $\chi$ of modern soil surfaces across the Loess Plateau (data from Porter et al., 2001). Compared with MAP, no improvement in the soil magnetism/climate correlation is evident using this soil moisture parameter. As noted previously (Maher, 1998), a study of climate effects on B horizon pH in soils sampled across the full climate range of the USA makes an interesting corollary (Folkoff, 1987). Of a host of climatic and soil factors (e.g. annual rainfall, annual potential evapotranspiration, actual evapotranspiration, leaching and moisture indices, A and B horizon soil textures), the factor with the highest explanatory power ($R^2 = 0.77$) was found to be annual rainfall. The dominance of this particular factor is due to its over-riding control of soil moisture. Perhaps the spatial limit of soil magnetic enhancement might be marked by the transition in 'aridity index' (MAP/ET), to an aridity index of >1 or an actual ET (P-measured ET) of >350 mm (Fig. 58, data from Thomas, 2008).

The strength of the observed correlation between MAP and pedogenic susceptibility in the Chinese Loess Plateau supports its use as a robust proxy for MAP in this large region. Its speed of measurement also means that it can meet the need for spatially and temporally dense palaeorainfall data for climate model validation and improved understanding of monsoon dynamics. Reported anomalies in the MAP/pedogenic susceptibility relationship (e.g. Guo et al., 2001) may reflect particular circumstances at sites across the Chinese Loess Plateau, such as the influence of local meteorological effects, or local soil factors inimical to magnetic enhancement (e.g. conditions too dry, too wet or too acidic for magnetite formation and preservation). It is also well established that the soil micro-environmental factors favouring formation of magnetite and of haematite are significantly different (e.g. Balsam et al., 2004); hence, direct correlation between $\chi$ and, for example, total free iron is unlikely. Similarly, comparisons between $\chi$ and weathering indicators (such as Rb/Sr ratios) require caution; mobility and redistribution of calcium carbonate can create stratigraphic anomalies in such indices (Bloemendal and Liu, 2005). Such mobility can include late-stage, post-pedogenic injection of carbonate into stratigraphically lower horizons (Rowe and Maher, 2000).

As an example of local meteorological conditions, enhancement of ET and aridity can result from the impact of regional fohn winds descending from upland areas such as the Liupan Shan. Shifts in the dominant moisture-bearing wind direction may also have an effect. On the western, rain-shadow side of the Liupan Shan, Baicaoyuan presently receives only ~350 mm MAP, from a rain shadow effect. In contrast, during the last interglacial (MIS 5e), it experienced an estimated MAP of ~600 mm. Such an increase indicates the possibility of a major shift in summer monsoon wind directions at this period, to southwesterly moisture-bearing winds (Indian monsoon-sourced) rather than southeasterly as at present (Maher and Thompson, 1994).

For the Chinese Loess Plateau, several studies have suggested that maghemite is the major mineral contributing the pedogenic magnetic enhancement (e.g. Verosub et al., 1993; Liu et al., 2007; Chen et al., 2010). However, analysis and quantification of the loess and palaeosol magnetic contributions (Fig. 55) shows that more- or less-oxidised, SP/SD magnetite is the key pedogenic component, contributing >90% of the susceptibility differences between the palaeosols and the loess (Maher and Thompson, 1992) and up to two thirds of the total IRM of the palaeosols (Spassov et al., 2003a, 2003b). These estimates are based on IRM acquisitions, partial ARMs, $\chi$ and frequency-dependent susceptibility, and thermomagnetic and electron microscopy analyses of magnetic extracts

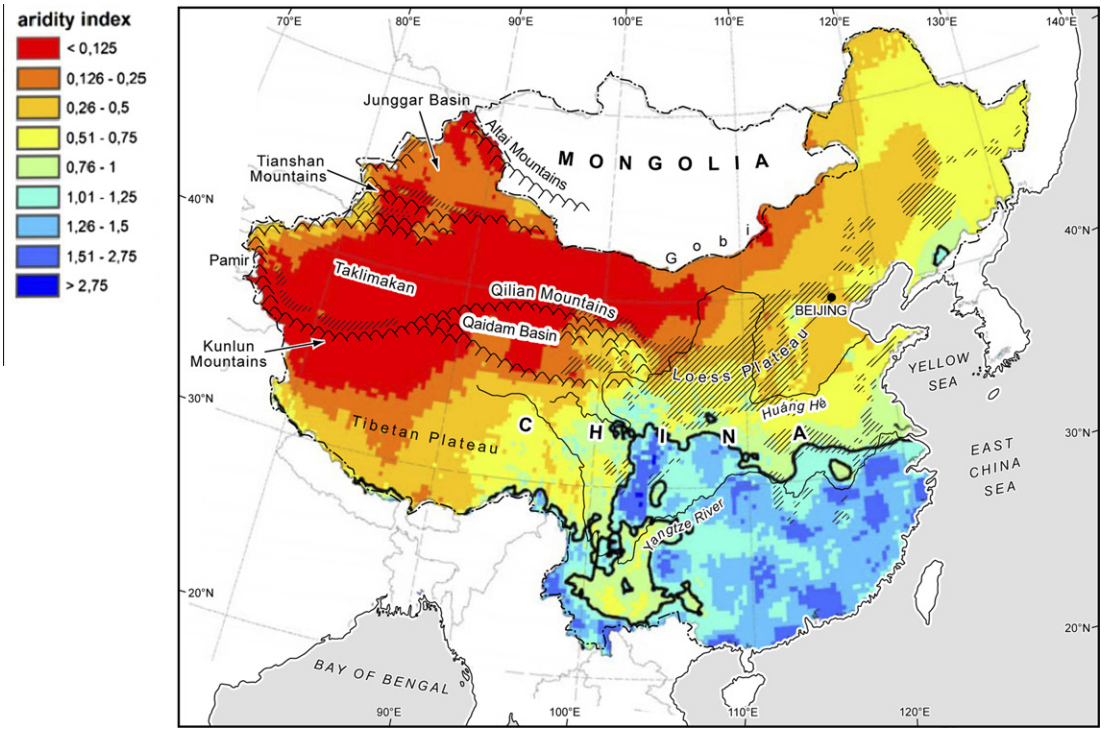


**Fig. 58.** Spatial distribution of the aridity index (i.e. precipitation – actual evapotranspiration); the solid black line delineates an aridity index of 1. Data from Thomas (pers. comm.)

(Maher and Thompson, 1992) and of particle-sized soil and loess fractions (Oldfield et al., 2009; Spassov et al., 2003a, 2003b; Sartori et al., 2005). Other studies have supported these original findings, for example, further quantifying the grain size distribution of the pedogenic ferrites (e.g. Liu et al., 2005a,c). Based on the Neél theory, Liu et al. (2005b) confirmed the existence of a continuous distribution of pedogenic magnetite grain sizes, with a maximum number of grains close to the SP/SD threshold (~0.025 μm).

### *9.5.3. Rainfall reconstructions from the Chinese Loess Plateau: significance for the evolution and future intensity of the East Asian monsoon*

Critically, the origins of the loess/palaeosol susceptibility differences across the Chinese Loess Plateau have been interrogated by an increasing range of detailed magnetic granulometric and thermomagnetic analyses, combined with quantitative magnetic extraction and independent morphological and compositional analyses. Such detailed analysis in turn enables use of the magnetic susceptibility data as a rainfall proxy for this extensive region. The value of the rainfall reconstructions obtained from the Chinese loess/soil magnetic climofunction can be illustrated with regard to rainfall variations for past interglacial (Fig. 59) and glacial stages (Fig. 60) over the last 600 kyr. Capitalising on sensitive, fast and easy measurements of $\chi$ as a climate proxy, these rainfall reconstructions come from 1000s of $\chi$ measurements, of samples from 50 loess/palaeosol sections across the Chinese Loess Plateau, of which 29 were newly measured by Hao and Guo (2005), and at 7 of these, samples were taken at 10 cm depth intervals. $\chi$ data for the other 21 loess/palaeosol sections were obtained from the published literature.

The striking regional coherence of the loess/palaeosol $\chi$ distributions through space and time (0–600 kyr BP), and their associated strong correlation with the marine oxygen isotope record, underlines the value of loess/soil magnetic properties (i.e. *sensu lato*) for identifying globally-significant climate change, and, specifically, latitudinal differences in effective rainfall.

The spatial variations in interglacial-stage $\chi$ strongly resemble present day NW-SE gradients in precipitation and temperature (Fig. 61). This indicates that regional atmospheric circulation patterns have changed relatively little over these timescales, except for evident variations in the intensity, and degree of inland penetration, of the East Asian summer monsoon. With the exception of the mid-Holocene, when the summer monsoon front extended >80 km further north, into the present day deserts, Holocene $\chi$ values and MAP estimates are lower than those for previous interglaciations.

Extending the MAP reconstructions to the last ~1 Myr (Fig. 62), the wettest periods are identified as MIS 5, 7, 11 and 13. The driest stage is MIS 22, at ~800 ka BP. Prior to ~700 ka BP, the amplitude of the $\chi$ and MAP variations is much less than in the later Pleistocene, a pattern mirrored by the marine oxygen isotope record. At MIS13 (~500 ka BP), mismatch is apparent between the high $\chi$/MAP – indicating a period of particularly intense East Asian palaeomonsoon – but only moderately light $\delta^{18}O$ (global ice volume) values (Maher and Thompson, 1995). This interglacial stage displays other anomalous characteristics, including cooler Antarctic temperatures, lower SSTs in the S. Atlantic, lower atmospheric $CO_2$ and $CH_4$ concentrations, and strong Indian and African monsoons (Guo et al., 2009). Warm climate conditions are evidenced by high-latitude northern hemisphere regions. These data combine to indicate a warmer northern hemisphere and cooler southern hemisphere during MIS13, under relatively low greenhouse gas concentrations. This hemispheric asymmetry of climate offers an explanation for intensification of the major monsoon systems, without recourse to any higher-latitude, ice sheet-driven forcing.

The glacial/stadial-stage distributions of $\chi$/MAP display markedly reduced values and weaker south-north gradients, indicating much less intense summer monsoon activity during these time periods (Fig. 62). These glacial decreases in available moisture

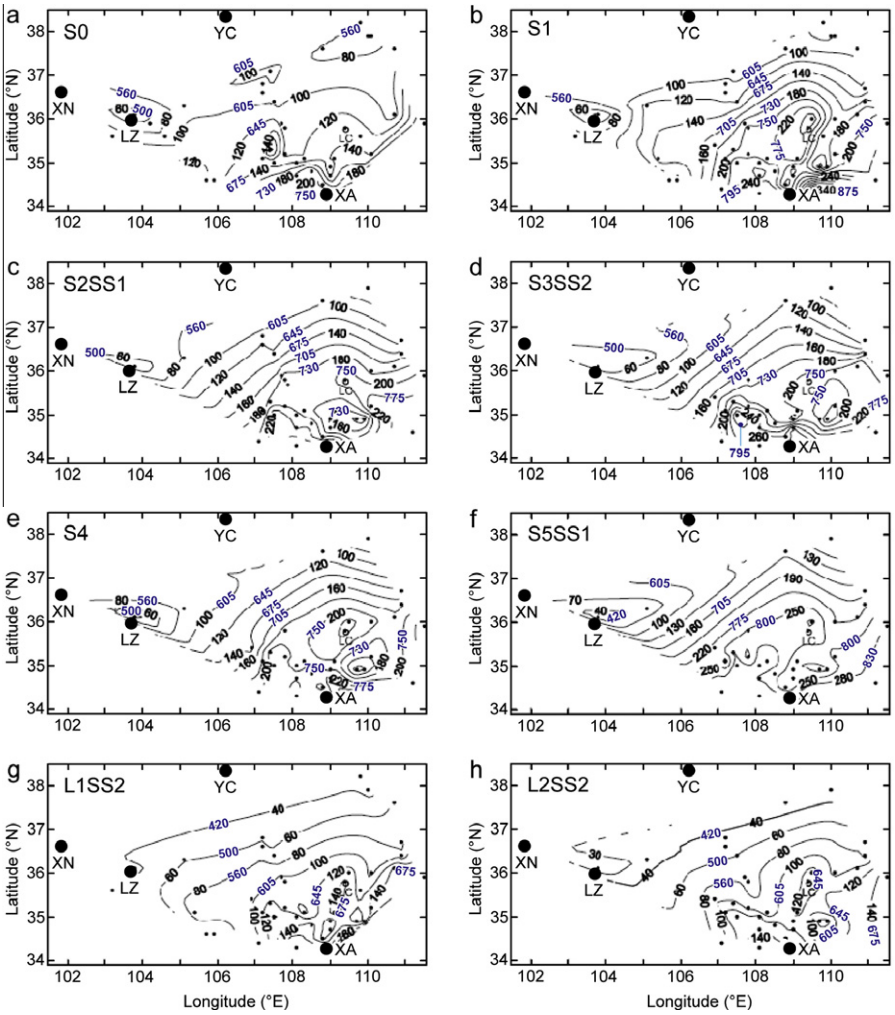


**Fig. 59.** Spatial and temporal distributions of $\chi$ (black numbers) and $\chi$-derived MAP estimates (mm/yr) for past interglacial and interstadial stages (blue numbers), across the Chinese Loess Plateau. The MAP estimates were calculated from the soil magnetism/MAP relationship shown in Fig. 56, fitted with a power law curve (MAP = 189.4 × pedogenic $\chi^{0.27}$). The circles indicate each individual loess/palaeosol site contributing to the susceptibility and palaeoprecipitation isolines. Adapted from Hao and Guo (2005).

are particularly marked towards the northwest margins of the Loess Plateau, signalling much less inland penetration by the moisture-bearing southeasterlies. Towards the southeastern margins of the Plateau, MAP values are reduced by a lesser amount (~20%).

### *9.5.4. The Holocene record of rainfall and East Asian summer monsoon intensity*

For the Holocene, records of monsoonal rain have been reported previously, obtained by oxygen isotope analysis of speleothems from Chinese caves, including the Dongge cave (e.g. Dykoski et al., 2005; Wang et al., 2005; Cheng et al., 2009; Cai et al., 2010). In apparent tandem with the Indian summer monsoon, the cave isotopic records suggest a gradual decline in East Asian monsoonal rainfall from the mid-Holocene, in association will precession-driven insolation changes (Fig. 63). These records have been used to indicate strong coupling between the Indian and East Asian monsoon systems, and teleconnections with events in the N. Atlantic Ocean (e.g. Cheng et al., 2009).

However, this pattern of Holocene rainfall correlates neither with lake-level data for the cave region (An et al., 2000), nor with the magnetically-derived MAP archive recorded at the western edge of the Loess Plateau (Fig. 63). The Duowa MAP record indicates rather variable summer monsoon activity through the Holocene, an increase in MAP from ~5 ka BP, and rapid, sub-millennial scale variations from ~2.5 ka BP (Maher and Hu, 2006). The discrepancy between the Dongge Cave $\delta^{18}O$ and the lake-level and magnetic records of precipitation might be attributable to shifts in moisture source and isotopic signal. For example, the shift to isotopically heavier $\delta^{18}O$ values from the mid-Holocene might reflect an increasing proportion of less-fractionated moisture sourced from the adjacent Pacific Ocean, rather than far-travelled and significantly lighter moisture sourced from the Indian summer monsoon (Maher, 2008).

### *9.6. The Russian steppe*

Because dust flux rates and MAP show (inverse) co-variation from the northwest to the southeast across the Loess Plateau, their respective role in determining the observed gradient in $\chi$ has been disputed. It has been argued that the $\chi$ distribution reflects dilution by differing amounts of low-$\chi$ dust; as much as 84% of the $\chi$ variance of the modern soils across the Plateau has been attributed to this present day 'dust-dilution' effect (Porter et al., 2001). The Russian steppe region provides the opportunity to test these competing hypotheses, since whilst it experiences a strong MAP gradient from the Caucasus towards the Caspian Sea, dust accumulation rates are minimal at the present day (Maher et al., 2003; Alekseeva et al., 2007).

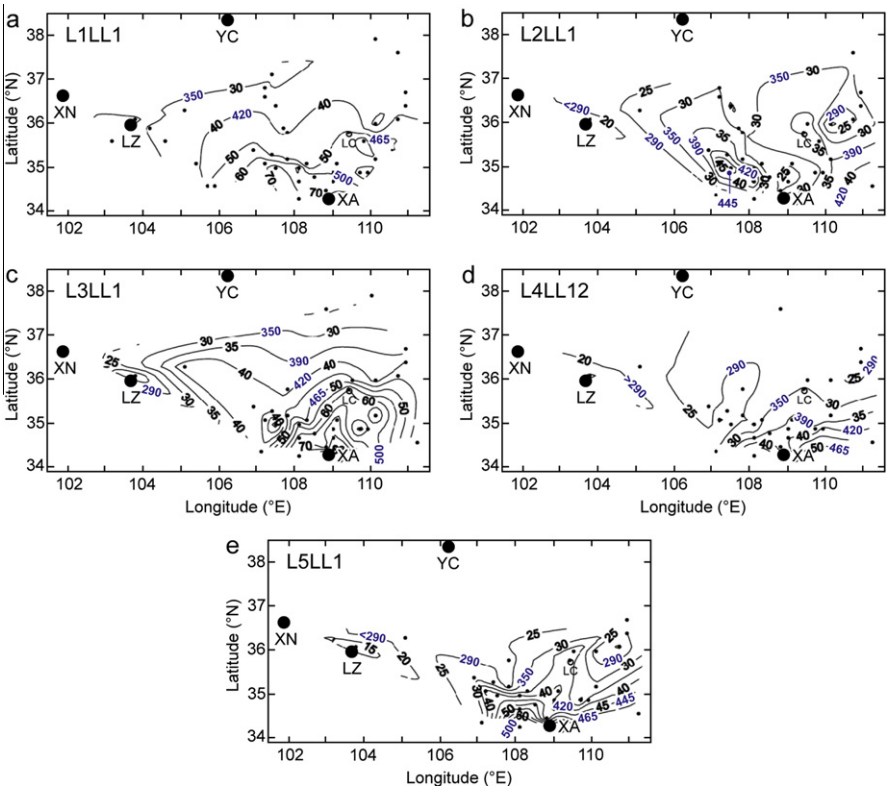


**Fig. 60.** Spatial and temporal distributions of susceptibility (black numbers) and susceptibility-derived MAP estimates (mm/yr; blue numbers) for past glacial and stadial stages (modified from Hao and Guo, 2005). The MAP estimates were calculated from the soil magnetism/MAP relationship shown in Fig. 56, fitted with a power law curve (MAP = 189.4 × pedogenic $\chi^{0.27}$). The circles indicate each individual loess/palaeosol site contributing to the susceptibility and palaeoprecipitation isolines.

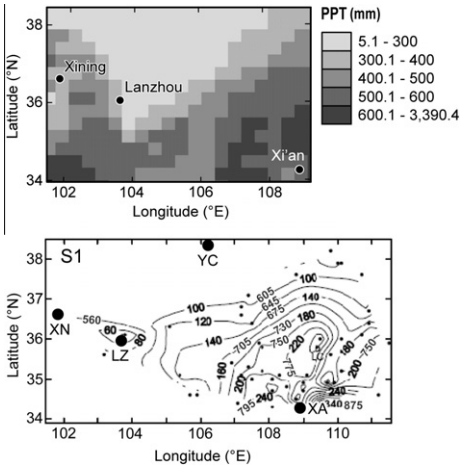


**Fig. 61.** Comparison between modern MAP distribution (mm/yr, upper panel) and magnetically-derived MAP (mm/yr, blue numbers) reconstructed from palaeosol S1 (MIS 5e) across the Loess Plateau (lower panel). Black numbers = measured magnetic susceptibility (from Hao and Guo, 2005). The circles indicate each individual loess/palaeosol site contributing to the susceptibility and palaeoprecipitation isolines.

Much of the Russian steppe is mantled in homogenous, weakly-magnetic loess, the grassland cover is virtually uninterrupted, and little source of magnetic contamination exists in this large, uninhabited region. Magnetic and mineralogical analyses identify *in situ*, pedogenic formation of ferrimagnets in the steppe soils, and, as in the Chinese case, increased ferrimagnetic concentrations are associated with higher MAP values. XRD and electron microscopy show that the pedogenic ferrites are ultrafine-grained (<~50 nm), substitution-free. Ferrimagnetic contributions to Mossbauer spectra range from 17% in the parent loess to 42% for a subsoil sample from the highest rainfall area. The haematite contribution decreases from ~40% in the parent material to ~21% in the most magnetic topsoil. Moving southwest from lower to higher MAP values, the total soil iron content varies little but the systematic magnetic increases are accompanied by decreased $Fe^{2+}$ content, reflecting increased silicate weathering. The corollaries of this region with the Chinese Loess Plateau are strong. The steppe parent materials are mostly loessial deposits, topography is rolling to flat; duration of soil formation effectively constant. Thus, climate, and, critically, MAP is identified statistically as the key control on the soil $\chi$ distribution in this region. The strongest correlations exists between MAP and $\chi$ and $\chi_{ARM}$ ($r = 0.93$), and between summer rainfall and $\chi$ and $\chi_{ARM}$ ($r = 0.85$ and 0.84, respectively). A negative correlation exists between MAP and HIRM ($r = -0.68$).

Such strong correlation between the steppe, with no dust accumulation at present, and the Chinese Loess Plateau, both substantiates the soil magnetism/MAP link and negates the significance of dust flux as a major control on soil magnetic properties in these two large regions (Maher et al., 2002).

The strong statistical relationship between pedogenic $\chi$ and MAP enables palaeorainfall reconstructions through the Holocene, based on palaeosols buried beneath funerary mounds across the Russian steppe (Alekseeva et al., 2007). The palaeo-MAP data indicate marked climate variations, with MAP minima at ~5, ~3.8, and 1.6 ka BP, and enhanced MAP at ~1.9 and 0.6 ka BP. Some synchrony is apparent between these MAP variations and changes in precipitation and lake levels in the Middle East; causal links with the North Atlantic Oscillation may exist (Alekseeva et al., 2007).

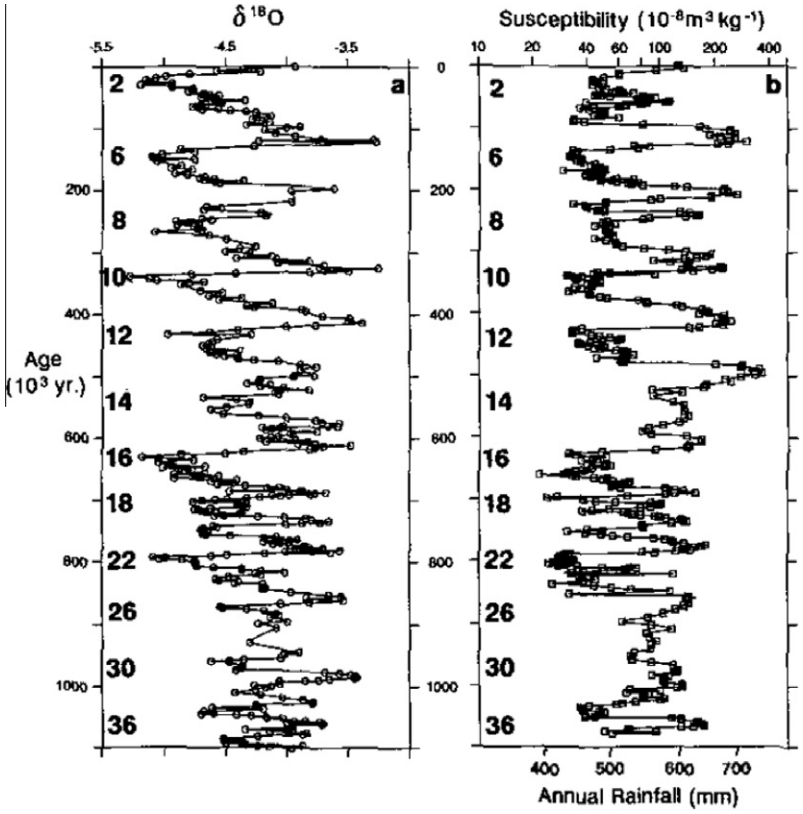


**Fig. 62.** Magnetic susceptibility and MAP reconstructions (mm/yr) for the last ~1 Ma, for Xifeng in the central Loess Plateau. From Maher and Thompson (1995).

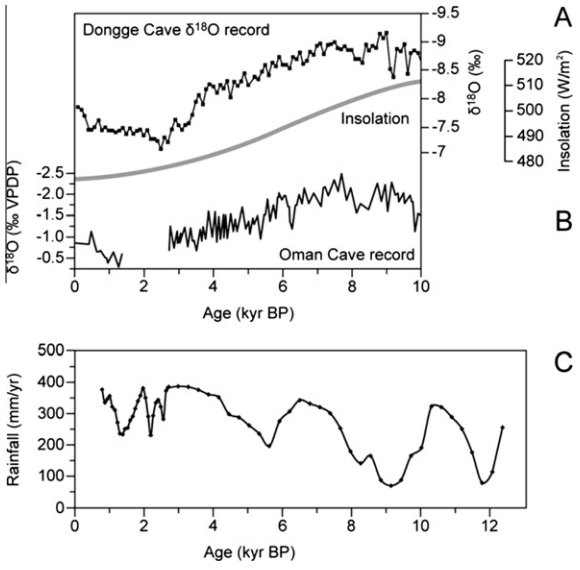


**Fig. 63.** (a) Holocene variations in oxygen isotope composition of speleothem calcite samples, from Dongge Cave, S. China, and the precessional change in N. hemisphere summer insolation (June–August), calculated for 20°N (from Wang et al., 2005); (b) Indian monsoon intensity, from oxygen isotope analysis of a speleothem from the Qunf Cave, Oman (Fleitmann et al., 2003); (c) rainfall record from Duowa, western edge of the Chinese Loess Plateau, from the soil magnetism/rainfall transfer function (Maher and Hu, 2006); at this marginal site, rainfall varies by as much as +50% and –75% from the estimated present day total (~265 mm/yr). N.B. The lowest MAP value in the MAP/pedogenic $\chi$ modern calibration set is 250 mm; hence, reconstructed MAP values <250 mm at Duowa are an extrapolation from the modern training set.

### 9.7. Alternative models of pedogenic enhancement

An alternative pathway of ferrimagnet formation in soils has recently been proposed, whereby pedogenic ferrimagnets are supposed to comprise not magnetite but maghemite, formed by ageing from ferrihydrite en route to its final transformation to haematite (Barron and Torrent, 2002; Torrent et al., 2006). Such a pathway requires no reductive step for production of $Fe^{2+}$ (the essential precursor for the mixed $Fe^{2+}/Fe^{2+}$ compound, magnetite). In the laboratory, the rate of formation of such maghemite depends log-linearly upon temperature (Barron and Torrent, 2002). Pedogenic ferrite formation would thus show direct association with temperature and aridity, rather than the observed correlation with rainfall (e.g. Maher, 1998; Sartori et al., 2005; Nie et al., 2010). Further, again based on laboratory results (Barron and Torrent, 2002), mineral transformations along the ferrihydrite–maghemite–haematite route would require very long timescales at ambient soil-forming temperatures (~$10^5$ years) to produce magnetically significant amounts of maghemite. In contrast, soil magnetic enhancement is found even in Holocene palaeosols having had only a few hundred years of soil-forming duration (Roberts et al., 2001; Maher et al., 2003; Nie et al., 2010).

Further, pedogenic maghemite would be found in association with haematite, not goethite (Michel et al., 2009). However, pedogenic ferrites co-occur with goethite and haematite (Ji et al., 2002, 2004; Balsam et al., 2004). For the palaeosols of the Russian steppe, for example, the concentrations of pedogenic magnetite and haematite show some inverse relationship (Fig. 64, Maher et al., 2003). Co-association between pedogenic magnetite/maghemite and goethite is not unexpected, given that goethite formation is – like magnetite – favoured by wetter soil micro-site conditions (Taylor and Graley, 1967; Schwertmann, 1988). Although more dif-

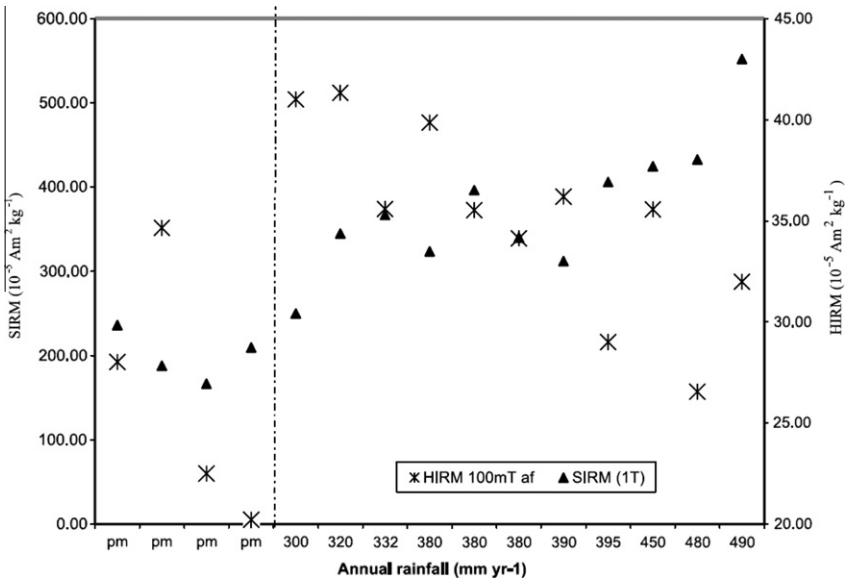


**Fig. 64.** SIRM and high-field remanence (HIRM) measured for parent materials (pm) and modern soils across the Russian steppe, plotted against modern-day MAP. From Maher et al. (2003).

ficult to quantify accurately than the pedogenic SP/SD ferrites, soil goethite may also represent a robust proxy for effective rainfall (see Section 9.8).

It seems possible that nanoscale pedogenic haematite can be over-estimated using DRS methods, depending on the spectroscopic peaks selected to discriminate between haematite and goethite (Scheinost and Schwertmann, 1999), and on whether or not the background colour of the sediment matrix has been accounted for. For example, whilst Balsam et al. (2004) report haematite concentrations for the Luochuan sequence (central Loess Plateau) of up to ~0.35 wt%, Hao et al. (2009) suggest concentrations as high as ~1.2 wt%. Using the HIRM data reported in Hao et al. (2009, and pers. comm.), maximum haematite concentrations are broadly estimated at ~0.42 wt%, and goethite concentrations at ~0.48 wt%.

### 9.8. Goethite as an indicator of rainfall

Goethite and haematite are likely to display contrasting behaviour in soils and palaeosols (e.g. Liu et al., 2006a), reflecting their different pathways of formation. Because goethite is likely to form from solution (i.e. upon dissolution of ferrihydrite) – in competition with haematite formation (which results from dehydration and topotactic rearrangement of ferrihydrite) – soil goethite also shows some relationship with soil wetness and thus effective rainfall. Fig. 65, for example, shows the direct relationship between effective rainfall and the ratio of goethite to total goethite + haematite in well-drained oxisols and ultisols in southern Brazilian soils (Kampf and Schwertmann, 1983).

With regard to the surface soils of the Chinese Loess Plateau, a similar, direct relationship between goethite content (wt%) and mean annual rainfall has also been recorded (Fig. 66; Balsam, pers. comm.). Although more costly and time-consuming to achieve, low-temperature, high-field magnetic analyses (e.g. 77–293 K, and up to ~7 T) of the goethite content of the loess/palaeosol sequences around the world may provide another route to quantification of palaeo-rainfall on regional scales. Improved quantification of the pedogenic haematite content may also enable improved understanding of changes in temperature and, especially, seasonality, as recorded in the loessic palaeosols.

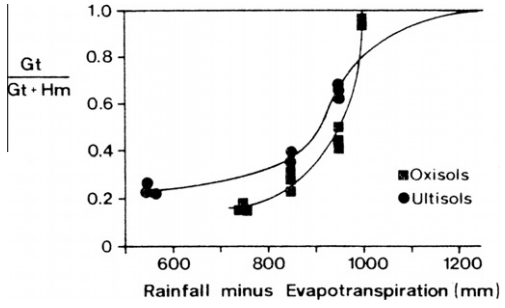


**Fig. 65.** The ratio of goethite to total goethite + haematite (from XRD) in well-drained oxisols and ultisols in southern Brazilian soils plotted against effective rainfall (Kampf and Schwertmann, 1983).

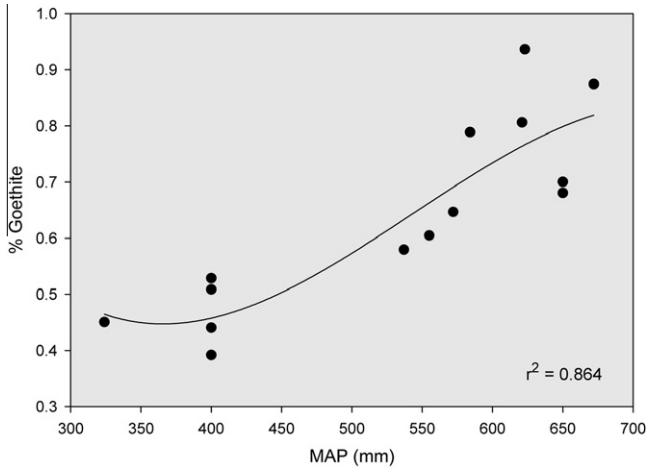


**Fig. 66.** Goethite (wt%, from diffuse reflectance spectrometry) vs modern-day MAP for soils across the Chinese Loess Plateau (Balsam, pers. comm.).

## 10. Summary; analytical techniques, future prospects

The sensitivity, speed and non-destructive nature of magnetic analyses of natural samples provides a key tool for identifying changes in dust sources, properties and fluxes, both at the present day and for a global range of palaeoclimatic archives, terrestrial and marine.

Whilst many environmental scientists are familiar with the use of one magnetic parameter, magnetic susceptibility, measurements of magnetic susceptibility are normally just the first, and most basic, step in characterising the magnetic properties of any sample. In order to interrogate the nature of the mixture of magnetic minerals, concentrations and grain sizes within a sample, a range of additional magnetic experiments will be required, ideally, supplemented by independent mineralogical analysis of representative subsets of the larger sample set. In practice, a relatively small number of magnetic measurements can often provide sufficient, discriminatory information to identify both the major magnetic components, and the magnetic differences between samples. This type of routine, room-temperature characterisation can be applied easily to large numbers of samples, offering the potential for high-resolution data in both the temporal and spatial domain.

Additional magnetic analyses, for example, making use of SQUID magnetometers, at low-and high temperatures, and a larger range of magnetising fields (up to $\sim$10 T), may be required for environmental samples containing very low concentrations of magnetic minerals (e.g. polar ice), and/or weakly magnetic minerals. High-field, low-temperature measurements might usefully be applied to key samples containing haematite and goethite mixtures, which, as shown here, are often critical in carrying a record of dust flux from arid zone sources. Similarly, more detailed understanding of the pedogenic formation of haematite and goethite in relation to soil moisture and temperature, especially in the famous Chinese Loess Plateau sequences, would also be valuable.

It is clear that climate and environmental change often induces not only changes in dust supply, transport and deposition, but also in the post-depositional environment and in the subsequent preservation and fidelity of the detrital aeolian signal. Diagenetic alteration or erasure of magnetic minerals can be selective and variable in intensity, introducing another climatically-modulated factor to the interpretation of sediment magnetic properties in any organic-rich, sub-oxic environment. A key advantage of sediment magnetic analysis, in comparison with DRS, is that such diagenetic transformations are often magnetically distinctive, enabling robust recognition of sequence sections periodically affected by reductive dissolution and authigenic (chemical and/or biogenic) mineral formation. As is clear from the examples discuss here, there is no simple correlation between sediment depth and diagenetic stage. Rather, diagenetic activity is a variable response to possibly multi-factorial changes in sedimentary environment, including organic content and sedimentation and burial rates, and levels of oxygenation at the sediment/water interface. Hence, detailed understanding of the sources of sediment magnetic particles is essential if robust palaeoclimatic reconstructions are to be made.

Whilst magnetic data on their own cannot as yet identify uniquely the precise mineralogy and source of the carriers of magnetisation, ongoing developments in magnetic instrumentation, analyses and data processing continue to increase their diagnostic power. Independent complementary analysis on smaller, representative subsets of samples can provide additional key information on the morphology, composition and mineralogical source of the magnetic carriers. Given that magnetic minerals often exist in minor or trace concentrations, such analysis may entail magnetic extraction and concentration of the constituent magnetic particles, for X-ray diffraction, electron microscopy and elemental analysis. The efficiency of magnetic extraction should be evaluated (e.g. by before- and after-extraction magnetic measurements) in order to ensure that the extracts are representative of the parent sample.

Inter-calibration between magnetic measurements and, for example, elemental iron concentrations are another useful way of capitalising on the speed and abundance of magnetic data collection. Similarly, inter-calibration between magnetic characterisation and DRS techniques may provide a powerful means of defining dust iron mineralogy and crystallinity, with regard both to radiative impacts and potential iron bioavailability in the HNLC marine environment.

In terms of future prospects, magnetic analyses of aeolian dusts can undoubtedly provide key information on the sources, properties and fluxes of mineral dusts both at the present day, and at high spatial and temporal resolution through the past glacial and interglacial stages of the Quaternary (and beyond). Increased collaboration between the magnetic and dust and climate research communities can only enhance the development of sample availability, sampling protocols and resultant new magnetic dust datasets. Improved quantification of magnetic mineral abundances in dusts, and inter-calibration between magnetic measurements and independent mineralogical analyses, can lead to dust magnetic measurements acting as robust proxies for dust and iron fluxes, of key importance in the context of direct climate effects, especially radiative forcing and cloud condensation effects, and indirect climate modification through the iron fertilisation of HNLC ocean regions.

For the present day, magnetic monitoring of mineral dusts can provide a sensitive, fast and cost-effective means of identifying dust sources and anthropogenic modifications to atmospheric mineral dust. Such magnetic monitoring of anthropogenic dust loadings might be of particular value in assessing the impacts of mitigation programmes planned or underway at either the national or international scale. As with any overview of present day dust research, the under-representation of dust sampling in many areas of the world, perhaps especially in the southern hemisphere, cannot go unremarked.

For the palaeo-dust record, improved understanding of the magnetic characteristics of haematite and goethite seems warranted, given the global significance of these minerals in tracing aeolian fluxes through space and time. For the marine and lacustrine realms, it is equally important to identify the respective roles of changes in aeolian flux, and changes in diagenetic activity, in determining the measured absolute and relative abundances of haematite and goethite in the sedimentary record. For the loess sequences around the world, further deconvolution of the inter-relationships between haematite, goethite and magnetite, and between these minerals and regional climate change, especially in the East Asian monsoon region, will enable even more detailed palaeoclimatic reconstruction. Extension of magnetic climo-(precipitation) functions to other regions, including Africa, represents another major development in magnetic studies of dust and soils.

## 11. Conclusions

The sources, properties and fluxes of mineral dust are significant with regard to climate modification at the present day and in the past. Because magnetic (remanence-bearing) iron oxides and oxyhydroxides occur ubiquitously in aeolian dusts, magnetic measurements of modern and palaeo-dusts provide a sensitive, fast and non-destructive means of analysing dusts, even when present in trace quantities (as in polar ice caps).

Discriminatory magnetic measurements can distinguish between dusts from different sources, based on differences in their

magnetic mineralogy, concentration, magnetic grain size and degree of magnetic interaction.

Even quite complex natural samples can often be characterised using a relatively small number of magnetic measurements, enabling large numbers of samples to be processed and offering high resolution datasets both in the temporal and spatial realm.

Palaeo-dust archives occur on every continent and in every ocean. For the marine realm outstanding magnetic records of past aeolian, climatic and palaeoceanographic change have been obtained. Notwithstanding these achievements, untapped potential still exists for detailed, quantitative retrieval of palaeo-dust and iron fluxes from the magnetic properties and records of oxic marine sediments. Given the global importance of the weakly magnetic minerals, haematite and goethite, as dust flux indicators, improved understanding of their varying sources, grain sizes and composition is essential. These minerals carry the potential for sensitive source discrimination, but also for quantitative assessment of dust fluxes and iron fluxes through time and space.

For any marine sediment affected by post-depositional reductive diagenesis, changes in sediment magnetic mineralogy must be carefully evaluated in order to ensure robust attribution of mineral sources and climatic roles. Unlike DRS techniques, which can also measure changes in haematite and goethite concentrations, magnetic analysis of sediments can identify those core sections affected by diagenesis, and which are thus unlikely to offer an accurate reflection of dust flux changes through time.

For the continental realm, magnetic discrimination of dust sources and fluxes is possible for the worldwide sequences of loesses and palaeosols but also for other terrestrial sediments, including ice, lake and desert records.

For loessic regions where post-depositional formation of soils is dominated by the soil-forming factor, climate, quantitative reconstruction of changes in palaeo-precipitation (and possibly temperature, via rainfall and potential evapotranspiration relationships) can be achieved. However, the magnetic properties of (unweathered) loess depend first on its source, and transport, and then on its post-depositional soil-forming regime.

It is possible (and valuable) to use the magnetic properties of least-weathered loess, together with other independent analyses (e.g. elemental composition) to identify and/or discount possible dust source area(s).

Palaeosol magnetic properties can be quantitatively calibrated against climate parameters (especially rainfall) in *suitable* soils, i.e. in accretionary and generally well-drained and well-buffered soils, such as occur across the Chinese Loess Plateau. Given a weakly magnetic parent material, like the Chinese loess, then pedogenic magnetic susceptibility precisely captures the palaeorainfall signal, is very easy to measure, and can provide temporally- and spatially-dense datasets, as required for validation of GCM hindcasting, and essential improvement in our knowledge of monsoon dynamics.

It is more challenging to calibrate palaeosol magnetic properties with climate in 'suitable' soils where the loess parent material is strongly magnetic and/or spatially variable (e.g. the Pampean sequences of South America). However, use of those magnetic parameters sensitive to the presence of SP/SD pedogenic ferrites, preferably combined with particle size-specific analyses, may resolve climate variations in such areas.

Gleying partially or completely erases soil ferrites, whether of detrital or pedogenic origin.

There are no 'competing models' of soil magnetism/climate (e.g. there is no 'Chinese model' or 'wind vigour' model). For any loess/palaeosol location, detailed, site-specific magnetic analysis is required, to establish the respective roles and influences of the relevant soil-forming factors.

## Acknowledgements

The author gratefully acknowledges financial support through a Royal Society Wolfson Research Merit Award. Thanks are due to Lonnie Thompson, Charlie Bristow, and Axel Thomas for kindly providing ice core samples from Dunde, dust samples from the Bodélé Depression, and the aridity index data for China, respectively. Simon Chew and Gemma Davies assisted greatly with the diagrams. I also appreciate the patience and helpfulness of the journal editors.

## Appendix A. Summary of acronyms

| | |
|---|---|
| ADIOS | Asian dust input to the oceanic system |
| A horizon | upper mineral soil horizon |
| B horizon | lower mineral soil horizon |
| $(B_0)_{CR}$ | the coercivity of remanence (see Fig. 2) |
| $\chi$ | initial, reversible, low-field magnetic susceptibility (see Table 1 and Fig. 2) |
| $\chi_{fd}$ | frequency dependent susceptibility (see Table 1) |
| $\chi_{ARM}$ | the anhysteretic susceptibility (the anhysteretic remanent magnetisation normalised by the dc biasing field in which it was acquired) |
| $\delta^{18}O$ | deviation in the $^{18}O/^{16}O$ ratio, compared with a standard ratio (e.g. Vienna Standard Mean Ocean Water, VSMOW) |
| DRS | diffuse reflectance spectroscopy |
| EDC | the EPICA Concordia Dome ice core |
| ET | evapotranspiration |
| FORC | first-order reversal curve |
| **H** | magnetic field |
| $H_{Cool\%}$ | the change in high-field remanence upon cooling from room temperature to 77 K (liquid nitrogen temperature) |
| *H* events | Heinrich (iceberg-rafting) events |
| HIRM | high-field remanent magnetisation (e.g. the remanence acquired in applied fields of between 300 mT and 1 T, $HIRM_{300\ mT-1\ T}$) |
| $HIRM_{100\ mT\ ac}$ | the high-field remanence remaining after ac demagnetisation in a field of 100 mT |
| HNLC | high nutrient-low chlorophyll |
| ICP-MS | inductively coupled plasma mass spectrometry |
| IPCC | Intergovernmental Panel on Climate Change |
| IRD | iceberg-rafted debris |
| ITCZ | inter-tropical convergence zone |
| K | temperature Kelvin |
| kyr BP | thousand years before present |
| LCC | long chain compounds |
| LGM | last glacial maximum |
| LRT | long range transport |
| ***m*** | magnetic moment |
| Ma BP | million years before present |
| MAR | mass accumulation rate |
| MAP | Mean annual precipitation |
| MBB | Matuyama–Brunhes boundary (~0.78 Ma BP) |
| mbsf | metres below sea floor |
| MD | multidomain (e.g. >~1 μm in magnetite) |
| MDF | median destructive field, the dc field required to reduce an acquired remanence to 50% of its initial value (e.g. $MDF_{ARM}$, $MDF_{IRM}$) |

(*continued on next page*)

**Appendix A** (*continued*)

| | |
|---|---|
| $M_i$ | induced magnetisation |
| MIS | marine oxygen isotope stage |
| mT | milliTesla |
| NGRIP | North Greenland ice core project |
| ODP | Ocean Drilling Program |
| PD | present day |
| PET | potential evapotranspiration |
| ppmv | parts per million by volume |
| PTFE | polytetrafluoroethylene ('Teflon') |
| SEAREX | air–sea exchange programme |
| SIRM | saturation isothermal remanent magnetisation |
| SP | superparamagnetic (e.g. <~0.03 μm in magnetite) |
| SSD | stable single domain (e.g. between ~0.03 and 0.1 μm in magnetite). |
| SST | sea surface temperature |
| S ratio | the ratio of the remanence remaining after dc demagnetisation at e.g. 100 mT and the SIRM saturation isothermal remanent magnetisation |
| SQUID | superconducting quantum interference device |
| T | Tesla |
| TOC | total organic carbon |
| TOMS | Nimbus-7 Total Ozone Mapping Spectrometer |
| XRD | X-ray diffraction |

## References


Abrajevitch, A., Van der Voo, R., Rea, D.K., 2009. Variations in relative abundances of goethite and hematite in Bengal Fan sediments: climatic vs. diagenetic signals. Marine Geology 267, 191–206.

Aleinikoff, J.N., Muhs, D.R., Bettis, E.A., Johnson, W.C., Fanning, C.M., Benton, R., 2008. Isotopic evidence for the diversity of late Quaternary loess in Nebraska: glaciogenic and nonglaciogenic sources. Geological Society of America Bulletin 120, 1362–1377.

Alekseeva, T., Alekseev, A., Maher, B.A., Demkin, V., 2007. Late Holocene climate reconstructions for the Russian steppe, based on mineralogical and magnetic properties of buried palaeosols. Palaeogeography Palaeoclimatology Palaeoecology 249, 103–127.

Alfaro, S.C., Gaudichet, A., Gomes, L., Maille, M., 1997. Modeling the size distribution of a soil aerosol produced by sandblasting. Journal of Geophysical Research-Atmospheres 102, 11239–11249.

Alfaro, S.C., Lafon, S., Rajot, J.L., Formenti, P., Gaudichet, A., Maille, M., 2004. Iron oxides and light absorption by pure desert dust: an experimental study. Journal of Geophysical Research-Atmospheres 109.

An, Z.S., 2000. The history and variability of the East Asian paleomonsoon climate. Quaternary Science Reviews 19, 171–187.

An, Z.S., Porter, S.C., Kutzbach, J.E., Wu, X.H., Wang, S.M., Liu, X.D., Li, X.Q., Zhou, W.J., 2000. Asynchronous Holocene optimum of the East Asian monsoon. Quaternary Science Reviews 19, 743–762.

An, Z.S., Liu, T.S., Lu, Y.C., Porter, S.C., Kukla, G., Wu, X.H., Hua, Y., 1990. The long-term paleomonsoon variation recorded by the loess-paleosol sequence in central China. Quaternary International 7, 91–96.

Arnold, E., Merrill, J., Leinen, M., King, J., 1998. The effect of source area and atmospheric transport on mineral aerosol collected over the North Pacific Ocean. Global and Planetary Change 18, 137–159.

Baker, A.R., Croot, P.L., 2010. Atmospheric and marine controls on aerosol iron solubility in seawater. Marine Chemistry 120, 4–13.

Baker, A.R., Jickells, T.D., Witt, M., Linge, K.L., 2006. Trends in the solubility of iron, aluminium, manganese and phosphorus in aerosol collected over the Atlantic Ocean. Marine Chemistry 98, 43–58.

Balkanski, Y., Schulz, M., Claquin, T., Guibert, S., 2007. Reevaluation of Mineral aerosol radiative forcings suggests a better agreement with satellite and AERONET data. Atmospheric Chemistry and Physics 7, 81–95.

Balsam, W., Ji, J.F., Chen, J., 2004. Climatic interpretation of the Luochuan and Lingtai loess sections, China, based on changing iron oxide mineralogy and magnetic susceptibility. Earth and Planetary Science Letters 223, 335–348.

Barbeau, K., Rue, E.L., Bruland, K.W., Butler, A., 2001. Photochemical cycling of iron in the surface ocean mediated by microbial iron(III)-binding ligands. Nature 413, 409–413.

Barron, V., Torrent, J., 2002. Evidence for a simple pathway to maghemite in Earth and Mars soils. Geochimica Et Cosmochimica Acta 66, 2801–2806.

Beer, J., Shen, C.D., Heller, F., Liu, T.S., Bonani, G., Dittrich, B., Suter, M., Kubik, P.W., 1993. Be-10 and magnetic-susceptibility in Chinese loess. Geophysical Research Letters 20, 57–60.

Ben-Ami, Y., Koren, I., Rudich, Y., Artaxo, P., Martin, S.T., Andreae, M.O., 2010. Transport of North African dust from the Bod, l, depression to the Amazon Basin: a case study. Atmospheric Chemistry and Physics 10, 7533–7544.

Bergametti, G., Gomes, L., Coudegaussen, G., Rognon, P., Lecoustumer, M.N., 1989. African dust observed over Canary Islands – source-regions and transport pattern for some summer situations. Journal of Geophysical Research-Atmospheres 94, 14855–14864.

Bidegain, J.C., Evans, M.E., van Velzen, A.J., 2005. A magnetoclimatological investigation of Pampean loess, Argentina. Geophysical Journal International 160, 55–62.

Bidegain, J.C., van Velzen, A.J., Rico, Y., 2007. The Brunhes/Matuyama boundary and magnetic parameters related to climatic changes in Quaternary sediments of Argentina. Journal of South American Earth Sciences 23, 17–29.

Bigg, G.R., Clark, C.D., Hughes, A.L.C., 2008. A last glacial ice sheet on the Pacific Russian coast and catastrophic change arising from coupled ice-volcanic interaction. Earth and Planetary Science Letters 265, 559–570.

Bigler, M., Rothlisberger, R., Lambert, F., Stocker, T.F., Wagenbach, D., 2006. Aerosol deposited in East Antarctica over the last glacial cycle: detailed apportionment of continental and sea-salt contributions. Journal of Geophysical Research-Atmospheres 111.

Biscaye, P.E., Grousset, F.E., Revel, M., VanderGaast, S., Zielinski, G.A., Vaars, A., Kukla, G., 1997. Asian provenance of glacial dust (stage 2) in the Greenland Ice Sheet Project 2 Ice Core, Summit, Greenland. Journal of Geophysical Research-Oceans 102, 26765–26781.

Bishop, J.K.B., Davis, R.E., Sherman, J.T., 2002. Robotic observations of dust storm enhancement of carbon biomass in the North Pacific. Science 298, 817–821.

Blain, S., Queguiner, B., Armand, L., Belviso, S., Bombled, B., Bopp, L., Bowie, A., Brunet, C., Brussaard, C., Carlotti, F., Christaki, U., Corbiere, A., Durand, I., Ebersbach, F., Fuda, J.L., Garcia, N., Gerringa, L., Griffiths, B., Guigue, C., Guillerm, C., Jacquet, S., Jeandel, C., Laan, P., Lefevre, D., Lo Monaco, C., Malits, A., Mosseri, J., Obernosterer, I., Park, Y.H., Picheral, M., Pondaven, P., Remenyi, T., Sandroni, V., Sarthou, G., Savoye, N., Scouarnec, L., Souhaut, M., Thuiller, D., Timmermans, K., Trull, T., Uitz, J., van Beek, P., Veldhuis, M., Vincent, D., Viollier, E., Vong, L., Wagener, T., 2007. Effect of natural iron fertilization on carbon sequestration in the Southern Ocean. Nature 446, U1070–U1071.

Blakemore, R., 1975. Magnetotactic bacteria. Science 190, 377–379.

Bleil, U., von Dobeneck, T., 2003. Late Quaternary terrigenous sedimentation in the western equatorial Atlantic South American versus African Provenance discriminated by magnetic mineral analysis. In: Wefer, G., Mulitza, S., Ratmeyer, V. (Eds.), The South Atlantic in the Late Quaternary: Reconstruction of Material Budgets and Current Systems. Springer-Verlag, pp. 213–236.

Bloemendal, J., Lamb, B., King, J., 1988. Paleoenvironmental implications of rock–magnetic properties of Late Quaternary sediment cores from the eastern equatorial Atlantic. Palaeoceanography 3, 61–87.

Bloemendal, J., deMenocal, P., 1989. Evidence for a change in the periodicity of tropical climate cycles at 2.4 Myr from whole-core magnetic susceptibility measurements. Nature 342, 897–900.

Bloemendal, J., King, J.W., Hall, F.R., Doh, S.J., 1992. Rock magnetism of late neogene and pleistocene deep-sea sediments – relationship to sediment source, diagenetic processes, and sediment lithology. Journal of Geophysical Research-Solid Earth 97, 4361–4375.

Bloemendal, J., King, J.W., Hunt, A., Demenocal, P.B., Hayashida, A., 1993. Origin of the sedimentary magnetic record at ocean drilling program sites on the Owen ridge, Western Arabian Sea. Journal of Geophysical Research-Solid Earth 98, 4199–4219.

Bloemendal, J., Liu, X.M., 2005. Rock magnetism and geochemistry of two plio-pleistocene Chinese loess-palaeosol sequences – implications for quantitative palaeoprecipitation reconstruction. Palaeogeography Palaeoclimatology Palaeoecology 226, 149–166.

Bopp, L., Kohfeld, K.E., Le Quere, C., Aumont, O., 2003. Dust impact on marine biota and atmospheric $CO_2$ during glacial periods. Paleoceanography 18.

Bory, A.J.M., Biscaye, P.E., Grousset, F.E., 2003a. Two distinct seasonal Asian source regions for mineral dust deposited in Greenland (NorthGRIP). Geophysical Research Letters 30.

Bory, A.J.M., Biscaye, P.E., Grousset, F.E., Zdanowicz, C.M., Prospero, J.M., 2003b. East-Asian dust sources and long-range transport: mineralogical and isotopic (Sr and Nd) constraints. Geochimica Et Cosmochimica Acta 67, A43.

Bowler, J.M., 1976. Aridity in Australia – age, origins and expression in aeolian landforms and sediments. Earth-Science Reviews 12, 279–310.

Boyd, P.W., Ellwood, M.J., 2010. The biogeochemical cycle of iron in the ocean. Nature Geoscience 3, 675–682.

Boyd, P.W., Mackie, D.S., Hunter, K.A., 2010. Aerosol iron deposition to the surface ocean – modes of iron supply and biological responses. Marine Chemistry 120, 128–143.

Bradtmiller, L.I., Anderson, R.F., Fleisher, M.Q., Burckle, L.H., 2007. Opal burial in the equatorial Atlantic Ocean over the last 30 ka: implications for glacial–interglacial changes in the ocean silicon cycle. Paleoceanography 22.

Bristow, C.S., Drake, N., Armitage, S., 2009. Deflation in the dustiest place on Earth: the Bodele depression, Chad. Geomorphology 105, 50–58.

Canfield, D.E., Berner, R.A., 1987. Dissolution and pyritization of magnetite in anoxic marine-sediments. Geochimica Et Cosmochimica Acta 51, 645–659.

Canfield, D.E., Raiswell, R., Bottrell, S., 1992. The reactivity of sedimentary iron minerals toward sulfide. American Journal of Science 292, 659–683.

Carter-Stiglitz, B., Banerjee, S.K., Gourlan, A., Oches, E., 2006. A multi-proxy study of Argentina loess: marine oxygen isotope stage 4 and 5 environmental record from pedogenic hematite. Palaeogeography Palaeoclimatology Palaeoecology 239, 45–62.

Castaneda, I.S., Mulitza, S., Schefuss, E., dos Santos, R.A.L., Damste, J.S.S., Schouten, S., 2009. Wet phases in the Sahara/Sahel region and human migration patterns in North Africa. Proceedings of the National Academy of Sciences of the United States of America 106, 20159–20163.

Cai, Y.J., Tan, L.C., Cheng, H., An, Z.S., Edwards, R.L., Kelly, M.J., Kong, X.G., Wang, X.F., 2010. The variation of summer monsoon precipitation in central China since the last deglaciation. Earth and Planetary Science Letters 291, 21–31.

Chadwick, O.A., Derry, L.A., Vitousek, P.M., Huebert, B.J., Hedin, L.O., 1999. Changing sources of nutrients during four million years of ecosystem development. Nature 397, 491–497.

Chen, J., Chen, Y., Liu, L.W., Ji, J.F., Balsam, W., Sun, Y.B., Lu, H.Y., 2006. Zr/Rb ratio in the Chinese loess sequences and its implication for changes in the East Asian winter monsoon strength. Geochimica Et Cosmochimica Acta 70, 1471–1482.

Chen, T.H., Xie, Q.Q., Xu, H.F., Chen, J., Ji, J.F., Lu, H.Y., Balsam, W., 2010. Characteristics and formation mechanism of pedogenic hematite in Quaternary Chinese loess and paleosols. Catena 81, 217–225.

Chen, Y., Chen, J., Liu, L.W., Ji, J.F., Zhang, J.X., 2003. Spatial and temporal changes of summer monsoon on the Loess Plateau of Central China during the last 130 ka inferred from Rb/Sr ratios. Science in China Series D-Earth Sciences 46, 1022–1030.

Cheng, H., Edwards, R.L., Broecker, W.S., Denton, G.H., Kong, X.G., Wang, Y.J., Zhang, R., Wang, X.F., 2009. Ice age terminations. Science 326, 248–252.

Chlachula, J., Evans, M.E., Rutter, N.W., 1998. A magnetic investigation of a Late Quaternary loess/palaeosol record in Siberia. Geophysical Journal International 132, 128–132.

Claquin, T., Schulz, M., Balkanski, Y.J., 1999. Modeling the mineralogy of atmospheric dust sources. Journal of Geophysical Research-Atmospheres 104, 22243–22256.

Clemens, S.C., Prell, W.L., 1991. Late quaternary forcing of indian-ocean summer-monsoon winds - a comparison of fourier model and general-circulation model results. Journal of Geophysical Research-Atmospheres 96, 22683–22700.

Coudegaussen, G., Rognon, P., Rapp, A., Nihlen, T., 1987. Dating of peridesert loess in matmata, south tunisia, by radiocarbon and thermo-luminescence methods. Zeitschrift Fur Geomorphologie 31, 129–144.

da Silva, A.R., de Souza, I.G., da Costa, A.C.S., 2010. Suscetibilidade magnética do horizonte B de solos do Estado do Paraná. Rev. Bras. Ciênc. Solo (Online) 34 (2), 329–338.

Day, R., Fuller, M., Schmidt, V.A., 1977. Hystereis properties of titanomagnetites – grain size and compositional dependence. Physics of the Earth and Planetary Interiors 13, 260–267.

de Baar, H.J.W., Boyd, P.W., Coale, K.H., Landry, M.R., Tsuda, A., Assmy, P., Bakker, D.C.E., Bozec, Y., Barber, R.T., Brzezinski, M.A., Buesseler, K.O., Boye, M., Croot, P.L., Gervais, F., Gorbunov, M.Y., Harrison, P.J., Hiscock, W.T., Laan, P., Lancelot, C., Law, C.S., Levasseur, M., Marchetti, A., Millero, F.J., Nishioka, J., Nojiri, Y., van Oijen, T., Riebesell, U., Rijkenberg, M.J.A., Saito, H., Takeda, S., Timmermans, K.R., Veldhuis, M.J.W., Waite, A.M., Wong, C.S., 2005. Synthesis of iron fertilization experiments: from the iron age in the age of enlightenment. Journal of Geophysical Research-Oceans 110.

deMenocal, P., Bloemendal, J., King, J., 1991. A rock-magnetic record of monsoonal dust deposition to the Arabian Sea: evidence for a shift in the mode of deposition at 2.4 Ma. In: Prell, W.L., Niitsuma, N., et al. (Eds.), Proceedings Ocean Drilling Program Scientific Results, vol. 117. Ocean Drilling Program, College Station, TX, pp. 389–407.

Dearing, J.A., Dann, R.J.L., Hay, K., Lees, J.A., Loveland, P.J., Maher, B.A., Ogrady, K., 1996. Frequency-dependent susceptibility measurements of environmental materials. Geophysical Journal International 124, 228–240.

Dearing, J.A., Hay, K.L., Baban, S.M.J., Huddleston, A.S., Wellington, E.M.H., Loveland, P.J., 1996. Magnetic susceptibility of soil: an evaluation of conflicting theories using a national data set. Geophysical Journal International 127, 728–734.

Dearing, J.A., Livingstone, I.P., Bateman, M.D., White, K., 2001. Palaeoclimate records from OIS 8.0-5.4 recorded in loess/palaeosol sequences on the Matmata Plateau, southern Tunisia, based on mineral magnetism and new luminescence dating. Quaternary International 76/77, 43–56.

Dearing, J.A., Hannam, J.A., Anderson, A.S., Wellington, E.M.H., 2001. Magnetic, geochemical and DNA properties of highly magnetic soils in England. Geophysical Journal International 144, 183–196.

Dekkers, M.J., 1989. Magnetic-properties of natural goethite. 1. Grain-size dependence of some low-field and high-field related rock-magnetic parameters measured at room-temperature. Geophysical Journal-Oxford 97, 323–340.

Delmonte, B., Andersson, P.S., Schoberg, H., Hansson, M., Petit, J.R., Delmas, R., Gaiero, D.M., Maggi, V., Frezzotti, M., 2009. Geographic provenance of aeolian dust in East Antarctica during Pleistocene glaciations: preliminary results from Talos Dome and comparison with East Antarctic and new Andean ice core data. Quaternary Science Reviews 29, 256–264.

Ding, Z., Yu, Z., Rutter, N.W., Liu, T., 1994. Towards an orbital time-scale for Chinese loess deposits. Quaternary Science Reviews 13, 39–70.

Ding, Z.L., Derbyshire, E., Yang, S.L., Yu, Z.W., Xiong, S.F., Liu, T.S., 2002a. Stacked 2.6-Ma grain size record from the Chinese loess based on five sections and correlation with the deep-sea delta O-18 record. Paleoceanography 17.

Ding, Z.L., Ranov, V., Yang, S.L., Finaev, A., Han, J.M., Wang, G.A., 2002b. The loess record in southern Tajikistan and correlation with Chinese loess. Earth and Planetary Science Letters 200, 387–400.

Doh, S.J., King, J.W., Leinen, M., 1988. A rock-magnetic study of giant piston cores LL44-GPC3 from the central North Pacific and its paleoceanographic implications. Paleoceanography 3, 89–111.

Duce, R.A., Tindale, N., Zhuang, G., 1991a. Atmospheric iron and its impact on marine biological productivity and chemical cycling. Abstracts of Papers of the American Chemical Society 201, 20. 20-NUCL.

Duce, R.A., Unni, C.K., Ray, B.J., Prospero, J.M., Merrill, J.T., 1980. Long-range atmospheric transport of soil dust from Asia to the tropical North Pacific – temporal variability. Science 209, 1522–1524.

Duce, P.S., Liss, J.T., Merrill, E.L., Atlas, P., Buat-Menard, B.B., Hicks, J.M., Miller, J.M., Prospero, R., Arimoto, T.M., Church, W., Ellis, J.N., Galloway, L., Hansen, T.D., Jickells, A.H., Knap, K.H., Reinhardt, B., Schneider, A., Soudine, J.J., Tokos, S., Tsunogai, R., Wollast, M., Zhou, M., 1991b. The atmospheric input of trace species to the world ocean. Global Biogeochemical Cycles 5, 193–259.

Dykoski, C.A., Edwards, R.L., Cheng, H., Yuan, D.X., Cai, Y.J., Zhang, M.L., Lin, Y.S., Qing, J.M., An, Z.S., Revenaugh, J., 2005. A high-resolution, absolute-dated Holocene and deglacial Asian monsoon record from Dongge Cave, China. Earth and Planetary Science Letters 233, 71–86.

Egli, R., 2004a. Characterization of individual rock magnetic components by analysis of remanence curves, 1. Unmixing natural sediments. Studia Geophysica Et Geodaetica 48, 391–446.

Egli, R., 2004b. Characterization of individual rock magnetic components by analysis of remanence curves. 2. Fundamental properties of coercivity distributions. Physics and Chemistry of the Earth 29, 851–867.

Egli, R., 2004c. Characterization of individual rock magnetic components by analysis of remanence curves. 3. Bacterial magnetite and natural processes in lakes. Physics and Chemistry of the Earth 29, 869–884.

Egli, R., Chen, A.P., Winklhofer, M., Kodama, K.P., Horng, C.S., 2010. Detection of noninteracting single domain particles using first-order reversal curve diagrams. Geochemistry Geophysics Geosystems 11.

Engelbrecht, J.P., McDonald, E.V., Gillies, J.A., Jayanty, R.K.M., Casuccio, G., Gertler, A.W., 2009a. Characterizing mineral dusts and other aerosols from the Middle EastPart 1: ambient sampling. Inhalation Toxicology 21, 297–326.

Engelbrecht, J.P., McDonald, E.V., Gillies, J.A., Jayanty, R.K.M., Casuccio, G., Gertler, A.W., 2009b. Characterizing mineral dusts and other aerosols from the Middle EastPart 2: grab samples and re-suspensions. Inhalation Toxicology 21, 327–336.

Engelstaedter, S., Washington, R., 2007. Temporal controls on global dust emissions: the role of surface gustiness. Geophysical Research Letters 34.

Fang, X.M., Li, J.J., VanderVoo, R., MacNiocaill, C., Dai, X.R., Kemp, R.A., Derbyshire, E., Cao, J.X., Wang, J.M., Wang, G., 1997. A record of the Blake Event during the last interglacial paleosol in the western Loess Plateau of China. Earth and Planetary Science Letters 146, 73–82.

Fassbinder, J.W.E., Stanjek, H., Vali, H., 1990. Occurrence of magnetic bacteria in soil. Nature 343, 161–163.

Fischer, H., Fundel, F., Ruth, U., Twarloh, B., Wegner, A., Udisti, R., Becagli, S., Castellano, E., Morganti, A., Severi, M., Wolff, E., Littot, G., Rothlisberger, R., Mulvaney, R., Hutterli, M.A., Kaufmann, P., Federer, U., Lambert, F., Bigler, M., Hansson, M., Jonsell, U., de Angelis, M., Boutron, C., Siggaard-Andersen, M.L., Steffensen, J.P., Barbante, C., Gaspari, V., Gabrielli, P., Wagenbach, D., 2007a. Reconstruction of millennial changes in dust emission, transport and regional sea ice coverage using the deep EPICA ice cores from the Atlantic and Indian Ocean sector of Antarctica. Earth and Planetary Science Letters 260, 340–354.

Fischer, H., Siggaard-Andersen, M.L., Ruth, U., Rothlisberger, R., Wolff, E., 2007b. Glacial/interglacial changes in mineral dust and sea-salt records in polar ice cores: sources, transport, and deposition. Reviews of Geophysics 45.

Fleitmann, D., Burns, S.J., Mudelsee, M., Neff, U., Kramers, J., Mangini, A., Matter, A., 2003. Holocene forcing of the Indian monsoon recorded in a stalagmite from Southern Oman. Science 300, 1737–1739.

Folkoff, M.E., 1987. Climatic control of soil acidity in the B horizon of United States soils. Physical Geography 8, 82–97.

Forster, T., Evans, M.E., Heller, F., 1994. The frequency-dependence of low-field susceptibility in loess sediments. Geophysical Journal International 118, 636–642.

Forster, T., Heller, F., 1994. Loess deposits from the Tajik depression (Central-Asia) – magnetic-properties and paleoclimate. Earth and Planetary Science Letters 128, 501–512.

France, D.E., Oldfield, F., 2000. Identifying goethite and hematite from rock magnetic measurements of soils and sediments. Journal of Geophysical Research-Solid Earth 105, 2781–2795.

Franke, C., von Dobeneck, T., Drury, M.R., Meeldijk, J.D., Dekkers, M.J., 2007. Magnetic petrology of equatorial Atlantic sediments: electron microscopy results and their implications for environmental magnetic interpretation. Paleoceanography 22.

Frechen, M., Oches, E.A., Kohfeld, K.E., 2003. Loess in Europe – mass accumulation rates during the Last Glacial Period. Quaternary Science Reviews 22, 1835–1857.

Freed, W.K., Watkins, N.D., 1975. Volcanic eruptions – contribution to magnetism in deep-sea sediments downwind from Azores. Science 188, 1203–1205.

Gaiero, D.M., 2007. Dust provenance in Antarctic ice during glacial periods: from where in southern South America? Geophysical Research Letters 34.

Gajdardziska-Josifovska, M., McClean, R.G., Schofield, M.A., Sommer, C.V., Kean, W.F., 2001. Discovery of nanocrystalline botanical magnetite. European Journal of Mineralogy 13, 863–870.

Ganopolski, A., Kubatzki, C., Claussen, M., Brovkin, V., Petoukhov, V., 1998. The influence of vegetation–atmosphere–ocean interaction on climate during the mid-Holocene. Science 280, 1916–1919.
Geiss, C.E., Egli, R., Zanner, C.W., 2008. Direct estimates of pedogenic magnetite as a tool to reconstruct past climates from buried soils. Journal of Geophysical Research-Solid Earth 113.
Geiss, C.E., Zanner, C.W., 2006. How abundant is pedogenic magnetite? Abundance and grain size estimates for loessic soils based on rock magnetic analyses. Journal of Geophysical Research-Solid Earth 111.
Geiss, C.E., Zanner, C.W., 2007. Sediment magnetic signature of climate in modern loessic soils from the Great Plains. Quaternary International 162, 97–110.
Ginoux, P., Chin, M., Tegen, I., Prospero, J.M., Holben, B., Dubovik, O., Lin, S.J., 2001. Sources and distributions of dust aerosols simulated with the GOCART model. Journal of Geophysical Research-Atmospheres 106 (D17), 20255–20273.
Glaccum, R.A., Prospero, J.M., 1980. Saharan aerosols over the tropical North-Atlantic – mineralogy. Marine Geology 37, 295–321.
Goudie, A.S., Middleton, N.J., 2001. Saharan dust storms: nature and consequences. Earth-Science Reviews 56, 179–204.
Grini, A., Zender, C.S., 2004. Roles of saltation, sandblasting, and wind speed variability on mineral dust aerosol size distribution during the Puerto Rican Dust Experiment (PRIDE). Journal of Geophysical Research-Atmospheres 109.
Grousset, F.E., Biscaye, P.E., Zindler, A., Prospero, J., Chester, R., 1988. Neodymium Isotopes as Tracers in Marine-Sediments and Aerosols - North-Atlantic. Earth and Planetary Science Letters 87, 367–378.
Grousset, F.E., Biscaye, P.E., Revel, M., Petit, J.R., Pye, K., Joussaume, S., Jouzel, J., 1992a. Antarctic (Dome C) ice-core dust at 18 Ky Bp – isotopic constraints on origins. Earth and Planetary Science Letters 111, 175–182.
Grousset, F.E., Rognon, P., Coudegaussen, G., Pedemay, P., 1992b. Origins of peri-saharan dust deposits traced by their Nd and Sr isotopic composition. Palaeogeography Palaeoclimatology Palaeoecology 93, 203–212.
Guo, B., Zhu, R.X., Florindo, F., Ding, Z.L., Sun, J.M., 2002. A short, reverse polarity interval within the Jaramillo subchron: evidence from the Jingbian section, northern Chinese Loess Plateau. Journal of Geophysical Research-Solid Earth 107.
Guo, B., Zhu, R.X., Roberts, A.P., Florindo, F., 2001. Lack of correlation between paleoprecipitation and magnetic susceptibility of Chinese loess/paleosol sequences. Geophysical Research Letters 28, 4259–4262.
Guo, Z.T., Berger, A., Yin, Q.Z., Qin, L., 2009. Strong asymmetry of hemispheric climates during MIS-13 inferred from correlating China loess and Antarctica ice records. Climate of the Past 5, 21–31.
Haberzettl, T., Anselmetti, F.S., Bowen, S.W., Fey, M., Mayr, C., Zolitschka, B., Ariztegui, D., Mauz, B., Ohlendorf, C., Kastner, S., Lucke, A., Schabitz, F., Wille, M., 2009. Late Pleistocene dust deposition in the Patagonian steppe–extending and refining the paleoenvironmental and tephrochronological record from Laguna Potrok Aike back to 55 ka. Quaternary Science Reviews 28, 2927–2939.
Han, J.M., Lu, H.Y., Wu, N.Q., Gui, Z.T., 1996. The magnetic susceptibility of modern soils in China and its use for paleoclimate reconstruction. Studia Geophysica and Geodaetica 40, 262–275.
Hanesch, M., Scholger, R., 2005. The influence of soil type on the magnetic susceptibility measured throughout soil profiles. Geophysical Journal International 161, 50–56.
Hanesch, M., Scholger, R., Dekkers, M.J., 2001. The application of fuzzy c-means cluster analysis and non-linear mapping to a soil data set for the detection of polluted sites. Physics and Chemistry of the Earth Part A-Solid Earth and Geodesy 26, 885–891.
Hao, Q.Z., Guo, Z.T., 2005. Spatial variations of magnetic susceptibility of Chinese loess for the last 600 kyr: implications for monsoon evolution. Journal of Geophysical Research-Solid Earth 110.
Hao, Q.Z., Oldfield, F., Bloemendal, J., Torrent, J., Guo, Z.T., 2009. The record of changing hematite and goethite accumulation over the past 22 Myr on the Chinese Loess Plateau from magnetic measurements and diffuse reflectance spectroscopy. Journal of Geophysical Research-Solid Earth 114.
Harrison, R.J., Feinberg, J.M., 2008. FORCinel: an improved algorithm for calculating first-order reversal curve distributions using locally weighted regression smoothing. Geochemistry Geophysics Geosystems 9.
Harrison, S.P., Kohfeld, K.E., Roelandt, C., Claquin, T., 2001. The role of dust in climate changes today, at the last glacial maximum and in the future. Earth-Science Reviews 54, 43–80.
Hatfield, R.G., Maher, B.A., 2009. Fingerprinting upland sediment sources: particle size-specific magnetic linkages between soils, lake sediments and suspended sediments. Earth Surface Processes and Landforms 34, 1359–1373.
Haug, G.H., Maslin, M.A., Sarnthein, M., Stax, R., Tiedemann, R., 1995. Evolution of northwest Pacific sedimentation patterns since 6 Ma (site 882). In: Rea, D.K., Basov, I.A., Scholl, D.W., Allan, J.F. (Eds.), Proceedings of the Ocean Drilling Program, Scientific Results, vol. 145. Ocean Drilling Program, College Sation, TX.
Heil, C.W., King, J.W., Zarate, M.A., Schultz, P.H., 2010. Climatic interpretation of a 1.9 Ma environmental magnetic record of loess deposition and soil formation in the central eastern Pampas of Buenos Aires, Argentina. Quaternary Science Reviews 29, 2705–2718.
Heller, F., Liu, T.S., 1982. Magnetostratigraphical dating of Loess deposits in China. Nature 300, 431–433.
Heller, F., Liu, T.S., 1984. Magnetism of Chinese Loess deposits. Geophysical Journal of the Royal Astronomical Society 77, 125.
Heller, F., Liu, X.M., Liu, T.S., Xu, T.C., 1991. Magnetic-susceptibility of Loess in China. Earth and Planetary Science Letters 103, 301–310.
Heller, F., Shen, C.D., Beer, J., Liu, X.M., Liu, T.S., Bronger, A., Suter, M., Bonani, G., 1993. Quantitative estimates of pedogenic ferromagnetic mineral formation in Chinese loess and paleoclimatic implications. Earth and Planetary Science Letters 114, 385–390.
Heller, F., Tungsheng, L., 1986. Paleoclimatic and sedimentary history from magnetic-susceptibility of Loess in China. Geophysical Research Letters 13, 1169–1172.
Heslop, D., Dekkers, M.J., Kruiver, P.P., van Oorschot, I.H.M., 2002a. Analysis of isothermal remanent magnetization acquisition curves using the expectation–maximization algorithm. Geophysical Journal International 148, 58–64.
Heslop, D., Dekkers, M.J., Langereis, C.G., 2002b. Timing and structure of the mid-Pleistocene transition: records from the loess deposits of northern China. Palaeogeography Palaeoclimatology Palaeoecology 185, 133–143.
Heslop, D., Dillon, M., 2007. Unmixing magnetic remanence curves without a priori knowledge. Geophysical Journal International 170, 556–566.
Heslop, D., Langereis, C.G., Dekkers, M.J., 2000. A new astronomical timescale for the loess deposits of Northern China. Geologica Carpathica 51, 202.
Hesse, P.P., 1997. Mineral magnetic 'tracing' of aeolian dust in southwest Pacific sediments. Palaeogeography Palaeoclimatology Palaeoecology 131, 327–353.
Hounslow, M.W., Maher, B.A., 1996. Quantitative extraction and analysis of carriers of magnetization in sediments. Geophysical Journal International 124, 57–74.
Hounslow, M.W., Maher, B.A., 1999. Source of the climate signal recorded by magnetic susceptibility variations in Indian Ocean sediments. Journal of Geophysical Research-Solid Earth 104, 5047–5061.
Hovan, S.A., Rea, D.K., Pisias, N., 1991. Late pleistocene continental climate and oceanic variability recorded in Northwest Pacific sediments. Paleoceanography 6 (3), 349–370.
Hovan, S.A., Rea, D.K., Pisias, N.G., Shackleton, N.J., 1989. A direct link between the China Loess and Marine Delta-O-18 records – aeolian flux to the North Pacific. Nature 340, 296–298.
Hsu, N.C., Tsay, S., King, M.D., Diner, D.J., 2007. Dust in the wind. In: King, M.D., Parkinson, C.L., Partington, K.C., Williams, R.G. (Eds.), Our Changing Planet. CUP.
Huang, J., Zhang, C., Prospero, J.M., 2009. Large-scale effect of aerosols on precipitation in the West African Monsoon region. Quarterly Journal of the Royal Meteorological Society 135, 581–594.
Husar, R.B., Prospero, J.M., Stowe, L.L., 1997. Characterization of tropospheric aerosols over the oceans with the NOAA advanced very high resolution radiometer optical thickness operational product. Journal of Geophysical Research-Atmospheres 102, 16889–16909.
IPCC, 2007. P. Forster, V. Ramaswamy, P. Artaxo, T. Berntsen, R. Betts, D.W. Fahey, J. Haywood, J. Lean, D.C. Lowe, G. Myhre, J. Nganga, R. Prinn, G. Raga, M. Schulz, R. Van Dorland, 2007. Changes in atmospheric constituents and in radiative forcing. In: Solomon, S., Qin, D., Manning, M., Chen, Z., Marquis, M., Averyt, K.B., Tignor, M., Miller, H.L. (Eds.), Climate Change 2007: The Physical Science Basis. Contribution of Working Group I to the Fourth Assessment Report of the Intergovernmental Panel on Climate Change. Cambridge University Press, Cambridge, United Kingdom, New York, NY, USA.
Itambi, A.C., von Dobeneck, T., Dekkers, M.J., Frederichs, T., 2010. Magnetic mineral inventory of equatorial Atlantic Ocean marine sediments off Senegal-glacial and interglacial contrast. Geophysical Journal International 183, 163–177.
Itambi, A.C., von Dobeneck, T., Mulitza, S., Bickert, T., Heslop, D., 2009. Millennial-scale northwest African droughts related to Heinrich events and Dansgaard–Oeschger cycles: evidence in marine sediments from offshore Senegal. Paleoceanography 24.
Jahn, B.M., Gallet, S., Han, J.M., 2001. Geochemistry of the Xining, Xifeng and Jixian sections, Loess Plateau of China: eolian dust provenance and paleosol evolution during the last 140 ka. Chemical Geology 178, 71–94.
Jenny, H., 1941. Factors of Soil Formation. McGraw Hill.
Ji, J.F., Balsam, W., Chen, J., Liu, L.W., 2002. Rapid and quantitative measurement of hematite and goethite in the Chinese loess-paleosol sequence by diffuse reflectance spectroscopy. Clays and Clay Minerals 50, 208–216.
Ji, J.F., Chen, J., Balsam, W., Lu, H.Y., Sun, Y.B., Xu, H.F., 2004. High resolution hematite/goethite records from Chinese loess sequences for the last glacial–interglacial cycle: rapid climatic response of the East Asian Monsoon to the tropical Pacific. Geophysical Research Letters 31.
Jiles, D., 1998. Introduction to Magnetism and Magnetic Materials. Chapman & Hall, London.
Kampf, N., Schwertmann, U., 1983. Goethite and hematite in a climosequence in Southern Brazil and their application in classification of Kaolinitic soils. Geoderma 29, 27–39.
Karlin, R., 1990. Magnetite diagenesis in marine-sediments from the Oregon continental-margin. Journal of Geophysical Research-Solid Earth and Planets 95, 4405–4419.
Karlin, R., Levi, S., 1983. Diagenesis of magnetic minerals in recent Hemipelagic sediments. Nature 303, 327–330.
Kemp, R.A., Zarate, M., Toms, P., King, M., Sanabria, J., Arguello, G., 2006. Late Quaternary paleosols, stratigraphy and landscape evolution in the Northern Pampa, Argentina. Quaternary Research 66, 119–132.
Kim, W., Doh, S.J., Yu, Y., Lee, M., 2008. Role of Chinese wind-blown dust in enhancing environmental pollution in Metropolitan Seoul. Environmental pollution 153, 333–341.
King, J.W., Heil, C., Peck, J.A., 2008. Paleomagnetic and mineral–magnetic results from the Lake Bosumtwi drilling project. Eos Trans. AGU, 89(53), Fall Meet. Suppl., Abstract: GP14A-03.
Kodama, K.P., 1995. Magnetic fabrics. Reviews of Geophysics, IUGG Report, 33.

Kohfeld, K.E., 2002. The role of dust in climate cycles. Geochimica Et Cosmochimica Acta 66, A409.
Kohfeld, K.E., Harrison, S.P., 2001. DIRTMAP: the geological record of dust. Earth-Science Reviews 54, 81–114.
Kohfeld, K.E., Le Quere, C., Harrison, S.P., Anderson, R.F., 2005. Role of marine biology in glacial–interglacial $CO_2$ cycles. Science 308, 74–78.
Kravchinsky, V.A., Zykina, V.S., Zykin, V.S., 2008. Magnetic indicator of global paleoclimate cycles in Siberian loess-paleosol sequences. Earth and Planetary Science Letters 265, 498–514.
Krinner, G., Boucher, O., Balkanski, Y., 2006. Ice-free glacial northern Asia due to dust deposition on snow. Climate Dynamics 27, 613–625.
Kropelin, S., Verschuren, D., Lezine, A.M., Eggermont, H., Cocquyt, C., Francus, P., Cazet, J.P., Fagot, M., Rumes, B., Russell, J.M., Darius, F., Conley, D.J., Schuster, M., von Suchodoletz, H., Engstrom, D.R., 2008. Climate-driven ecosystem succession in the Sahara: the past 6000 years. Science 320, 765–768.
Kukla, G., 1987. Loess stratigraphy in central China. Quaternary Science Reviews 6, 191–219.
Kukla, G., An, Z.S., Melice, J.L., Gavin, J., Xiao, J.L., 1990. Magnetic-susceptibility record of Chinese loess. Transactions of the Royal Society of Edinburgh-Earth Sciences 81, 263–288.
Kukla, G., Heller, F., Ming, L.X., Chun, X.T., Sheng, L.T., Sheng, A.Z., 1988. Pleistocene climates in china dated by magnetic-susceptibility. Geology 16, 811–814.
Kurtz, A.C., Derry, L.A., Chadwick, O.A., 2001. Accretion of Asian dust to Hawaiian soils: isotopic, elemental, and mineral mass balances. Geochimica Et Cosmochimica Acta 65, 1971–1983.
Lafon, S., Rajot, J.L., Alfaro, S.C., Gaudichet, A., 2004. Quantification of iron oxides in desert aerosol. Atmospheric Environment 38, 1211–1218.
Lafon, S., Sokolik, I.N., Rajot, J.L., Caquineau, S., Gaudichet, A., 2006. Characterization of iron oxides in mineral dust aerosols: implications for light absorption. Journal of Geophysical Research-Atmospheres 111.
Lagroix, F., Banerjee, S.K., Jackson, M.J., 2004. Magnetic properties of the Old Crow tephra: identification of a complex iron titanium oxide mineralogy. Journal of Geophysical Research-Solid Earth 109.
Lambert, F., Delmonte, B., Petit, J.R., Bigler, M., Kaufmann, P.R., Hutterli, M.A., Stocker, T.F., Ruth, U., Steffensen, J.P., Maggi, V., 2008. Dust-climate couplings over the past 800,000 years from the EPICA Dome C ice core. Nature 452, 616–619.
Lancaster, N., Ollier, C.D., 1983. Sources of sand for the Namib sand sea. Zeitschrift für Geomorphologie, Supplementband 45, 71–83.
Lanci, L., Delmonte, B., Maggi, V., Petit, J.R., Kent, D.V., 2008. Ice magnetization in the EPICA-Dome C ice core: implication for dust sources during glacial and interglacial periods. Journal of Geophysical Research-Atmospheres 113.
Lanci, L., Kent, D.V., 2006. Meteoric smoke fallout revealed by superparamagnetism in Greenland ice. Geophysical Research Letters 33.
Lanci, L., Kent, D.V., Biscaye, P.E., Bory, A., 2001. Isothermal remanent magnetization of Greenland ice. preliminary results. Geophysical Research Letters 28, 1639–1642.
Lanci, L., Kent, D.V., Biscaye, P.E., Steffensen, J.P., 2004. Magnetization of Greenland ice and its relationship with dust content. Journal of Geophysical Research-Atmospheres 109.
Larrasoana, J.C., Roberts, A.P., Rohling, E.J., 2008. Magnetic susceptibility of eastern Mediterranean marine sediments as a proxy for Saharan dust supply? Marine Geology 254, 224–229.
Larrasoana, J.C., Roberts, A.P., Rohling, E.J., Winklhofer, M., Wehausen, R., 2003. Three million years of monsoon variability over the northern Sahara. Climate Dynamics 21, 689–698.
Laskar, J., Robutel, P., Joutel, F., Gastineau, M., Correia, A.C.M., Levrard, B., 2004. A long-term numerical solution for the insolation quantities of the Earth. Astronomy & Astrophysics 428, 261–285.
Lau, K.M., Kim, M.K., Kim, K.M., 2006. Asian summer monsoon anomalies induced by aerosol direct forcing: the role of the Tibetan Plateau. Climate Dynamics 26, 855–864.
Le Borgne, E., 1955. Susceptbilite magnetique anoramle du sol superficiel. Annales Geophysicae 16, 159–195.
Li, F., Ginoux, P., Ramaswamy, V., 2008. Distribution, transport, and deposition of mineral dust in the Southern Ocean and Antarctica: Contribution of major sources. Journal of Geophysical Research-Atmospheres, 113.
Liu, T.-S., 1988. Loess in China. Springer-Verlag, Berlin. 224 p..
Lindsay, W.L., 1979. Chemical Equilibria in Soils. Wiley Interscience.
Liu, Q.S., Banerjee, S.K., Jackson, M.J., Zhu, R.X., Pan, Y.X., 2002. A new method in mineral magnetism for the separation of weak antiferromagnetic signal from a strong ferrimagnetic background. Geophysical Research Letters 29.
Liu, Q.S., Deng, C.L., Yu, Y.J., Torrent, J., Jackson, M.J., Banerjee, S.K., Zhu, R.X., 2005a. Temperature dependence of magnetic susceptibility in an argon environment: implications for pedogenesis of Chinese loess/palaeosols. Geophysical Journal International 161, 102–112.
Liu, Q.S., Torrent, J., Maher, B.A., Yu, Y.J., Deng, C.L., Zhu, R.X., Zhao, X.X., 2005b. Quantifying grain size distribution of pedogenic magnetic particles in Chinese loess and its significance for pedogenesis. Journal of Geophysical Research-Solid Earth, 110.
Liu, Q.S., Bloemendal, J., Torrent, J., Deng, C.L., 2006a. Contrasting behavior of hematite and goethite within paleosol S5 of the Luochuan profile, Chinese Loess Plateau. Geophysical Research Letters 33.
Liu, Q.S., Deng, C.L., Torrent, J., Zhu, R.X., 2007. Review of recent developments in mineral magnetism of the Chinese loess. Quaternary Science Reviews 26, 368–385.
Liu, Q.S., Roberts, A.P., Rohling, E.J., Zhu, R.X., Sun, Y.B., 2008. Post-depositional remanent magnetization lock-in and the location of the Matuyama–Brunhes geomagnetic reversal boundary in marine and Chinese loess sequences. Earth and Planetary Science Letters 275, 102–110.
Liu, Q.S., Torrent, J., Maher, B.A., Yu, Y.J., Deng, C.L., Zhu, R.X., Zhao, X.X., 2005c. Quantifying grain size distribution of pedogenic magnetic particles in Chinese loess and its significance for pedogenesis. Journal of Geophysical Research-Solid Earth 110.
Liu, Q.S., Yu, Y.J., Torrent, J., Roberts, A.P., Pan, Y.X., Zhu, R.X., 2006b. Characteristic low-temperature magnetic properties of aluminous goethite [alpha-(Fe,Al)OOH] explained. Journal of Geophysical Research-Solid Earth 111.
Liu, X.M., Hesse, P., Beget, J., Rolph, T., 2001. Pedogenic destruction of ferrimagnetics in Alaskan loess deposits. Australian Journal of Soil Research 39, 99–115.
Liu, X.M., Rolph, T., Bloemendal, J., Shaw, J., Liu, T.S., 1995. Quantitative Estimates of palaeoprecipitation at Xifeng, in the loess plateau of China. Palaeogeography Palaeoclimatology Palaeoecology 113, 243–248.
Longworth, G., Becker, L.W., Thompson, R., Oldfield, F., Dearing, J.A., Rummery, T.A., 1979. Mossbauer-effect and magnetic studies of secondary iron-oxides in soils. Journal of Soil Science 30, 93–110.
Lovley, D.R., Stolz, J.F., Nord, G.L., Phillips, E.J.P., 1987. Anaerobic production of magnetite by a dissimilatory iron-reducing microorganism. Nature 330, 252–254.
Luo, C., Mahowald, N., Bond, T., Chuang, P.Y., Artaxo, P., Siefert, R., Chen, Y., Schauer, J., 2008. Combustion iron distribution and deposition. Global Biogeochemical Cycles 22.
Lyons, R., Oldfield, F., Williams, E., 2010. Mineral magnetic properties of surface soils and sands across four North African transects and links to climatic gradients. Geochemistry Geophysics Geosystems 11.
Madureira, L.A.S., vanKreveld, S.A., Eglinton, G., Conte, M., Ganssen, G., vanHinte, J.E., Ottens, J.J., 1997. Late Quaternary high-resolution biomarker and other sedimentary climate proxies in a northeast Atlantic core. Paleoceanography 12, 255–269.
Maher, B.A., 1986. Characterization of soils by mineral magnetic measurements. Physics of the Earth and Planetary Interiors 42, 76–92.
Maher, B.A., Mutch, T.J., in prep. Magnetic identification of dust fluxes and provenance in deep sea sediments of the North Atlantic IRD belt.
Maher, B.A., 1988. Magnetic-properties of some synthetic sub-micron magnetites. Geophysical Journal-Oxford 94, 83–96.
Maher, B.A., 1998. Magnetic properties of modern soils and Quaternary loessic paleosols: paleoclimatic implications. Palaeogeography Palaeoclimatology Palaeoecology 137, 25–54.
Maher, B.A., 2005. Loess. McGraw-Hill Encyclopedia of Science & Technology, McGraw Hill, New York.
Maher, B.A., 2007. Environmental magnetism and climate change. Contemporary Physics 48, 247–274.
Maher, B.A., 2008. Holocene variability of the East Asian summer monsoon from Chinese cave records: a re-assessment. Holocene 18, 861–866.
Maher, B.A., Kohfeld, K. 2009, http://www.lec.lancs.ac.uk/research/LU_themes/inqua_working_group.php.
Maher, B.A., Alekseev, A., Alekseeva, T., 2002. Variation of soil magnetism across the Russian steppe: its significance for use of soil magnetism as a palaeorainfall proxy. Quaternary Science Reviews 21, 1571–1576.
Maher, B.A., Alekseev, A., Alekseeva, T., 2003. Magnetic mineralogy of soils across the Russian Steppe: climatic dependence of pedogenic magnetite formation. Palaeogeography Palaeoclimatology Palaeoecology 201, 321–341.
Maher, B.A., Dennis, P.F., 2001. Evidence against dust-mediated control of glacial–interglacial changes in atmospheric $CO_2$. Nature 411, 176–180.
Maher, B.A., Hu, M.Y., Roberts, H.M., Wintle, A.G., 2003. Holocene loess accumulation and soil development at the western edge of the Chinese Loess Plateau: implications for magnetic proxies of palaeorainfall. Quaternary Science Reviews 22, 445–451.
Maher, B.A., Hu, M.Y., 2006. A high-resolution record of Holocene rainfall variations from the western Chinese Loess Plateau: antiphase behaviour of the African/Indian and East Asian summer monsoons. Holocene 16, 309–319.
Maher, B.A., Karloukovski, V.V., Mutch, T.J., 2004. High-field remanence properties of synthetic and natural submicrometre haematites and goethites: significance for environmental contexts. Earth and Planetary Science Letters 226, 491–505.
Maher, B.A., Mutch, T.J., Cunningham, D., 2009a. Magnetic and geochemical characteristics of Gobi Desert surface sediments: implications for provenance of the Chinese Loess Plateau. Geology 37, 279–282.
Maher, B.A., Prospero, J.M., Mackie, D., Gaiero, D., Hesse, P.P., Balkanski, Y., 2010. Global connections between aeolian dust, climate and ocean biogeochemistry at the present day and at the last glacial maximum. Earth-Science Reviews 99, 61–97.
Maher, B.A., Thompson, R., 1992. Paleoclimatic significance of the mineral magnetic record of the Chinese loess and paleosols. Quaternary Research 37, 155–170.
Maher, B.A., Thompson, R., 1995. Paleorainfall reconstructions from pedogenic magnetic susceptibility variations in the Chinese loess and paleosols. Quaternary Research 44, 383–391.
Maher, B.A., Thompson, R., 1999. Paleomonsoons. I. The paleoclimatic record of the Chinese loess and palaeosols. In: Maher, B.A., Thompson, R. (Eds.), Quaternary Climates, Environments and Magnetism. Cambridge University Press, pp. 81–125.
Maher, B.A., Thompson, R., Hounslow, M.W., 1999. Introduction to Quaternary climates, environments and magnetism. In: Maher, B.A., Thompson, R. (Eds.), Quaternary Climates, Environments and Magnetism. Cambridge University Press, pp. 1–48.

Maher, B.A., Thompson, R., Zhou, L.P., 1994. Spatial and temporal reconstructions of changes in the Asian palaeomonsoon – a new mineral magnetic approach. Earth and Planetary Science Letters 125, 461–471.
Maher, B.A., Watkins, S.J., Brunskill, G., Alexander, J., Fielding, C.R., 2009b. Sediment provenance in a tropical fluvial and marine context by magnetic 'fingerprinting' of transportable sand fractions. Sedimentology 56, 841–861.
Maher, B.A., in prep. Dust and diagenesis in Quaternary-age sediments of the Coral Sea.
Mahowald, N., Kohfeld, K., Hansson, M., Balkanski, Y., Harrison, S.P., Prentice, I.C., Schulz, M., Rodhe, H., 1999. Dust sources and deposition during the last glacial maximum and current climate: a comparison of model results with paleodata from ice cores and marine sediments. Journal of Geophysical Research-Atmospheres 104, 15895–15916.
Mahowald, N.M., Baker, A.R., Bergametti, G., Brooks, N., Duce, R.A., Jickells, T.D., Kubilay, N., Prospero, J.M., Tegen, I., 2005. Atmospheric global dust cycle and iron inputs to the ocean. Global Biogeochemical Cycles 19.
Mahowald, N.M., Muhs, D.R., Levis, S., Rasch, P.J., Yoshioka, M., Zender, C.S., Luo, C., 2006. Change in atmospheric mineral aerosols in response to climate: last glacial period, preindustrial, modern, and doubled carbon dioxide climates. Journal of Geophysical Research-Atmospheres 111 (D10), D10202.
Maring, H., Savoie, D.L., Izaguirre, M.A., Custals, L., Reid, J.S., 2003. Mineral dust aerosol size distribution change during atmospheric transport. Journal of Geophysical Research-Atmospheres 108.
Marino, F., Castellano, E., Ceccato, D., De Deckker, P., Delmonte, B., Ghermandi, G., Maggi, V., Petit, J.R., Revel-Rolland, M., Udisti, R., 2008. Defining the geochemical composition of the EPICA Dome C ice core dust during the last glacial–interglacial cycle. Geochemistry Geophysics Geosystems 9.
Marticorena, B., Bergametti, G., Aumont, B., Callot, Y., Ndoume, C., Legrand, M., 1997. Modeling the atmospheric dust cycle. 2. Simulation of Saharan dust sources. Journal of Geophysical Research-Atmospheres 102, 4387–4404.
Martin, J.H., 1990. Glacial–interglacial $CO_2$ change: the iron hypothesis. Paleoceanography 5 (1), 1–13.
Martinez-Garcia, A., Rosell-Mele, A., Geibert, W., Gersonde, R., Masque, P., Gaspari, V., Barbante, C., 2009. Links between iron supply, marine productivity, sea surface temperature, and $CO_2$ over the last 1.1 Ma. Paleoceanography 24.
Matasova, G., Petrovsky, E., Jordanova, N., Zykina, V., Kapicka, A., 2001. Magnetic study of Late Pleistocene loess/palaeosol sections from Siberia: palaeoenvironmental implications. Geophysical Journal International 147, 367–380.
McGee, D., Broecker, W.S., Winckler, G., 2010. Gustiness: the driver of glacial dustiness? Quaternary Science Reviews 29, 2340–2350.
McTainsh, G., Chan, Y.C., McGowan, H., Leys, J., Tews, K., 2005. The 23rd October 2002 dust storm in eastern Australia: characteristics and meteorological conditions. Atmospheric Environment 39, 1227–1236.
Michel, F.M., Barron, V., Torrent, J., Morales, M.P., Serna, C.J., Boily, J.F., Liu, Q.S., Ambrosini, A., Cismasu, A.C., Brown, G.E., 2009. Ordered ferrimagnetic form of ferrihydrite reveals links among structure, composition, and magnetism. Proceedings of the National Academy of Sciences of the United States of America 107, 2787–2792.
Miller, R.L., Perlwitz, J., Tegen, I., 2004a. Feedback upon dust emission by dust radiative forcing through the planetary boundary layer. Journal of Geophysical Research-Atmospheres 109.
Miller, R.L., Tegen, I., Perlwitz, J., 2004b. Surface radiative forcing by soil dust aerosols and the hydrologic cycle. Journal of Geophysical Research-Atmospheres 109.
Minasny, B., McBratney, A.B., 2002. FuzME version 3.0. Australian Centre for Precision Agriculture, The University of Sydney, Australia. Available from: <http://www.usyd.edu.au/su/agric/acpa> (10 July 2008).
Moore, J.K., Braucher, O., 2008. Sedimentary and mineral dust sources of dissolved iron to the world ocean. Biogeosciences 5, 631–656.
Morris, R.V. et al., 2000. Mineralogy, composition, and alteration of Mars Pathfinder rocks and soils: evidence from multispectral, elemental, and magnetic data on terrestrial analogue, SNC meteorite, and Pathfinder samples. Journal of Geophysical Research 105 (E1), 1757–1817. doi:10.1029/1999JE001059.
Mulitza, S., Heslop, D., Pittauerova, D., Fischer, H.W., Meyer, I., Stuut, J.B., Zabel, M., Mollenhauer, G., Collins, J.A., Kuhnert, H., Schulz, M., 2010. Increase in African dust flux at the onset of commercial agriculture in the Sahel region. Nature 466, 226–228.
Mulitza, S., Prange, M., Stuut, J.B., Zabel, M., von Dobeneck, T., Itambi, A.C., Nizou, J., Schulz, M., Wefer, G., 2008. Sahel megadroughts triggered by glacial slowdowns of Atlantic meridional overturning. Paleoceanography 23.
Mullins, C.E., 1977. Magnetic-susceptibility of soil and its significance in soil science – review. Journal of Soil Science 28, 223–246.
Myhre, G., 2009. Consistency between satellite-derived and modeled estimates of the direct aerosol effect. Science 325, 187–190.
Nie, J.S., Song, Y.G., King, J.W., Egli, R., 2010. Consistent grain size distribution of pedogenic maghemite of surface soils and Miocene loessic soils on the Chinese Loess Plateau. Journal of Quaternary Science 25, 261–266.
Norrish, K., Taylor, R.M., 1961. Isomorphous replacement of iron by aluminium in soil goethites. Journal of Soil Science 12, 294.
Oldfield, F., Hunt, A., Jones, M.D.H., Chester, R., Dearing, J.A., Olsson, L., Prospero, J.M., 1985. Magnetic differentiation of atmospheric dusts. Nature 317, 516–518.
Oldfield, F., Hao, Q.Z., Bloemendal, J., Gibbs-Eggar, Z., Patil, S., Guo, Z.T., 2009. Links between bulk sediment particle size and magnetic grain-size: general observations and implications for Chinese loess studies. Sedimentology 56, 2091–2106.
Orgeira, M.J., Egli, R., Compagnucci, R.H., 2011. A quantitative model of magnetic enhancement in loessic soils. Studia Geophysica et Geodaetica.
Orgeira, M.J., Vasquez, C.A., Compagnucci, R.H., Raposo, I., Pereyra, F.X., 2009. Rock magnetism in soils of the Pampean plain. Buenos Aires province, Argentina. Linking climate and magnetic behaviour. Revista Mexicana De Ciencias Geologicas 26, 65–78.
Ozdemir, O., Dunlop, D.J., Moskowitz, B.M., 1993. The effect of oxidation on the Verwey transition in magnetite. Geophysical Research Letters 20, 1671–1674.
Pailhe, N., Wattiaux, A., Gaudon, M., Demourgues, A., 2008. Impact of structural features on pigment properties of alpha-$Fe_2O_3$ haematite. Journal of Solid State Chemistry 181, 2697–2704.
Pan, Y.X., Zhu, R.X., Liu, Q.S., Guo, B., Yue, L.P., Wu, H.N., 2002. Geomagnetic episodes of the last 1.2 Myr recorded in Chinese loess. Geophysical Research Letters 29.
Pavich, M.J., Brown, L., Harden, J., Klein, J., Middleton, R., 1986. Be-10 distribution in soils from Merced River terraces, California. Geochimica et Cosmochimica Acta 50, 1727–1735.
Peck, J.A., Green, R.R., Shanahan, T., King, J.W., Overpeck, J.T., Scholz, C.A., 2004. A magnetic mineral record of Late Quaternary tropical climate variability from Lake Bosumtwi, Ghana. Palaeogeography Palaeoclimatology Palaeoecology 215, 37–57.
Petit, J.R., Jouzel, J., Raynaud, D., Barkov, N.I., Barnola, J.M., Basile, I., Bender, M., Chappellaz, J., Davis, M., Delaygue, G., Delmotte, M., Kotlyakov, V.M., Legrand, M., Lipenkov, V.Y., Lorius, C., Pepin, L., Ritz, C., Saltzman, E., Stievenard, M., 1999. Climate and atmospheric history of the past 420,000 years from the Vostok ice core, Antarctica. Nature 399, 429–436.
Pike, C.R., Roberts, A.P., Verosub, K.L., 1999. Characterizing interactions in fine magnetic particle systems using first order reversal curves. Journal of Applied Physics 85, 6660–6667.
Pike, C.R., Roberts, A.P., Verosub, K.L., 2001. First-order reversal curve diagrams and thermal relaxation effects in magnetic particles. Geophysical Journal International 145, 721–730.
Porder, S., Chadwick, O.A., 2009. Climate and soil-age constraints on nutrient uplift and retention by plants. Ecology 90, 623–636.
Porter, S.C., Hallet, B., Wu, X.H., An, Z.H., 2001. Dependence of near-surface magnetic susceptibility on dust accumulation rate and precipitation on the Chinese Loess Plateau. Quaternary Research 55, 271–283.
Prins, M.A., Vriend, M., Nugteren, G., Vandenberghe, J., Lu, H.Y., Zheng, H.B., Weltje, G.J., 2007. Late Quaternary aeolian dust input variability on the Chinese Loess Plateau: inferences from unmixing of loess grain-size records. Quaternary Science Reviews 26, 230–242.
Prospero, J.M., 1996a. The atmospheric transport of particles to the Ocean. In: Ittekkot, V., Schafer, P., Honjo, S., Depetris, P.J. (Eds.), Particle Flux in the Ocean. John Wiley & Sons Ltd., New York, p. 372.
Prospero, J.M., 1996b. Saharan dust transport over the North Atlantic Ocean and Mediterranean: an overview. Environmental Science and Technology Library 11, 133–151.
Prospero, J.M., Ginoux, P., Torres, O., Nicholson, S.E., Gill, T.E., 2002. Environmental characterization of global sources of atmospheric soil dust identified with the Nimbus 7 Total Ozone Mapping Spectrometer (TOMS) absorbing aerosol product. Reviews of Geophysics 40 (1), RG1002.
Prospero, J.M., Lamb, P.J., 2003. African droughts and dust transport to the Caribbean: climate change implications. Science 302 (5647), 1024–1027.
Prospero, J.M., Nees, R.T., 1986. Impact of the North African drought and El Niño on mineral dust in the Barbados trade winds. Nature 320 (6064), 735–738.
Prospero, J.M., Uematsu, M., Savoie, D., 1989. Mineral aerosol transport to the Pacific Ocean. In: Riley, J.P., Chester, R., Duce, R. (Eds.), Chemical Oceanography. Academic Press, New York, pp. 187–218.
Pugh, R.S., McCave, I.N., Hillenbrand, C.D., Kuhn, G., 2009. Circum-Antarctic age modelling of Quaternary marine cores under the Antarctic Circumpolar Current: ice-core dust-magnetic correlation. Earth and Planetary Science Letters 284, 113–123.
Pye, K., 1989. Processes of fine particle formation, dust source regions, and climatic changes. In: Leinen, M., Sarnthein, M. (Eds.), Paleoclimatology and Paleometeorology: Modern and Past Patterns of Global Atmospheric Transport. Kluwer Academic Pubs, Dordrecht, pp. 3–30.
Pye, K., 1981. Rate of dune reddening in a humid tropical climate. Nature 290, 582–584.
Pye, K., Zhou, L.P., 1989. Late Pleistocene and holocene aeolian dust deposition in North China and the Northwest Pacific-Ocean. Palaeogeography Palaeoclimatology Palaeoecology 73, 11–23.
Quayle, B.M., Mather, T.A., Witt, M.L.I., Maher, B.A., Mitchell, R., Martin, R.S., Calabrese, S., 2010. Application and evaluation of biomagnetic and biochemical monitoring of the dispersion and deposition of volcanically-derived particles at Mt. Etna, Italy. Journal of Volcanology and Geothermal Research 191, 107–116.
Rea, D.K., Hovan, S.A., 1995. Grain-size distribution and depositional processes of the mineral component of Abyssal sediments – lessons from the North Pacific. Paleoceanography 10, 251–258.
Revel-Rolland, M., De Deckker, P., Delmonte, B., Hesse, P.P., Magee, J.W., Basile-Doelsch, I., Grousset, F., Bosch, D., 2006. Eastern Australia: a possible source of dust in East Antarctica interglacial ice. Earth and Planetary Science Letters 249, 1–13.
Reynolds, R., Belnap, J., Reheis, M., Lamothe, P., Luiszer, F., 2001. Aeolian dust in Colorado Plateau soils: nutrient inputs and recent change in source. Proceedings of the National Academy of Sciences of the United States of America 98, 7123–7127.

Reynolds, R., Neff, J., Reheis, M., Lamothe, P., 2006. Atmospheric dust in modem soil on aeolian sandstone, Colorado Plateau (USA): variation with landscape position and contribution to potential plant nutrients. Geoderma 130, 108–123.
Reynolds, R.L., Goldstein, H.L., Miller, M.E., 2010. Atmospheric mineral dust in dryland ecosystems: applications of environmental magnetism. Geochemistry Geophysics Geosystems 11, Q07009. doi:10.1029/2010GC003103.
Roberts, A.P., Liu, Q.S., Rowan, C.J., Chang, L., Carvallo, C., Torrent, J., Horng, C.S., 2006. Characterization of hematite (alpha-$Fe_2O_3$), goethite (alpha-FeOOH), greigite ($Fe_3S_4$), and pyrrhotite ($Fe_7S_8$) using first-order reversal curve diagrams. Journal of Geophysical Research-Solid Earth 111.
Roberts, H.M., 2008. The development and application of luminescence dating to loess deposits: a perspective on the past, present and future. Boreas 37, 483–507.
Roberts, H.M., Muhs, D.R., Wintle, A.G., Duller, G.A.T., Bettis, E.A., 2003. Unprecedented last-glacial mass accumulation rates determined by luminescence dating of loess from western Nebraska. Quaternary Research 59, 411–419.
Roberts, H.M., Wintle, A.G., Maher, B.A., Hu, M.Y., 2001. Holocene sediment-accumulation rates in the western Loess Plateau, China, and a 2500-year record of agricultural activity, revealed by OSL dating. Holocene 11, 477–483.
Robinson, S.G., 1986. The late pleistocene paleoclimatic record of North-Atlantic deep-sea sediments revealed by mineral–magnetic measurements. Physics of the Earth and Planetary Interiors 42, 22–47.
Robinson, S.G., Maslin, M.A., McCave, I.N., 1995. Magnetic-susceptibility variations in upper pleistocene deep-sea sediments of the Ne Atlantic – implications for ice rafting and paleocirculation at the last glacial maximum. Paleoceanography 10, 221–250.
Rochette, P., Mathe, P.E., Esteban, L., Rakoto, H., Bouchez, J.L., Liu, Q.S., Torrent, J., 2005. Non-saturation of the defect moment of goethite and fine-grained hematite up to 57 Teslas. Geophysical Research Letters, 32.
Rohling, E.J., Cane, T.R., Cooke, S., Sprovieri, M., Bouloubassi, I., Emeis, K.C., Schiebel, R., Kroon, D., Jorissen, F.J., Lorre, A., Kemp, A.E.S., 2002. African monsoon variability during the previous interglacial maximum. Earth and Planetary Science Letters 202, 61–75.
Rossignol-Strick, M., 1983. African monsoons, an immediate climate response to orbital insolation. Nature 304, 46–49.
Rothlisberger, R., Mulvaney, R., Wolff, E.W., Hutterli, M.A., Bigler, M., Sommer, S., Jouzel, J., 2002. Dust and sea salt variability in central East Antarctica (Dome C) over the last 45 kyrs and its implications for southern high-latitude climate. Geophysical Research Letters 29.
Rowe, P.J., Maher, B.A., 2000. 'Cold' stage formation of calcrete nodules in the Chinese Loess Plateau: evidence from U-series dating and stable isotope analysis. Palaeogeography Palaeoclimatology Palaeoecology 157, 109–125.
Ruddiman, W.F., 1977. Late Quaternary deposition of ice-rafted sand in subpolar North-Atlantic (Lat 40-Degrees to 65-Degrees-N). Geological Society of America Bulletin 88, 1813–1827.
Ruth, U., Wagenbach, D., Steffensen, J.P., Bigler, M., 2003. Continuous record of microparticle concentration and size distribution in the central Greenland NGRIP ice core during the last glacial period. Journal of Geophysical Research-Atmospheres 108.
Sahota, J.T.S., Mayewski, P.A., Oldfield, F., Twickler, M.S., 1996. Magnetic measurements of Greenland and Himalayan ice-core samples. Holocene 6, 477–480.
Sarnthein, M., Tetzlaff, G., Koopmann, B., Wolter, K., Pflaumann, U., 1981. Glacial and inter-glacial wind regimes over the eastern sub-tropical Atlantic and Northwest Africa. Nature 293, 193–196.
Sartori, M., Evans, M.E., Heller, F., Tsatskin, A., Han, J.M., 2005. The last glacial/interglacial cycle at two sites in the Chinese Loess Plateau: mineral magnetic, grain-size and Be-10 measurements and estimates of palaeoprecipitation. Palaeogeography Palaeoclimatology Palaeoecology 222, 145–160.
Sassen, K., DeMott, P.J., Prospero, J.M., Poellot, M.R., 2003. Saharan dust storms and indirect aerosol effects on clouds: CRYSTAL-FACE results. Geophysical Research Letters 30.
Scheinost, A.C., Schwertmann, U., 1999. Color identification of iron oxides and hydroxysulfates: use and limitations. Soil Science Society of America Journal 63, 1463–1471.
Schellenberger, A., Veit, H., 2006. Pedostratigraphy and pedological and geochemical characterization of Las Carreras loess-paleosol sequence, Valle de Tafi, NW-Argentina. Quaternary Science Reviews 25, 811–831.
Schmidt, A.M., von Dobeneck, T., Bleil, U., 1999. Magnetic characterization of Holocene sedimentation in the South Atlantic. Paleoceanography 14, 465–481.
Schwertmann, U., Taylor, R.M., 1987. Iron oxides. In: Dixon, J.B., Weed, S.B. (Eds.), Minerals in Soil Environments, second ed. Soil Science Society of America, Madison.
Schwertmann, U., 1988. Some properties of soil and synthetic iron oxides. In: Stucki, J.W., Goodman, B.A., Schwertmann, U. (Eds.), Iron in Soils and Clay Minerals, D. Reidel Publishing, Holland.
Sedwick, P., Sholkovitz, E.R., Church, T., 2007. Impact of anthropogenic combustion emissions on the fractional solubility of aerosol iron: evidence from the Sargasso Sea. Geochemistry Geophysics Geosystems 8 (10), Q10Q06.
Shao, Y.P., Leys, J.F., McTainsh, G.H., Tews, K., 2007. Numerical simulation of the October 2002 dust event in Australia. Journal of Geophysical Research-Atmospheres 112.
Shi, Z.B., Krom, M.D., Benning, L.G., Bonneville, S., Baker, A., Jickells, T., 2009a. Formation of iron nanoparticles during dust cloud processing. Geochimica Et Cosmochimica Acta 73, A1211.
Shi, Z.B., Krom, M.D., Bonneville, S., Baker, A.R., Jickells, T.D., Benning, L.G., 2009b. Formation of iron nanoparticles and increase in iron reactivity in mineral dust during simulated cloud processing. Environmental Science & Technology 43, 6592–6596.
Shigemitsu, M., Narita, H., Watanabe, Y.W., Harada, N., Tsunogai, S., 2007. Ba, Si, U, Al, Sc, La, Th, C and C-13/C-12 in a sediment core in the western subarctic Pacific as proxies of past biological production. Marine Chemistry 106, 442–455.
Sokolik, I.N., Toon, O.B., 1999. Incorporation of mineralogical composition into models of the radiative properties of mineral aerosol from UV to IR wavelengths. Journal of Geophysical Research-Atmospheres 104, 9423–9444.
Spassov, S., Heller, F., Evans, M.E., Yue, L.P., von Dobeneck, T., 2003a. A lock-in model for the complex Matuyama–Brunhes boundary record of the loess/palaeosol sequence at Lingtai (Central Chinese Loess Plateau). Geophysical Journal International 155, 350–366.
Spassov, S., Heller, F., Kretzschmar, R., Evans, M.E., Yue, L.P., Nourgaliev, D.K., 2003b. Detrital and pedogenic magnetic mineral phases in the loess/palaeosol sequence at Lingtai (Central Chinese Loess Plateau). Physics of the Earth and Planetary Interiors 140, 255–275.
Spracklen, D.V., Carslaw, K.S., Kulmala, M., Kerminen, V.M., Sihto, S.L., Riipinen, I., Merikanto, J., Mann, G.W., Chipperfield, M.P., Wiedensohler, A., Birmili, W., Lihavainen, H., 2008. Contribution of particle formation to global cloud condensation nuclei concentrations. Geophysical Research Letters 35.
Stanjek, H., Fassbinder, J.W.E., Vali, H., Wagele, H., Graf, W., 1994. Evidence of biogenic Greigite (Ferrimagnetic $Fe_3S_4$) in soil. European Journal of Soil Science 45, 97–103.
Sugden, D.E., McCulloch, R.D., Bory, A.J.M., Hein, A.S., 2009. Influence of Patagonian glaciers on Antarctic dust deposition during the last glacial period. Nature Geoscience 2, 281–285.
Sun, D.H., Chen, F.H., Bloemendal, J., Su, R.X., 2003. Seasonal variability of modern dust over the Loess Plateau of China. Journal of Geophysical Research-Atmospheres 108.
Sun, D.H., Shaw, J., An, Z.S., Rolph, T., 1993. Matuyama/Brunhes (M/B) transition recorded in Chinese loess. Journal of Geomagnetism and Geoelectricity 45, 319–330.
Sun, D.H., Wu, X.H., Liu, D.S., 1996. Regime over the evolution of the summer monsoon Loess Plateau of the last 150 ka. Science in China Series D-Earth Sciences 39, 503–511.
Sun, Y., Tada, R., Liu, J., Chen, Q.S., Shin, T., Tani, A., Ji, J., Yuko, I., 2008. Tracing the provenance of fine-grained dust deposited on the central Chinese Loess Plateau. Geophysical Research Letters 35, L01804. doi:10.1029/2007GL031672.
Swap, R., Garstang, M., Greco, S., Talbot, R., Kallberg, P., 1992. Saharan dust in the Amazon Basin. Tellus Series B-Chemical and Physical Meteorology 44, 133–149.
Tagliabue, A., Bopp, L., Aumont, O., 2009a. Evaluating the importance of atmospheric and sedimentary iron sources to Southern Ocean biogeochemistry. Geophysical Research Letters 36.
Tagliabue, A., Bopp, L., Roche, D.M., Bouttes, N., Dutay, J.C., Alkama, R., Kageyama, M., Michel, E., Paillard, D., 2009b. Quantifying the roles of ocean circulation and biogeochemistry in governing ocean carbon-13 and atmospheric carbon dioxide at the last glacial maximum. Climate of the Past 5, 695–706.
Tanaka, T.Y., Chiba, M., 2006. A numerical study of the contributions of dust source regions to the global dust budget. Global and Planetary Change 52, 88–104.
Tarduno, J.A., 1995. Superparamagnetism and reduction diagenesis in pelagic sediments – enhancement or depletion. Geophysical Research Letters 22, 1337–1340.
Tauxe, L., Herbert, T., Shackleton, N.J., Kok, Y.S., 1996. Astronomical calibration of the Matuyama–Brunhes boundary: consequences for magnetic remanence acquisition in marine carbonates and the Asian loess sequences. Earth and Planetary Science Letters 140, 133–146.
Taylor, R.M., Graley, A.M., 1967. Influence of ionic environment on nature of iron oxides in soils. Journal of Soil Science 18, 341.
Taylor, R.M., Maher, B.A., Self, P.G., 1987. Magnetite in soils. 1. The synthesis of single-domain and superparamagnetic magnetite. Clay Minerals 22, 411–422.
Tegen, I., Fung, I., 1995. Contribution to the atmospheric mineral aerosol load from land–surface modification. Journal of Geophysical Research-Atmospheres 100, 18707–18726.
Tegen, I., Harrison, S.P., Kohfeld, K., Prentice, I.C., Coe, M., Heimann, M., 2002. Impact of vegetation and preferential source areas on global dust aerosol: results from a model study. Journal of Geophysical Research-Atmospheres 107.
Thomas, A., 2008. Development and properties of 0.25-degree gridded evapotranspiration data fields of China for hydrological studies. Journal of Hydrology 358, 145–158.
Thompson, L.G., Mosley-Thomson, E., Davis, M.E., Bolzan, J.F., Dai Klein, L., Gundestrup, N., Yao, T., Wu, X., Xie, Z., 1990. Glacial stage ice-core records from the subtropical Dunde Ice Cap, China. Annals of Glaciology 14, 288–297.
Thompson, L.G., Mosley-Thompson, E., Brecher, H., Davis, M., Leon, B., Les, D., Lin, P.N., Mashiotta, T., Mountain, K., 2006. Abrupt tropical climate change: past and present. Proceedings of the National Academy of Sciences of the United States of America 103, 10536–10543.
Thompson, L.G., Yao, T., Davis, M.E., Henderson, K.A., MosleyThompson, E., Lin, P.N., Beer, J., Synal, H.A., ColeDai, J., Bolzan, J.F., 1997. Tropical climate instability: the last glacial cycle from a Qinghai-Tibetan ice core. Science 276, 1821–1825.
Thompson, R., 1986. Modeling magnetization data using simplex. Physics of the Earth and Planetary Interiors 42, 113–127.
Thompson, R., Maher, B.A., 1995. Age models, sediment fluxes and paleoclimatic reconstructions for the Chinese loess and paleosol sequences. Geophysical Journal International 123, 611–622.

Tiedemann, R., Sarnthein, M., Stein, R., 1989. Climate changes in the western Sahara: aeolo-marine sediment record of the last 8 million years (sites 657–661). In: Ruddiman, W., Sarnthein, M., Baldauf, Jetal (Eds.), Proceedings of the Ocean Drilling Program. Scientific Results, vol. 108. Ocean Drilling Program, College Station, TX, pp. 241–278.

Torrent, J., Barron, V., Liu, Q.S., 2006. Magnetic enhancement is linked to and precedes hematite formation in aerobic soil. Geophysical Research Letters 33.

Torrent, J., Schwertmann, U., Fechter, H., Alferez, F., 1983. Quantitative relationships between soil color and hematite content. Soil Science 136, 354–358.

Torii, M., Lee, T.Q., Fukuma, K., Mishima, T., Yamazaki, T., Oda, H., Ishikawa, N., 2001. Mineral magnetic study of the Taklimakan desert sands and its relevance to the Chinese loess. Geophysical Journal International 146 (2), 416–424.

Trauth, M.H., Larrasoana, J.C., Mudelsee, M., 2009. Trends, rhythms and events in Plio-Pleistocene African climate. Quaternary Science Reviews 28, 399–411.

Tsoar, H., Pye, K., 1987. Dust transport and the question of desert loess formation. Sedimentology 34, 139–153.

Tsuda, A., Takeda, S., Saito, H., Nishioka, J., Nojiri, Y., Kudo, I., Kiyosawa, H., Shiomoto, A., Imai, K., Ono, T., Shimamoto, A., Tsumune, D., Yoshimura, T., Aono, T., Hinuma, A., Kinugasa, M., Suzuki, K., Sohrin, Y., Noiri, Y., Tani, H., Deguchi, Y., Tsurushima, N., Ogawa, H., Fukami, K., Kuma, K., Saino, T., 2003. A mesoscale iron enrichment in the western Subarctic Pacific induces a large centric diatom bloom. Science 300 (5621), 958–961.

Uematsu, M., Duce, R.A., Prospero, J.M., Chen, L., Merrill, J.T., McDonald, R.L., 1983. Transport of mineral aerosol from Asia over the north Pacific Ocean. Journal of Geophysical Research-Oceans and Atmospheres 88 (NC9), 5343–5352.

Uematsu, M., Merrill, J.T., Duce, R.A., Prospero, J.M., 1986. Atmospheric fluxes of Asian desert dust to the North Pacific – temporal and spatial variability. Atmospheric Environment 20, 2073.

Uematsu, M., Wang, Z.F., Uno, I., 2003. Atmospheric input of mineral dust to the western North Pacific region based on direct measurements and a regional chemical transport model. Geophysical Research Letters 30 (6), L1342.

Urbat, M., Pletsch, T., 2003. Pleistocene deep-sea sediment in ODP Hole 1149A, Nadezhda Basin: sources, alteration, and age controls (0-800 ka). In: Ludden, J.N., Plank, T., Escutia, C. (Eds.), Proc. ODP, Sci. Results, vol. 185 (Online). Available from: <http://wwodp.tamu.edu/publications/185_SR/012/012.htm>.

Van Andel, T.H., Tzedakis, P.C., 1996. Palaeolithic landscapes of Europe and environs, 15,0000–25,000 years ago: an overview. Quaternary Science Reviews 15, 481–500.

van Velzen, A.J., Dekkers, M.J., 1999. Low-temperature oxidation of magnetite in loess-paleosol sequences: a correction of rock magnetic parameters. Studia Geophysica Et Geodaetica 43, 357–375.

VanCuren, R.A., Cahill, T.A., 2002. Asian aerosols in North America: frequency and concentration of fine dust. Journal of Geophysical Research-Atmospheres 107.

Verma, S., Venkataraman, C., Boucher, O., 2008. Origin of surface and columnar Indian Ocean Experiment (INDOEX) aerosols using source- and region-tagged emissions transport in a general circulation model. Journal of Geophysical Research-Atmospheres 113.

Verosub, K.L., Fine, P., Singer, M.J., Tenpas, J., 1993. Pedogenesis and paleoclimate – interpretation of the magnetic-susceptibility record of Chinese loess-paleosol sequences. Geology 21, 1011–1014.

Vidic, N.J., Singer, M.J., Verosub, K.L., 2004. Duration dependence of magnetic susceptibility enhancement in the Chinese loess-palaeosols of the past 620 ky. Palaeogeography Palaeoclimatology Palaeoecology 211, 271–288.

Virina, E.I., Faustov, S.S., Heller, F., 2000. Magnetism of loess-palaeosol formations in relation to soil-forming and sedimentary processes. Physics and Chemistry of the Earth Part A-Solid Earth and Geodesy 25, 475–478.

Vlag, P.A., Oches, E.A., Banerjee, S.K., Solheid, P.A., 1999. The paleoenvironmental-magnetic record of the Gold Hill Steps loess section in central Alaska. Physics and Chemistry of the Earth Part A-Solid Earth and Geodesy 24, 779–783.

von Suchodoletz, H., Oberhansli, H., Hambach, U., Zoller, L., Fuchs, M., Faust, D., 2010. Soil moisture fluctuations recorded in Saharan dust deposits on Lanzarote (Canary Islands) over the last 180 ka. Quaternary Science Reviews 29, 2173–2184.

Wagener, T., Guieu, C., Losno, R., Bonnet, S., Mahowald, N., 2008. Revisiting atmospheric dust export to the Southern Hemisphere ocean: biogeochemical implications. Global Biogeochemical Cycles 22.

Walden, J., Oldfield, F., Smith, J.P. (Eds.), 1999. Environmental magnetism: apractical guide. Technical Guide No. 6, Quaternary Research Association, London.

Walden, J., White, K.H., Kilcoyne, S.H., Bentley, P.M., 2000. Analyses of iron oxide assemblages within Namib dune sediments using high field remanence measurements (9 T) and Mossbauer analysis. Journal of Quaternary Science 15, 185–195.

Wang, H.Z., Zhao, Quanhong., Lizhong, Yu., Zhang, Weiguo., 2008. Late Quaternary eolian records in the northwest Pacific with glacial cycles: a comparison. Science in China Series D: Earth Sciences 41 (1), 28–34. doi:10.1007/BF02932417.

Wang, X.M., Dong, Z.B., Zhang, J.W., Liu, L.C., 2004. Modern dust storms in China: an overview. Journal of Arid Environments 58, 559–574.

Wang, Y.J., Cheng, H., Edwards, R.L., He, Y.Q., Kong, X.G., An, Z.S., Wu, J.Y., Kelly, M.J., Dykoski, C.A., Li, X.D., 2005. The Holocene Asian monsoon: links to solar changes and North Atlantic climate. Science 308, 854–857.

Watkins, S.J., Maher, B.A., 2003. Magnetic characterisation of present-day deep-sea sediments and sources in the North Atlantic. Earth and Planetary Science Letters 214, 379–394.

Watkins, S.J., Maher, B.A., Bigg, G.R., 2007. Ocean circulation at the Last Glacial Maximum: a combined modeling and magnetic proxy-based study. Paleoceanography 22.

Watson, A.J., Lefevre, N., 1999. The sensitivity of atmospheric $CO_2$ concentrations to input of iron to the oceans. Tellus Series B-Chemical and Physical Meteorology 51, 453–460.

Werner, M., Tegen, I., Harrison, S.P., Kohfeld, K.E., Prentice, I.C., Balkanski, Y., Rodhe, H., Roelandt, C., 2002. Seasonal and interannual variability of the mineral dust cycle under present and glacial climate conditions. Journal of Geophysical Research-Atmospheres 107.

Westgate, J.A., Stemper, B.A., Pewe, T.L., 1990. A 3-My record of pliocene-pleistocene loess in interior Alaska. Geology 18, 858–861.

Winckler, G., Anderson, R.F., Fleisher, M.Q., McGee, D., Mahowald, N., 2008. Covariant glacial–interglacial dust fluxes in the equatorial Pacific and Antarctica. Science 320, 93–96.

Worobiec, A., Szaloki, I., Osan, J., Maenhaut, W., Stefaniak, E.A., Van Grieken, R., 2007. Characterisation of Amazon Basin aerosols at the individual particle level by X-ray microanalytical techniques. Atmospheric Environment 41, 9217–9230.

Xie, Q.Q., Chen, T.H., Xu, H.F., Chen, J., Ji, J.F., Lu, H.Y., Wang, X.Y., 2009a. Quantification of the contribution of pedogenic magnetic minerals to magnetic susceptibility of loess and paleosols on Chinese Loess Plateau: paleoclimatic implications. Journal of Geophysical Research-Solid Earth 114.

Xie, Q.Q., Chen, T.H., Xu, X.C., Qing, C.S., Xu, H.F., Sun, Y.B., Ji, J.F., 2009b. Transformation relationship among different magnetic minerals within loess-paleosol sediments of the Chinese Loess Plateau. Science in China Series D-Earth Sciences 52, 313–322.

Yamazaki, T., 2009. Environmental magnetism of Pleistocene sediments in the North Pacific and Ontong-Java Plateau: temporal variations of detrital and biogenic components. Geochemistry Geophysics Geosystems 10.

Yamazaki, T., Ioka, N., 1997. Environmental rock-magnetism of pelagic clay: implications for Asian eolian input to the North Pacific since the Pliocene. Paleoceanography 12, 111–124.

Yancheva, G., Nowaczyk, N.R., Mingram, J., Dulski, P., Schettler, G., Negendank, J.F.W., Liu, J.Q., Sigman, D.M., Peterson, L.C., Haug, G.H., 2007. Influence of the intertropical convergence zone on the East Asian monsoon. Nature 445, 74–77.

Zavarzina, D.G., 2001. Biogeochemical Factors of Iron Compounds Transformation in Redox Conditions. Ph.D. Thesis, Moscow State University.

Zhang, D.Z., Iwasaka, Y., 2004. Size change of Asian dust particles caused by sea salt interaction: measurements in southwestern Japan. Geophysical Research Letters 31.

Zhou, L.P., Shackleton, N.J., 1999. Misleading positions of geomagnetic reversal boundaries in Eurasian loess and implications for correlation between continental and marine sedimentary sequences. Earth and Planetary Science Letters 168, 117–130.

Zhu, A., Ramanathan, V., Li, F., Kim, D., 2007. Dust plumes over the Pacific, Indian, and Atlantic oceans: climatology and radiative impact. Journal of Geophysical Research-Atmospheres 112.

Zhu, R.X., Coe, R.S., Guo, B., Anderson, R., Zhao, X.X., 1998. Inconsistent palaeomagnetic recording of the Blake event in Chinese loess related to sedimentary environment. Geophysical Journal International 134, 867–875.

Zhu, R.X., Pan, Y.X., Liu, Q.S., 1999. Geomagnetic excursions recorded in Chinese loess in the last 70,000 years. Geophysical Research Letters 26, 505–508.

Zhu, R.X., Zhou, L.P., Laj, C., Mazaud, A., Ding, Z.L., 1994. The blake geomagnetic polarity episode recorded in Chinese loess. Geophysical Research Letters 21, 697–700.